Bacterial Transport and Deposition in an Intact Soil Lysimeter and Packed Sand Columns

---

A thesis

submitted in partial fulfillment

of the requirements for the Degree of

Master of Applied Science

at

Lincoln University

by

Guangming Jiang

Lincoln University

2005

Abstract of a thesis submitted in partial fulfillment of the

requirements for the Degree of Master of Applied Science

Bacterial Transport and Deposition in an Intact Soil Lysimeter and Packed Sand Columns

by Guangming Jiang

Microbial transport in porous media is mainly facilitated by flowing water, whilst retention is due to adsorption to phase interfaces. Water flow in porous media depends greatly on water content and pore size distribution. Microbial adsorption to air-water interfaces is especially important in unsaturated porous media. Bacterial transport in unsaturated soils is much less well understood than in saturated conditions, especially for intact soils. The first experiment was designed to investigate the fate and transport of bacteria in intact soils with different water saturations, and particularly the effect of low suction (and hence removal of water flow in the largest macropores).

An intact soil column (50 cm diameter × 70 cm depth) with a tension infiltrometer was used to investigate the transport and deposition of *Bacillus subtilis* endospores (i.e. dormant and persistent bacteria) during both saturated and unsaturated flows. Soil porosity and pore size distribution were measured. Porosity decreased with depth and macropores were concentrated in the topsoil. Three tensiometers and a temperature sensor were installed along the soil column to monitor matric suction and temperature. Breakthrough curves for bacteria and chemical tracer Br^- at 0 kPa and 0.5 kPa suction were obtained during the three-month leaching experiment.

Bacterial breakthrough occurred earlier than the inert chemical tracer, which is consistent with effects of pore size exclusion. Also, saturated flow gave a significantly higher concentration and recovery ratio of leached bacteria, i.e. 51% vs. 0.88%. Recovery of Br^- in leachate at both suctions reached above 85%. The column was destructively sampled

for deposited endospores at the completion of leaching. Bacterial deposition was concentrated in the top ten centimeters, then decreased abruptly and was relatively constant with column depth, although showing some irregularity at the bottom of the column.

To more thoroughly investigate the factors which influence bacterial transport in porous media, a sand column leaching system with well-controlled degree of water saturation and flow rate was built to investigate the effects of water content, particle size, and column length on bacterial transport.

Adsorption of *E. coli* strain D to silica sands was measured in batch adsorption tests. The average percent of adsorption for coarse and fine sands was 45.9 ± 7.8 % and 96.9 ± 3.2 %, respectively. The applicability of results from batch adsorption experiments to bacterial transport was limited because of the dynamic feature of bacteria in sand columns.

The early breakthrough of *E. coli* relative to bromide was clear for all sand columns, namely *c.* 0.15~0.3 pore volume earlier. The column length had no significant effects on the *E. coli* peak concentration and total recovery in leachate, which supported the observation that bacteria were retained in top layer of sands. Tailing of breakthrough curves was more prominent for all fine sand columns than their coarse sand counterparts. Bacterial recovery in leachate from coarse and saturated sand columns was significantly higher than fine and unsaturated columns.

Observed data were fitted by equilibrium, one-site, two-site and their AWI amended convection-dispersion kinetic models. Two-site + AWI model achieved constant high model efficiency for both coarse and fine sands, under either saturated or unsaturated flow conditions. However, f in two-site model could not be physically measured and the fitted value might just be an artifact. Although the intrinsic flaw associated with two-site + AWI model, it is still a simple and effective modeling approach.

Keywords:

Bacillus subtilis; *Escherichia coli*; microbial transport; unsaturated intact soil; tension infiltrometer; silica sand columns; matric suction; water content; pore size exclusion; air-water interface; bacterial adsorption; breakthrough curve; CXTFIT 2.1; STANMOD 2.2; convection-dispersion equation; modeling.

Acknowledgments

It is through the support of many that this Masters thesis has been completed after one and a half years of field and laboratory trials.

My thanks go first to my supervisors, Dr Michael Noonan and Dr Graeme Buchan, Lincoln University, for their clear guidance, advice, and encouragement throughout my study at Lincoln University. Thank you for your help with my courses and language when I was first landed in New Zealand. You are always prompt reviewing and editing my papers, experimental plans. The research couldn't be done without your excellent supervision. Your consistent support and friendship are very much appreciated.

I am grateful for my postgraduate scholarship funded from NZAID (New Zealand Agency for International Development) to support my studies. I also appreciate that Southwest University of Science and Technology, China gave me the opportunity to further my education.

Appreciation is given to B. N. Dancer at University of Wales Institute of Science and Technology for supplying bacteria used in the research.

I also thank Michelle Pattison and Neil Smith for their generous assistance in laboratory and field experiments. Neil helped me throughout my field trial and laboratory experiments, including calibration of sensors, installation of devices, writing and debugging datalogger programs, collection of samples. You are such a great guy, not only helping me with the experiments, but also bringing me fun and humor. Thank Michelle Pattison for showing me the basic microbiological laboratory techniques.

Appreciation is also given to Dr Verwoerd Wynands at Lincoln University, who helped me solve partial differential equations used to model bacterial transport. I would like to thank Professor Arturo Keller at Bren School of Environmental Science and Management, University of California for generously sending me source code of COLLOIDFIT model. Thanks to my former colleague Qingyang Wu at Sichuan University, who encouraged and

helped me with mathematical modeling.

I would like to acknowledge support from the Soil and Physical Science Group, Lincoln University, especially Jason Breitmeyer and Joy Jiao for analysis of bromide samples, and Barry Thompson for measurement of soil porosity and pore size distribution.

I also thank Shuang Jiang for her discussion and comments on my proposal and experimental results.

Thanks to my friend Wenyu Sun. Your emails and phone calls have been so supportive, enabling me to pass through much lonely time.

To my friends Yue Zhang, Xiaolong Yang, King Hei, Tao Peng, Zhi Xie, and all the badminton guys in the recreation centre. Thanks buddies. The badminton time makes me fit for the heavy study and that's really wonderful time we spent together.

I also feel deeply grateful to my father for his endless love and support, for his endeavor and encouragement to further my education.

Publications

1. Jiang GM, Noonan MJ, Buchan GD, Smith NP (2005) Transport and deposition of *Bacillus subtilis* through an intact soil column. *Australian Journal of Soil Research* **43**, 695-703.

2. Buchan GD, Cameron KC, Noonan MJ, Jiang GM, Close M (2005) Pathogen transport via soils from land-applied animal wastes. In 'European Geosciences Union General Assembly'. Vienna

3. Jiang GM, Noonan MJ, Buchan GD, Smith NP (2005) Transport and trapping of bacteria in an intact soil column. *Water in the Soil-Plant-Atmosphere System (WISPAS)* **90**.

Preface

This thesis starts with a literature review on microbial transport and retention in porous media (Chapter I), followed by Chapter II describing the research objectives. Chapter III describes the first series of experiments with an outdoor soil lysimeter which studied the effects of macropore water flow (i.e. at very low suction) and the bacterial spatial distribution in the soil after leaching events. Chapter IV discusses experimental designs to achieve well-controlled unsaturated steady flow in sand columns. Chapter V presents experimental and mathematical modelling results from the sand column transport experiments. Appendix I extends the results and discussion on mathematical modelling of bacterial transport. Appendix II gives results for the water infiltration rates and suctions in all sand columns. The remaining appendices delineate experimental methods and programs used in this thesis.

Table of Contents

List of Tables

List of Figures

Abbreviations

mL	Milliliter
L	Litre
g	Gram
mg	Milligram
µg	Microgram
hr	Hour
min	Minute
sec	Second
AWI	Air water interface
BTC	Breakthrough curve
cfu	Colony forming unit
CDE	Convection diffusion equation
COS	Coarse Oamaru sand
DLVO	Derjaguin-Landau-Verwey-Overbeek theory
FIA	Flow injection analysis
FOS	Fine Oamaru sand
GEM	Genetically engineered microorganisms
IEC	Ion Exchange Chromatography

NC	Normalized concentration
ND	Normalized depth
PV	Pore volume
SMC	Soil (sand) moisture characteristics
SWI	Solid water interface
TPB	Triple phase boundary

List of Symbols

c	Bacterial concentration in the drainage water (cfu cm^{-3}).
c'	Concentration of conservative chemical tracer, i.e. bromide (mg L^{-1}).
c_0	Initial bacterial concentration (cfu cm^{-3}).
c_0'	Initial concentration of inert chemical tracer (mg L^{-1}).
C_s	Bacterial concentrations on solid (cfu g^{-1}) for equilibrium adsorption.
C_w	Bacterial concentrations in liquid (cfu g^{-1}) for equilibrium adsorption.
d_m	Media grain size (μm).
d_p	Diameter of transported particles (μm).
f	The fraction of exchange sites assumed to be at equilibrium adsorption.
D	Dispersion coefficient (cm^2 min^{-1}).
g	Gravitational acceleration (m s^{-2}).
J	Microbial flux density in the direction of flow (the number of microbes passing through a unit cross-sectional area per unit time, cfu cm^{-2} min^{-1}).
k_0, k	Bacterial attachment coefficient to air-water interface (min^{-1}).
k_1, K_f	Bacterial attachment coefficient to solid-water interface (min^{-1}).
k_2, K_r	Bacterial detachment coefficient from solid-water interface (min^{-1}).
K_d	Distribution coefficient for equilibrium bacterial adsorption (mL g^{-1}).
K_f	Bacterial attachment coefficient to solid-water interface (min^{-1}).
K_L	A constant related to binding energy (mL/cfu) in Langmuir isotherm;
K_r	Bacterial detachment coefficient from solid-water interface (min^{-1}).
$K_r(S)$	Relative hydraulic conductivity as a function of suction.
L	The tube length (cm).
m	For van Genuchten conductivity model, m is assumed to be 1 – 1/n. For Freundlich isotherm, m is a constant indicating sorption intensity.
M_s	Weight of sand for density measurement (g).
n	$n = 1 + \lambda$, λ is pore size index.
N_w	Total number of bacteria in the supernatant (cfu) after centrifugation.
N_t	Total number of bacteria added in batch bacterial adsorption test (cfu).

PA	The percentage of bacterial adsorption to Oamaru sand (%).
Pe	The Peclet number, $Pe=vL/D$. The ratio of advection to dispersion processes
ΔP	Pressure gradient (Pa).
Q	Water flux ($cm^3\ s^{-1}$).
r	The radius of the capillary tube (cm); or tube radius for Poiseuille's law.
R	The bacterial transport retardation factor.
R_d	The rate of microbial decay (number of microbes per unit volume of porous media per unit time, cfu cm^{-3} min^{-1}).
R_g	The rate of microbial regrowth (number of microbes per unit volume of porous media per unit time, cfu cm^{-3} min^{-1}).
s	The concentration of bacteria reversibly attached to soil grains (cfu g^{-1}).
S, h	Matric suction (kPa); h is also the height of water rise in a capillary tube (cm).
S_{max}	The maximum adsorption sites per gram of sand (cfu/g).
S_w	Degree of water saturation.
t	Time lapsed after injection of bacterial suspension (min)
$\overline{u}$	Mean flow velocity through the tube (cm s^{-1}).
v	Pore water velocity (cm min^{-1})
v_g	Sedimentation velocity of bacteria (cm min^{-1})
v_x	Chemotactic velocity of bacteria (cm min^{-1})
W	Mass of sand used in the mixture of batch bacterial adsorption test (g).
W_a	Weight of cleaned an empty 100 mL flask (g).
W_s	Weight of a 100 mL flask plus soil, corrected to 105 °C oven dry water content (g).
W_{sw}	Weight of fifty grams sand plus a 100 mL flask with boiled, and cooled distilled water (g).
W_w	Weight of a 100 mL flask with boiled cooled distilled water (g).
V	Volume of fluid in the mixture of batch bacterial adsorption test (mL).
V_s	Volume of sand for density measurement (mL).
x, z	The longitudinal distance from the point of inlet (cm).

Greek

α	Equivalent to the inverse of air entry suction.
ρ_b	Soil or sand bulk density (g cm^{-3}).
ρ_w	Water density (g cm^{-3}).
ρ_p	Particle density (g cm^{-3}).
θ_v	Volumetric water content.
$\theta_{v,s}$, ε	Saturated water content; or total porosity.
θ_r	Residual water content.
θ_{sat}	Saturated water content.
μ	Water dynamic viscosity (Pa s).
σ	The surface tension of water (kg s^{-2}).
Ψ_m	Soil matric potentials (kPa).

Chapter One
Introduction and Literature Review

1.1. Introduction

For more than a century, scientists have been working on the fate and transport of microbes through porous media, especially soils. Pathogen transport through subsurface and subsequent contamination of water resources usually coincides with increased water flow in soils (heavy precipitation, irrigation) (Gerba and Smith 2005; Martin and Noonan 1977; Unc and Goss 2004).

For example, Martin and Noonan (1977) found that groundwater was contaminated by coliform bacteria when effluent from an oxidation pond was applied at the rate of approximately 200 mm H_2O and following a heavy rainfall, but was not polluted when rainfall was less intense. Findings of many researchers have revealed that microbes can be removed from the water phase by adsorption, filtration, or deposition at phase interfaces. Noonan (personal communication) has also found that spray irrigation of a dairy pasture at the rate of 50 mm every 12 days allows water to penetrate 1.7 m of soil and gravel strata but the percolate was free of coliform bacteria. On one occasion, when 30 mm of rain followed the application of 50 mm of irrigation water, the percolate was found to contain coliform bacteria. Subsequent irrigation of 80 mm also produced coliform bacteria in the percolate. While the vast majority of bacteria from the cow faeces were trapped in the top layer of the soil, under some conditions of water flow, bacteria would penetrate the strata. There is much unknown about the retention and movement of microbes in soil and other strata, phenomena such as that reported by Noonan and others can not be predicted with any degree of confidence.

Microbial transport, in many aspects, is similar to abiotic colloids. These are a group of very fine particles in suspension that have effective diameters ranging from 1 nm to 10 μm, roughly comparable to those of virus, bacteria, and *Cryptosporidium* sp. (Sirivithayapakorn and Keller 2003). However, because microbes are living organisms, their transport in porous media is more complex than is the case for abiotic colloids (Ginn,

Wood *et al.* 2002). Not only are microbes subject to the same physicochemical interactions as are colloids, but there are also a number of strictly biological processes that affect the transport processes. Generally, microbial transport is facilitated by flowing water in the porous media; and retention is mainly caused by adsorption at phase interfaces, i.e. the solid-water interface (SWI), air-water interface (AWI), and the triple phase boundary (TPB).

Although these observations are important in predicting bacterial transport and retention, the relative importance of water flow and microbial adsorption at phase interfaces on microbial transport and retention is not understood thoroughly. This thesis aims to elucidate the effects of water flow and bacterial adsorption on bacterial transport and retention, and to help explain the observation of Noonan and others.

1.2. Passive microbial transport facilitated by flowing water

1.2.1. Introduction

Microbial transport by water flow in porous media is called passive transport, as the motility of microbes (induced by bacterial flagellar movement, or cell contraction and expansion) does not contribute much to the overall movement facilitated by the flow (Robert and Chenu 1992). Although some microorganisms can survive under quite dry conditions, for transport through porous media, water flow is by far the most important carrier.

Water flow is caused by a potential gradient in porous media (Hillel 1998), and is influenced dramatically by pore size distribution, degree of saturation and especially by macroporosity (Beven and Germann 1982; Czapar and Fawcett 1992; Jabro, Lotse *et al.* 1991; Silva, Cameron *et al.* 2000; Singh and Kanwar 1991; Thomas and Phillips 1979). In porous media, water flow is usually divided into two mechanisms: mass flow driven by a potential (e.g. suction) gradient; and vapor diffusion driven by a moisture or temperature gradient. Liquid water flow is dominant in moister porous media, whereas the vapor diffusion mainly occurs in drier porous media. The liquid water flow is further divided into macropore flow and matric flow.

1.2.2. Effect of macropore water flow

In natural subsurface strata, macropore water flow is important because it conducts the majority of water flux and has high velocity. The water flux in different pore sizes at a given hydraulic gradient can be calculated using physical equations (Bouma 1991). According to Poiseuille's law, water flux is proportional to r^4 (where r is radius of pore throats) (Hillel 1998). This has strong implication that macropore water flow is responsible for the majority of water flow, and consequently microbial transport.

In porous media, such as soils, macropore flow includes preferential flow and bypass flow. In natural vadose (unsaturated) zone, preferential flow could be dominated by bypass flow (short-circuiting), fingering effect, and funneled flow that increase the mobility of harmful chemicals and microbial contaminants in applied water (Beven and Germann 1982; Munyankusi, Gupta *et al.* 1994; Natsch, Keel *et al.* 1996; Singh and Kanwar 1991; Thomas and Phillips 1979). Macropore flow paths were reported to exist in all undisturbed soil columns used to study solute transport (Singh and Kanwar 1991). Macropore flow under unsaturated conditions was found to result in the transport of large quantities of bromide and nitrate-nitrogen, and sometimes substantial leaching of nitrate when soil is at or near saturation (Jabro, Lotse *et al.* 1991; Silva, Cameron *et al.* 2000). Also, herbicide and chloride were found to be transported through soil columns only when continuous artificial macropores were present (Czapar and Fawcett 1992). Some research also showed that only when macropore flow was included in water flow models could solute and water transport be predicted more precisely (Munyankusi, Gupta *et al.* 1994; Williams and Vepraskas 1994). Given that macropore flow has a large effect on the transport of chemical solute; it could be expected to affect microbial transport, though not much research has been done to quantify the effects.

When heavy precipitation or irrigation occurrs, water-filled macropores (worm holes, plant root channels, clay soil cracks, fractures in consolidated soil) produced fast and relatively unrestricted water movement. For natural soils, macropores cause big variance of hydraulic conductivity, rendering predictions of water flow and microbial transport more difficult. In this thesis, we are going to address the effects of macropore flow by imposing certain suctions on an intact soil lysimeter and packed sand columns.

1.2.3. Effect of water content in porous media

Water flow rate is usually higher in saturated than unsaturated media assuming it is driven by the same pressure gradient. This is because the effective (water-filled) porosity decreases with lower saturation, and thus the sizes of channels conducting water are diminished. Also, even with the same effective porosity, porous media having macropores conduct water faster than those with smaller pores. Thus, the rate of migration of microbes in porous media depends strongly on the water content (which is related to suction).

When porous media is partially drained, microbes can still keep on moving through the adsorbed water films surrounding solid particles. Flagellar movement and the Brownian effect promote microbial transport through pores or sometimes along pore walls. However such movements may not be appreciable compared with movement in continuous water pathways, especially continuous macropores under saturated conditions.

Only pores, which are usually sufficiently greater than the size of a single microbe, with sufficient water content, can form a continuous pathway for the potential movement of the microbes. Considering the fact that water flow is mainly conducted through big pores, exclusion of microbes from pore throats is not usually determined by the ratio of sizes between microbes and pore throats, but the dramatically different water flow rates. Thus, microbes tend to travel much shorter distances in drier soils than under wet conditions, and transport mainly occurs through macropores rather than micropores (Ginn, Wood *et al.* 2002).

1.2.4. Effect of porosity and pore size distribution

Porous media usually contain a large number of pores with different shapes and sizes, and these are intricately interconnected (Hillel 1998). Among the factors influencing microbial transport in porous media, total porosity and pore-size distribution are critical parameters. These partly determine the water flow regime, and thus greatly influence the percent of total applied microbial cells recovered in percolate.

The size range of medium pores is from 0.1 μm to 10 μm, which is approximately 15% of the total porosity in sand and 33% in loam. Macropores are generally larger than 30 μm,

which provides unrestricted transport conduits for many microbes. Bacterial sizes are generally believed to be from about 200 nm to 5 μm, which is the size range from coarse clay to fine silt. Comparison of the sizes of microbes and soil pores is provided by (Matthess and Pekdeger 1985; McGechan and Lewis 2002; Robert and Chenu 1992) (see Figure 1). Therefore, it is easy for microbes to flow through the majority of soil pores if their size is compared to soil pores.

Effective porosity (water-filled or water-conducting) will decrease when a porous medium is dried. Therefore, effective porosity (rather than total porosity) should be used for quantifying interstitial water velocity. According to the capillary theory, bigger pores are emptied of water first when a porous medium is becoming unsaturated. Effective porosity of porous media with higher percent of larger diameter pores decreases sharply when they are dried under low suctions. Therefore, microbial transport in this kind of porous media varies dramatically between saturated and unsaturated conditions.

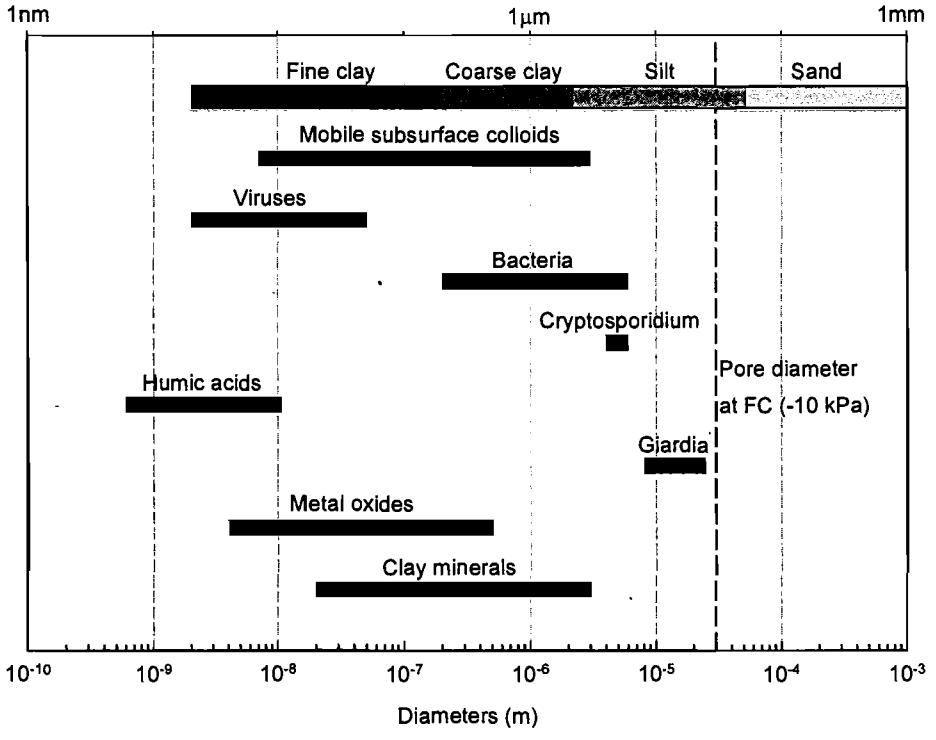

Figure 1. Size ranges of microorganisms and colloids. Pore diameter at field capacity is 30 μm; pore diameter at permanent wilting point is 0.2 μm.

1.2.5. Effect of microbial size (pore size exclusion)

Generally, transported particles move faster than the mean pore-water velocity or conservative/non-reacting tracers, due to the size of the particles being conveyed. Microbes appear to travel along faster streamlines at the centre of pore throats rather than next to pore walls (Germann and Alaoui 2002; Hendry, Lawrence *et al.* 1999). Sirivithayapakorn and Keller (2003) studied the size exclusion effect at pore-scale and demonstrated the accelerated transport velocity of bacteria. Sinton et al. (2000) postulated effects of pore size exclusion as the reason for the more rapid transport of bacteriophages adsorbed to bacteria through aquifers.

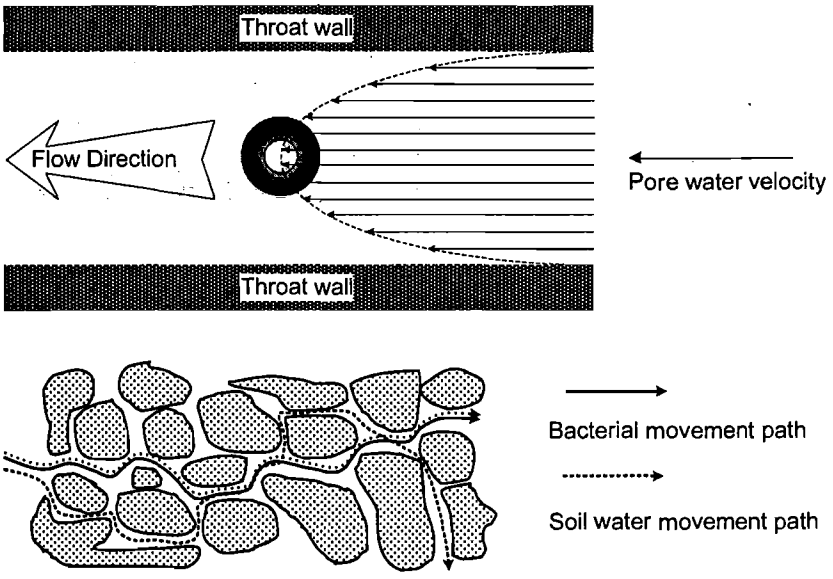

Figure 2. Different sized particles move along the velocity profile through a soil pore throat (Sirivithayapakorn and Keller 2003), and the detouring effect.

There are at least two processes causing exclusion: anionic and size effects; and size effects can be further divided into classical chromatographic and pore exclusion processes (Ginn, Wood *et al.* 2002). Anion exclusion mainly acts at the nanometer scale, and as such is not important for microbial transport. Size effects can also happen at the macroscopic scale. At this larger scale, colloid (including microbes) transport by rerouting to alternate pathways with bigger pores (detouring effect), is termed pore exclusion, volume exclusion, or pore size exclusion. In a microscale, size exclusion effect is facilitated by the large size of microbes relative to molecules of chemical tracers, or due

to the relatively low diffusion constant of microbes, which help to diffuse small particles into small soil pores. Bigger colloids travel at lower average velocity than smaller ones because they sample a broader range of the pore water velocity profile (Figure 2). However, in either case, the microbes are excluded from stagnant regions (with no or lower advective water velocity) in porous media. Thus, it is not necessary in practice to differentiate between the two processes (Jin and Flury 2002).

Comparisons of breakthrough of bacteria versus conservative chemical tracers (e.g. bromide, tritium etc.) are often made to determine whether they are transported differently through porous media and to elucidate the mechanisms of differential transport (Caron, Banton *et al.* 1996; Dong, Rothmel *et al.* 2000; Grolimund, Elimelech *et al.* 1998; Hekman, Heijnen *et al.* 1994; Jabro, Lotse *et al.* 1991; Jackson, Roy *et al.* 1994; McLeod, Aislabie *et al.* 2003; Silliman, Fletcher *et al.* 2001; Zhang, Johnson *et al.* 2001b). Size exclusion mechanisms are the most widely-used explanation for the differential transport (relative breakthrough) of microbes versus dissolved tracers. Zhang *et al.* (2001a) indicated that there are some potential artifacts associated with the traditional breakthrough curve methods. In addition to the size exclusion effect, attachment of bacteria to phase interfaces also contributes to the early breakthrough of bacteria relative to chemical tracers. Thus, Zhang *et al.* (2001a) suggested that the differential breakthrough caused by size exclusion can be discriminated from bacterial attachment by comparison of the observed peak shift with the estimated value from attachment.

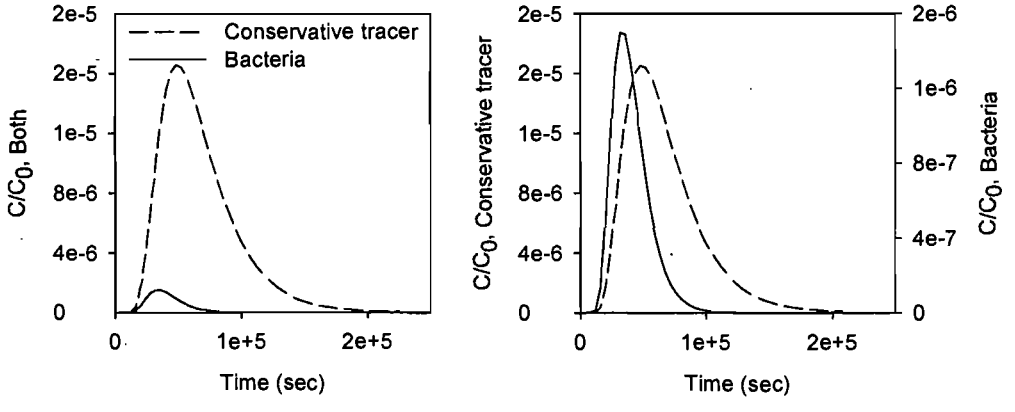

Figure 3. Simulated breakthrough curves of bacteria versus conservative chemical tracer, plotted with the same or different concentration scale.

A typical breakthrough curve (normalized concentration versus time) showing the differential microbial transport was simulated and is shown in Figure 3. The simulation is based on the one-dimensional advection-dispersion equation with a term accounting for adsorption (deposition, attachment, or filtration) (Grolimund, Elimelech *et al.* 1998; Zhang, Johnson *et al.* 2001a).

$$\frac{\partial c}{\partial t} = D\frac{\partial^2 c}{\partial x^2} - v\frac{\partial c}{\partial x} - kc \tag{1}$$

Zhang *et al.* (2001a) also reported that for a semi-infinite column initially free of the transported bacteria, and a unit pulse input, the solution for the bacterial concentration c at position x and time t is

$$c(x,t) = c_0 e^{-kt} \frac{x}{2\sqrt{\pi t^3 D}} e^{-(x-vt)^2/4Dt} \tag{2}$$

1.2.6. Conclusions

Microbial transport through natural or artificial porous media is mainly facilitated and controlled by the flowing water. Also, water flow velocity in porous media is determined by water content, and pore size distribution (especially existence of continuous preferential flow paths) when driven by same pressure gradient.

1.3. Microbial retention by adsorption to phase interfaces

1.3.1. Introduction

Microbes were shown to be removed from water by passage through porous media (Chu, Jin *et al.* 2001; Nicosia, Rose *et al.* 2001; Schijven, Medema *et al.* 2000). This removal was partly attributed to microbial die-off in unfavorable environmental conditions, such as low nutrient levels in soils, and unfavorable temperatures. Adsorption can cause retention of microbes at phase interfaces in porous media. The growth of microbes and ultimately the formation of a biofilm may produce more microbes in water or block pores.

Porous media can consist of three phases: solid media, water phase, and air phase. Because microbes are suspended in water phase, transport may occur only within water

phase or at water interfaces (i.e. air-water interface, solid-water interface). For saturated porous media, solid-water interface is the only adsorption site. Air-water interfaces and triple-phase boundaries are more effective microbial adsorption sites if porous media are unsaturated.

1.3.2. Microbial adsorption at solid-water interface

According to the size of microbes and accompanying particles (manure, organic matter, colloids, sand or clay) in water, caking, straining and filtration (adsorption) have been proposed as the main mechanisms for the removal of microbes. A surface cake is the collection and aggregation of particulates and associated microbes above the media surface. Straining tends to be insignificant when the size of microbes (or clump) is < 5% of average grain diameter (Ginn, Wood *et al.* 2002). Straining is mainly a mechanical and geometric process, while adsorption (filtration) is a physicochemical and biological process, which involves the van der Waals force, the electrostatic diffusing double layer effect, and development of extracellular polysaccharides.

Ginn *et al.* (2002) also gave a comprehensive description of processes in microbial transport in subsurfaces, and definitions of straining and filtration according to the soil pore capture mechanism were reviewed and summarized. Straining was defined as when 'a colloidal particle is physically larger than a pore or pore restriction it is attempting to pass through'. There are two types of filtration: mechanical filtration of large particles in matrix (which again is straining as defined above) and physicochemical filtration of small particles through molecular forces (which may be more properly regarded as adsorption).

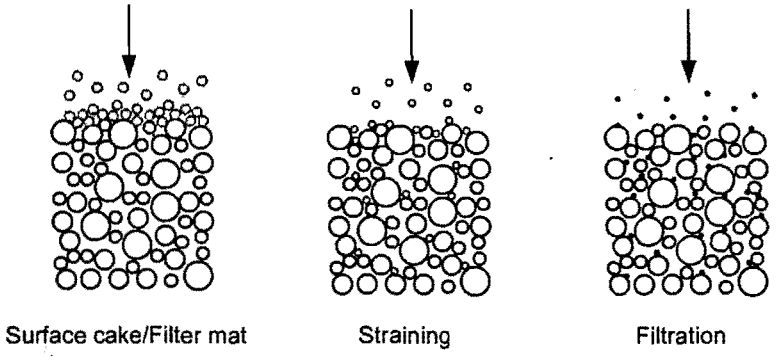

Figure 4. Surface caking, straining, and physicochemical filtration (adsorption) mechanisms for particle transport in the subsurface (McDowell-Boyer, Hunt *et al.* 1986).

A detailed review of microbial adhesion was completed by Hermansson (1999) in terms of the Derjaguin-Landau-Verwey-Overbeek (DLVO) theory of colloid stability. Because the traditional DLVO theory can only explain the total effects of the van der Waals force and diffusive electric double layer force, an extended DLVO theory was developed to include acid/base force (cell hydrophobicity) and extracellular polymer bridging effects (Hermansson 1999; Jin and Flury 2002). However, the DLVO theory (including 'classical' and extended theory) is usually used as a qualitative approach for microbial adsorption, though sometimes being employed to calculate adsorption free energy changes and to predict the probability of attachment.

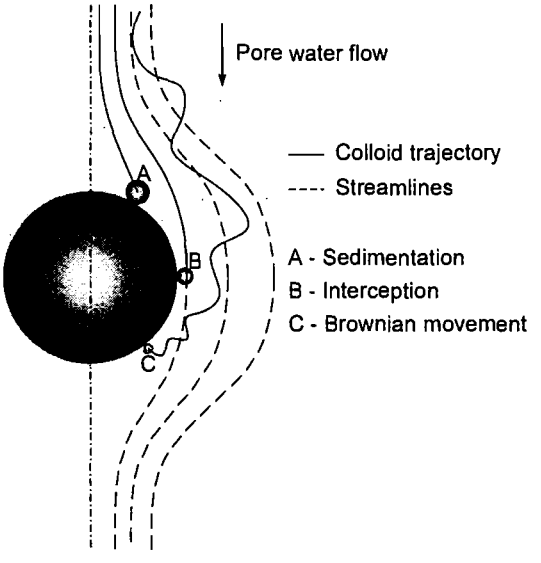

Figure 5. Sketch of particle collision and capture mechanisms(McDowell-Boyer, Hunt *et al.* 1986; Yao, Habibian *et al.* 1971).

The attachment of microbes to particle surface involves two processes: mass transport to the surface and interactions between the microbes and phase interfaces. Colloid filtration theory is usually employed to describe the microbe-SWI interactions (adsorption) (Bouwer and Rittmann 1992; Harvey and Garabedian 1991; Hermansson 1999; Schijven and Hassanizadeh 2000). The opportunity for and frequency of the transported particles to collide with immobilized soil particles is usually expressed as collector efficiency η; while the percentage of the microbes that finally attached to particles is indicated by collision (sticking) efficiency α, which is a process explained by the DLVO theory stated above.

The desorption of microbes from SWI is determined by the hydrodynamic shear force and attachment strength. Higher water flow velocity can remobilize attached microbes into the flowing water. Also, a change of water pH, ionic strength could result in detachment of adsorbed microbes (Banks, Yu *et al.* 2003; Fontes, Mills *et al.* 1991; Li and Logan 1999; Mills, Herman *et al.* 1994; Saiers and Lenhart 2003; Yee, Fein *et al.* 2000). Transient captured microbes can shift to an irreversible attached state by the formation of extracellular polymers (Ginn, Wood *et al.* 2002).

Small pores and pore throats are crucial for the retention of microbes by enhancement of adsorption and straining. A porous medium with more small pores also provides more opportunities for sorption to occur between cells and solid particulates, because of longer contact time and shorter distance between buoyant microbes and phase interfaces (McGechan 2002; McGechan and Lewis 2002). Thus, microbes transported by water flow through the smaller and more tortuous pores are greatly retained.

Cell properties, including geometric size and shape, presence of flagella or capsules, hydrophobicity and zeta potential (net surface charge) have been studied for their effects on bacterial transport and retention. Because microbial transport mainly depends on water flow, cell properties are usually related to their adsorption behavior. A brief review of effects of cell properties on microbial adsorption is given below.

Cell shape (defined as the ratio of cell width to cell length) was reported to affect bacterial transport through clean quartz sand columns (Weiss, Mills *et al.* 1995). It was shown that short rods with low contact angles underwent the greatest decreases in cell length after passing through a soil column. Dong *et al.* (2000) also reported that shorter cells with larger-diameter displayed a higher recovery of cells in percolate than longer, smaller-diameter cells. A recent study showed that bacterial cell wall type (Gram +/–) and shape (rod or coccus) showed minor effects on breakthrough through laboratory column packed with glass beads (Becker, Collins *et al.* 2004). In this paper, cell motility was showed to increase the adsorption rate and decrease desorption rate. In contrast, other researchers found that bacterial motility facilitates transport of microbes because nonmotile bacteria needed longer time to detach from sediment grains (McCaulou and Bales 1995).

It has also been found that high hydrophobicity values of cell surface were always

associated with enhanced attachment to the mineral particles for eight different strains including *Salmonella typhimurium*, *Enterococcus faecalis*, *Enterococcus faecium*, *Escherichia coli*, *Citrobacter freundii*, *Shigella sonnei*, and *Shigella boydii* (Stenstrom 1989). Similar results were observed for sixteen strains of bacteria (including six strains of *Pseudomonas*, two strains of *Escherichia*, four strains of *Arthrobacter*, *Micrococcus*, *Acinetobacter*, *Thiobacillus*, *Alcaligenes*, *Bacillus*, *Agrobacterium*, *Corynebacter*, *Azotobacter*, *Rhizobium* and *Mycobacter*) that attached to sulfated polystyrene (Loosdrecht, Lyklema *et al.* 1987). In contrast, one report indicated that bacterial transport was not correlated to hydrophobicity, net surface charges, and presence of capsules, but retention was statistically related to cell size (Gannon, Manilal *et al.* 1991). Recently, more concerns have been given to subpopulations of mono-colony bacteria, i.e. intrapopulation variability (Bolster, Mills *et al.* 2000; Mailloux, Fuller *et al.* 2003; Silliman, Fletcher *et al.* 2001).

Usually, microbial attachment to particle surfaces was assumed to be independent of each other, i.e. further attachment had the same kinetics as the initial attachment. This was based on the fact that microbes only occupy a very small percent of the total surface area of particles. However, increased (ripening) or decreased attachment (blocking) was observed when porous media exchange sites were saturated (Camesano, Unice *et al.* 1999; Rijnaarts, Norde *et al.* 1996).

Permanent adsorption and forming of a biofilm will change the hydraulic properties of porous media, i.e. permeability and conductivity (Dunsmore, Bass *et al.* 2004). In a physical sense, the size of pore throat is decreased by microbial attachment, and this facilitates further capture of free buoyant microbes. Also, the surface properties of particles and the adsorption process will be very different from adsorption onto initially clean surfaces.

1.3.3. Microbial adsorption at air-water interface

Unsaturated porous media have been reported to effectively remove viruses, bacteria, and colloids during unsaturated transport (Lance and Gerba 1984; Lenhart and Saiers 2002; Tan, Bond *et al.* 1992). Though some researchers suggest that the stagnant water in unsaturated media could exclude some favorable adsorption sites on SWI from colloids, it was generally found that unsaturated flow had high potential to trap and remove microbes

from water (Chu, Jin *et al.* 2003; Chu, Jin *et al.* 2001; Germann and Alaoui 2002; Keller and Sirivithayapakorn 2004; Lenhart and Saiers 2002; Schafer, Ustohal *et al.* 1998; Shein, Polyanskaya *et al.* 2002; Wan and Tokunaga 1997; Wan, Wilson *et al.* 1994). Powelson and Mills (2001) also reported that constant unsaturated water flow in a sand column resulted in higher removal of *E. coli* than saturated and changing unsaturated (with cyclic changes of water content) flow.

Several mechanisms have been suggested to explain the increased microbial retention observed in unsaturated compared with saturated systems. Jin *et al.* (2002) presented a detailed discussion of unsaturated virus transport. A general discussion of colloidal and bacterial transport in unsaturated media was presented by Keller *et al.* (2004) and Schafer *et al.* (1998). A short summary of the literature on microbial adsorption at air-water interfaces in unsaturated porous media is given below.

Mechanisms for adsorption of microbes at the AWI are different from the SWI, since the AWI is more dynamic, hydrophobic and possesses a low negative charge (Hermansson 1999). However, factors that have been shown to be important for adsorption at the SWI are also important for adsorption at the AWI, i.e. surface hydrophobicity, cell surface structures, solution ionic strength.

The AWI has been found to have a high affinity for both hydrophobic and hydrophilic microbes (Wan and Wilson 1994; Wan, Wilson *et al.* 1994), although hydrophobic microbes were found to be more reactive than hydrophilic microbes in adsorption both to solid-water and air-water interface (Corapcioglu and Choi 1996; Wan, Wilson *et al.* 1994). Adsorption of microbes to the AWI was usually shown to be irreversible because of the strong capillary force. In addition, the triple phase boundary of air, water, solid (TPB) was thought to be a favorable adsorption site for microbes (Powelson and Mills 2001; Thompson, Flury *et al.* 1998; Thompson and Yates 1999). In addition to enhanced adsorption to AWI, SWI, and TPB, film straining (microbes was trapped in thin water films surrounding particles) was suggested as another mechanism for the high retention capability of unsaturated porous media (Wan and Tokunaga 1997).

Although higher microbial retention and removal was related to lower water content, it is only valid in unsaturated porous media with a relatively stable water content. It has been observed that colloids retained at SWI and thin water films were released into the water

due to increasing water content (El-Farhan, Denovio *et al.* 2000). For a natural vadose zone under transient flow conditions caused by precipitation or application of effluents, microbes trapped at the AWI could be remobilized and this may result in high recovery in the outflow water. Also, the air phase (entrapped air bubbles in unsaturated media) could be mobilized or dissolved during rewetting in the event of dramatic change of water flow conditions (Sirivithayapakorn and Keller 2003).

1.3.4. Conclusions

In brief, for short-term microbial transport, without considering die-off and regrowth, the dominant factor for the removal of microbes from flowing water in porous media is adsorption at phase interfaces, namely SWI under saturated conditions, together with AWI, TPB for unsaturated microbial transport.

1.4. Modeling microbial transport in porous media

To model microbial transport, either a thorough understanding of the theoretical processes needs to be known, or large experimental and field data sets must be available for empirical models. Mechanistic models based on factors influencing microbial transport have been used widely, and most of these models were developed by improving the traditional convection-dispersion equation.

The most popular model is an advection-dispersion equation that includes microbial attachment to and detachment from phase interfaces (Bengtsson and Ekere 2001; Bolster, Mills *et al.* 2000; Grolimund, Elimelech *et al.* 1998; Scheibe and Wood 2003; Zhang, Johnson *et al.* 2001a; Zhang, Johnson *et al.* 2001b). Usually, the bacterial attachment/detachment processes are represented by equilibrium or first-order kinetic reaction terms. This model can be used to simulate microbial transport well, especially with respect to the phenomenon of size exclusion and the relatively faster average transport velocity. The general microbial transport model for a one-dimensional flow system in homogeneous porous media is expressed as follows:

$$\frac{\rho_b \partial s}{\partial t} + \frac{\theta \partial c}{\partial t} = -\frac{\partial J}{\partial x} - R_d + R_g \qquad (3)$$

Where c is the bacterial concentration in soil water (cfu cm^{-3}), x is the longitudinal

distance from the point of inlet (cm), s is the concentration of bacteria reversibly attached to soil grains (cfu g^{-1}), ρ_b is the soil bulk density (g cm^{-3}) and θ is the volumetric water content, J is the microbial flux density in the direction of flow (the number of microbes passing through a unit cross-sectional area per unit time, cfu cm^{-2} min^{-1}); R_d and R_g are the rates of decay and regrowth (number of microbes per unit volume of porous media per unit time, cfu cm^{-3} min^{-1}), respectively. The total flux of microbes is equal to the sum of the fluxes resulting from advective transport by water, random active movement (bacterial motility), diffusion, hydrodynamic dispersion, sedimentation, and chemotaxis:

$$J = -\theta D(\frac{\partial c}{\partial x}) + \theta(v + v_g + v_x)c \tag{4}$$

Where, v is interstitial water velocity (cm min^{-1}); v_g and v_x denote the sedimentation and chemotactic velocity of bacteria (cm min^{-1}). The dispersion coefficient D (cm^2 min^{-1}) accounts for random active movement, diffusion, and hydrodynamic dispersion. Sedimentation of bacteria is negligible due to the close approximation of the cell density to that of water, especially in absence of cell flocculation (Smith, Thomas *et al.* 1985). Besides, chemotaxis is not significant in the natural or engineering porous media without a macroscopic substrate concentration gradient. Thus, (4) is simplified to

$$J = -\theta D(\frac{\partial c}{\partial x}) + \theta vc \tag{5}$$

For conditions in which microbial growth and decay are limited (e.g. at low temperature), R_d and R_g may be neglected in (3). Substitution of (5) into (3), and omitting microbial die-off and regrowth yields

$$\frac{\rho_b}{\theta}\frac{\partial s}{\partial t} + \frac{\partial c}{\partial t} = D\frac{\partial^2 c}{\partial x^2} - v\frac{\partial c}{\partial x} \tag{6}$$

If the one-site first order kinetic model is employed to describe the microbial adsorption and desorption process in porous media, the governing partial differential equation is

$$\frac{\partial c}{\partial t} = D\frac{\partial^2 c}{\partial x^2} - v\frac{\partial c}{\partial x} - K_f c + \frac{\rho_b}{\theta}K_r S_r \tag{7}$$

$$\frac{\rho_b}{\theta}\frac{\partial s}{\partial t} = K_f c - \frac{\rho_b}{\theta} K_r s \tag{8}$$

Where K_f is the attachment coefficient (min^{-1}), and K_r is the detachment coefficient (min^{-1}). This model is common in bacterial transport modeling and has been proved to be very effective in demonstrating the breakthrough patterns. Many additions have been made to this model to include more factors, e.g. dual soil porosity, or dual bacterial sticking efficiency. These models have been tested and resulted in more accurate predictions.

1.5. Potential applications

The study of microbial transport in soils is of ongoing and considerable interest in soil science, and has been studied extensively in microbiology, soil physics, hydrology and epidemiology. This is not only because of its various applications and environmental implications, but also because it represents an intellectual challenge.

The research into bacterial transport in porous media was originally stimulated by concerns of waterborne bacterial diseases arising from the use of polluted groundwater. Animal wastes (manure, slurry and occasionally urine) or human septic wastes contain large numbers of different pathogens, such as *E. coli* O157:H7, *Campylobacter* spp., *Giardia* spp., *Cryptosporidium* spp., rotaviruses etc (Gerba and Smith 2005; Unc and Goss 2004). After application of animal wastes onto farmland, a large number of pathogens may be transported through the vadose zone in soils by infiltration water, and might cause pollution of groundwater. Therefore, the protection of public health and prevention of pathogen transport to water resources has highlighted the study of microbial transport in porous media (Morris and Foster 2000). Recently, it has also become important in the bioremediation of contaminated aquifers, including bioaugmentation, biostimulation, and natural attenuation. The applications of this research topic include the following.

1.5.1. Contamination of water by pathogens

Pathogen transport in soil and the subsequent contamination of underground or surface water resources can lead to microbiological problems with organic waste disposal

(Edmonds 1976; Gerba 1985; Morris and Foster 2000; Reddy, Khaleel *et al.* 1981; Unc and Goss 2003; Unc and Goss 2004). Especially in agricultural areas, where large amounts of animal manures or effluents are applied rather than chemical fertilizers, the potential contamination poses a threat to the potability and use of water resources (Huysman and Verstraete 1993a; Huysman and Verstraete 1993b). After pathogens are released into the environment, such as by waste application, they are partitioned into and transported by surface runoff or infiltrating water, which may lead to contamination of surface and/or subsurface water. Many tragic events in the history of public health involve pathogen contamination of drinking water following the transport of pathogens through various distances in soils. Such tragedies happen even under the current best management practices for waste disposal and protection of water resources, e.g. the Walkerton (Ontario, Canada) tragedy of May 2000 (Unc and Goss 2004).

Pathogens released into soils through septic tank effluent (Bitton and Harvey 1992), sewage irrigation (Wallach 1994) have been demonstrated to travel rather long distances under various soil conditions, especially following heavy rainfall (Hagedorn, Hansen *et al.* 1978). The results of the microbial transport in soils are the contamination and degradation of surface or subsurface water resources, and potential spreading of epidemics. The understanding of microbial transport patterns is useful for the planning, design, installation, and management of septic tanks, and biological wastewater treatment units such as sand filter beds and drainage outlets. Thus, this type of study is increasingly important nowadays for environmental and health issues, such as the release and transport of pathogenic microorganisms by agricultural activities involving animal wastes as manure or effluent, human waste disposal via septic tank systems and land-applied sludge.

1.5.2. Bioremediation of contaminated subsurface

Soil or groundwater polluted by recalcitrant substances, e.g. petroleum, radionuclides or organic chemicals, can be treated by bioremediation. A variety of microbes have been isolated that can degrade general chemical pollutants such as PAHs (polycyclic aromatic hydrocarbons), BTEX (benzene-toluene-ethylbenzene-xylene) compounds, or NAPLs (non-aqueous-phase liquids) such as petroleum and chlorinated aliphatics or aromatics. Also, biological sorption and reduction of uranium from the hexavalent to the nonsoluble

quadrivalent state has been proved to be an effective way to remediate uranium contaminated natural groundwater and mining wastewater (Finneran, Housewright *et al.* 2002; Liu, Gorby *et al.* 2002; Nelson, Cellan *et al.* 2002; Payne, Gentry *et al.* 2002; Suzuki, Kelly *et al.* 2003). One of the most effective methods to remedy soils contaminated by recalcitrant organic chemicals is to inoculate these sites with specific microbes, which can degrade the polluting compounds. In such a case, the transport and spatial distribution of the inoculated bacteria in the soil profile are at the very core of the *in situ* bioremediation. Data needed to predict bacterial transport in the field is rare.

In the case of *in situ* bioremediation, microbial transport in soils is critical in intrinsic bioremediation (natural attenuation), biostimulation (by the addition of water, oxygen, organic substrates, electron donors, etc. into the contaminated subsurface), and bioaugmentation (by the introduction of specific microbial cells able to degrade the contaminants) (Ginn 2002; Ginn, Wood *et al.* 2002). In practice, how and to what depth the amended microbes move downward through the soil profile is crucial for the success of a bioremediation project (Benyahia 2000; Pierzynski 2000). *In situ* bioremediation that is operated at the contamination site generally requires a high soil porosity and water content for the easy transport and biological activities of the cleanup microbes (Chapelle 1999). Many bioremediation projects have demonstrated the difficulty in controlling and monitoring the movement of specified bacteria in the soil profile.

1.5.3. Other agronomic applications

Other agronomic applications include research into genetically engineered microbes (GEMs). GEMs are inoculated into soil for the prevention of some plant diseases or to act as biocontrol agents and plant growth promoters (e.g. by nitrogen fixation) (Huysman and Verstraete 1993a; Huysman and Verstraete 1993b). The macropores created by plant root channels play an important role in such applications. Soil management and irrigation have been employed to optimize the movement of applied microbes.

Care must be taken with the deliberate release of GEMs into natural environments and its impact on ecosystems. Many GEMs may transfer small parts of their genomes to other biota in the environment and might be incorporated into intrinsic microbes. The measurement of the fate, transport, and distribution of released GEMs in soils is an important facet of many biotechnological research projects.

Chapter Two
Research Analysis and Objectives

2.1. Research analysis

2.1.1. Summary of literature review

Bacterial transport through the unsaturated and/or saturated subsurface might pose contamination problems when land disposal is adopted to treat animal manure, effluents, or biosolids from domestic wastewater treatment plants. The properties of both the bacteria and the porous media (soil, gravel aquifer, sand) were suggested as influential factors during bacterial transport.

From the literature review in chapter I, it is clear that bacterial migration through porous media mainly depends on water flow, and bacterial retention is mainly determined by bacterial adsorption at phase interfaces. For long term bacterial transport, die-off and regrowth probably contribute to the final outcome. Water flow is also closely related to pore size distribution and water content in porous media. Bacterial adsorption at SWI is a result of interactions between cells and particle surfaces, and is mainly related to surface area and chemical composition of particles. However, attached cells at AWI can be detached by chemical perturbation or shearing force of water flow. In contrast, bacterial adsorption at AWI is usually irreversible.

To date, much research has been focused in the area of saturated flow conditions, with increasing interest in unsaturated flow. Mechanisms for bacterial transport have been explored in both macroscopic and microscopic scales. Mechanistic models have been developed and implemented to simulate bacterial transport and retention in porous media.

2.1.2. Previous experiments

Previous research at Lincoln University about the effects of land disposal of oxidation pond effluent on groundwater microbial contamination have shown that indicator

microorganisms only appeared in groundwater following heavy rainfall and flood irrigation events (Martin and Noonan 1977). Also, it has been shown that spray irrigation at Lincoln University's new dairy farm (established in 2001) has had little or no impact on the level of microbial contamination of groundwater in the first three years of operation.

These two experiments suggest the importance of water flow on bacterial transport in soils. However, soil properties such as moisture characteristics and pore size distribution are not available to help explain the observations. These properties are directly related to water flow in soils. Besides, no tests were done to measure bacterial adsorption to soils. This makes the explanation more difficult. However, these experiments and observations encouraged us to explore factors related to soil water flow and bacterial adsorption.

2.1.3. Conclusions

The literature review and previous experiments suggest that bacterial contamination (if it occurs) will only emerge with flood irrigation and heavy precipitation. Water flow is thus one of the most important factors which control bacterial transport behaviour. Considering that water flow is directly related to pore size distribution (especially macropores) and initial water content of soils before water input, the effects of pore space properties and water content (determined by matric suction) were selected as the parameters for our experimental designs.

Compared with a conservative chemical tracer, such as bromide, bacteria are usually heavily reduced when transported through porous media. If decay or die-off of microbes is excluded (such as when persistent cells are used, and at a well-controlled environmental temperature), this reduction can be attributed to a combination of: irreversible adsorption at solid-water interfaces (SWI); adsorption at air-water interfaces (AWI) when an immobile air phase is formed in the subsurface; and physical straining by interstices smaller than bacteria.

Therefore, adsorption of bacteria was thought to be the key factor to retain bacteria passing through porous media. In this thesis, bacterial retention by means of attachment was studied by exploring the effects of adsorption to particle surfaces and air-water interfaces.

2.2. Objectives and methods

Based on the fact that bacterial transport and retention are controlled by water flow and bacterial adsorption respectively, the objectives of this thesis were to explore the relative significance of factors related to water flow and bacterial adsorption. In addition, one of the objectives was to develop mechanistic models which can be applied to experimental data to simulate and predict bacterial transport.

To fulfil these objectives, laboratory and field experiments using bacterial and bromide transport through both heterogeneous soil and homogeneous silica sands, under both saturated and unsaturated flow conditions, were carried out to gain bacterial breakthrough curves. *Bacillus subtilis* and *E. coli* were employed as tracer microbes in experiments with an outdoor soil lysimeter and indoor sand columns, respectively. The sand column/*E. coli* experiments were conducted in a cold room, while *B. subtilis* is persistent in soils. These two facts reduced die-off as a factor affecting bacterial retention. Retained bacteria were measured by enumerating bacterial concentration in soil and sand cores after the transport experiments. Bacterial adsorption to particle surfaces was determined by batch adsorption experiments. Particle size distribution, pore size distribution, and moisture release characteristics were obtained by tension table or Buchner funnel apparatus.

Mechanistic models including equilibrium adsorption, one-site first-order kinetic adsorption, and two-site kinetic/equilibrium adsorption at SWI were modified by including a term for an irreversible first-order attachment to AWI. These models were used to simulate bacterial and bromide breakthrough curves from the sand column experiments. The capabilities of existing microbial transport models were investigated with regard to our experimental observations. The best modelling approach was determined by comparing the applicability and efficiency of each model when applied to the sand columns experimental data. Based on the evaluation and modification of current models, a practical model (the convection dispersion model supplemented with two-site adsorption at SWI and first-order kinetic irreversible adsorption at AWI) for predicting bacterial transport was also constructed in this thesis.

Chapter Three

Transport and Deposition of *Bacillus subtilis* through an Intact Soil Column

3.1. Introduction

Although many field and laboratory column experiments on bacterial transport have been reported in the literature, most focus on saturated flow. Bacterial transport involves passage through both the unsaturated (or vadose) zone and saturated aquifers. A few researchers have found that retention of bacteria or colloids in porous media is greater under unsaturated than saturated conditions (Germann and Alaoui 2002; Lance and Gerba 1984; Lenhart and Saiers 2002; Schafer, Ustohal *et al.* 1998; Tan, Bond *et al.* 1992). However, bacterial transport through intact soil columns has not been investigated in respect of unsaturated water flow and macropore effects. In unsaturated porous media, high potential of bacterial retention was attributed to adsorption at AWI and film straining. However, experimental evidence to verify the effects of air-water interfaces and film straining is lacking (Jin and Flury 2002). This chapter will investigate effects of unsaturated water flow and macropores on bacterial transport through an intact soil lysimeter.

In recent years, unsaturated transport has gained increasing attention. However, most research has been carried out in sand columns, and so ignores effects of structural heterogeneity. Water flow in intact soils is conducted mainly through bigger pores, especially macropores. Very low suction will empty macropores of water and helps to clarify the effects of macropore flow. To investigate bacterial transport under unsaturated condition in heterogeneous soil, an intact soil column with sandy loam soil was used. The attractive feature of this experiment is the accurately controlled suction by a tension infiltrometer imposed on top of the soil lysimeter. To our knowledge, no similar experiments have been reported.

A previous experiment was carried out at Lincoln University when a tension infiltrometer

was used to enable study of nitrate leaching under controlled suctions (Silva 1999). That experiment selected 0.5 kPa and 0 kPa as the suctions to study the influence of macropore flow on nitrate leaching and bacterial movement. Bacterial concentration and the volume of leachate were monitored for about three months. It was showed that application of 0.5 kPa suction onto the soil column decreased the number and concentration of percolated *B. subtilis* endospores, compared to those at 0 kPa suction. To enable a direct comparison, we employed the same suctions, bacteria, soil type, and a lysimeter of the same size with that project for this thesis.

The objectives of the study were to (a) investigate the effects of soil matric suction (hence degree of saturation) on water flow and the concurrent bacterial and chemical tracer transport in intact soils, (b) determine the effect of macropore in undisturbed soils on bacterial transport and retention, and (c) provide a framework and experimental methods for subsequent research into modeling bacterial transport in intact soils and sand columns.

3.2. Materials and Methods

3.2.1. Bacteria and culture preparation

B. subtilis endospores were chosen as the tracer because they persist in natural environments such as soil and water, so die-off does not need to be taken into account (Slepecky and Hemphill 1992). *B. subtilis* forms orange colonies on tryptone glucose agar, which helps to distinguish it from other soil bacteria. The selected strain was rifampicin-resistant and was prepared according to Houston *et al.* (1989), and was thus distinguished from natural *B. subtilis* in soils. This strain was used at both suctions (0.5 kPa and 0 kPa) because of its low detection-limit and easy plate counting.

To prepare the endospore suspension for the 0.5 kPa unsaturated experiment, 3.3 mL of stock bacterial suspension was sonicated for 1 min and then heat-treated in a water bath at 80 °C for 10 minutes. Sonication was shown to be effective in breaking cell clumps caused by long-term storage (data not shown). The sonicated suspension and 4.4 g sodium bromide were added to 2.2 L of sterilized water. The diluted suspension was shaken vigorously and 2 × 1 mL samples were added to 9 mL 0.1% peptone water. Another 200 mL sub-sample was taken and stored in a freezer for later analysis. The remaining 2 L suspension (3.65×10^5 cells/ml, 2000 mg/L Br^-) was irrigated uniformly onto the soil

surface using a 2 L garden sprayer with an adjustable nozzle. The saturated leaching experiment used the same procedure to make up suspension of different concentration, i.e. 4.35×10^4 cells/ml, 4000 mg/L Br^-. The unintended different cell concentration used for 0 and 0.5 kPa suctions may have been caused by the change of bacteria with time in stock. This difference was circumvented by employing normalized concentration in data analysis.

3.2.2. Soil column experimental setup

The soil column was a lysimeter with 50 cm diameter and 70 cm depth, installed outdoors at Lincoln University, Canterbury, New Zealand. The soil was a free draining Templeton fine sandy loam (Udic-Ustochrept, coarse loamy, mixed, mesic) (Silva 1999). Texture changed from fine sandy loam in the A horizon into sandy loam in the subsoil. Details of the lysimeter collection and tension infiltrometer are described in Cameron *et al.* (1992) and Silva *et al.* (2000).

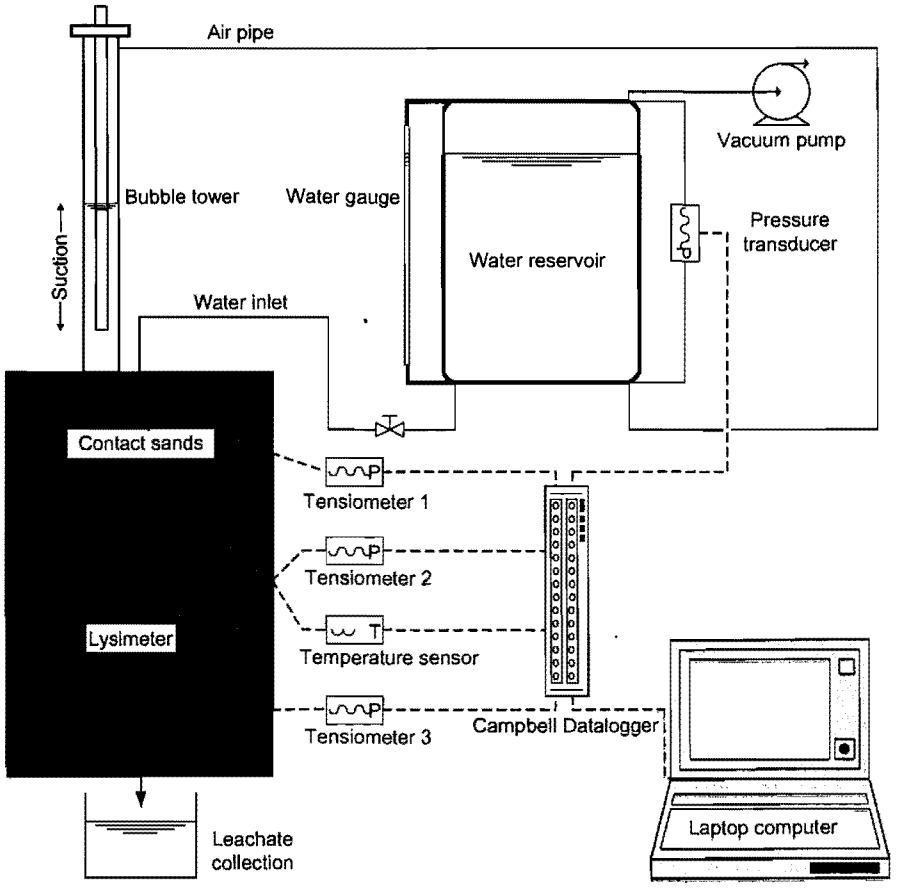

Figure 6. Schematic of the lysimeter experimental apparatus.

Figure 6 is a schematic diagram of the column setup. A temperature probe (LM35CZ, National Semiconductor), three pressure transducers (170 PC, Micro Switch) attached to three tensiometers (Fabricated from Soil Moisture Equipment Corp Ceramic Cups - Part 652X07B1M03), a pressure transducer (SCX01DNC, Sensym Co.), and a datalogger (CR10, Campbell Scientific Instruments) were calibrated in the laboratory. The temperature probe was inserted horizontally at 30 cm depth. The tensiometers were installed at 15, 30, and 60 cm depths, with 20° downward angle. A pressure transducer in the infiltrometer 200 L reservoir was used to record the infiltration rate.

3.2.3. Assay methods and procedures

Effluent samples collected during the leaching period were stored at –20 °C before analysis. Previous work had shown that freezing did not change endospore numbers (Data not shown). Samples were thawed at ambient temperature. About 20 mL subsample of each effluent sample was transferred to 30 mL vials for bromide analysis. *B. subtilis* endospores were enumerated by membrane filtration technique and plate counting. The culturing medium used was rifampicin supplemented tryptone-glucose-agar (TGA) medium (1% tryptone, 0.5% glucose, 1.5% agar, 5 μg/ml rifampicin). Bromide in the effluent was analyzed using a Dionex DX–120 Ion Exchange Chromatograph fitted with a Dionex AS 50 Autosampler and integrated by Chromeleon Peaknet 6.0.

To enumerate deposited endospores in soil, tetrasodium pyrophosphate ($Na_4P_2O_7 \cdot 10H_2O$) was added to 125 mL flasks as a soil dispersing agent to a final concentration of 0.18% (Lorch, Benckieser *et al.* 1995; Sylvia, Fuhrmann *et al.* 1998). A 10 g soil sample and 95 mL sterilized water were added into the flasks, which were shaken for 15 min in a horizontal rotary shaker at 200 rpm, and then settled for 15 min. After heat-treating flasks at 80 °C in a water bath for 25 min, serial dilution and plate counting with TGA medium were carried out. A subsample of each soil core was dried in a forced air-circulating oven at 70 °C to constant weight.

3.2.4. Column experiments

The tension infiltrometer's 200 L water reservoir (**Figure 6**) was filled with water, leaving a small volume on the top for air circulation. Grass in the lysimeter was trimmed to ground level without disturbing the soil. A polyester cloth (Just Screen, NZ) of 20 μm

mesh was laid on the surface of the lysimeter. Silica sand (Industrial Sands Ltd., NZ) of particle size 75-297 μm was poured on top of the polyester cloth to a thickness of about 10-15 mm, and was flattened for maximum contact with the infiltrometer disk.

The infiltrometer disk was immersed in a water bath to eliminate air from inside the disk. The air inlet pipe was used as a manometer to adjust the bubble tower, which maintained the suction (0.5 kPa) for unsaturated flow. A vacuum pump was connected to the water reservoir and maintained constant negative water pressure (suction) in the reservoir, bubble tower and soil lysimeter. The water-filled infiltrometer disk was installed on top of the contact sand. The lysimeter was allowed to reach stable water potentials under 0.5 kPa suction for two weeks.

Once the lysimeter reached stable condition, the polyester cloth and contact sand were removed from the top of the lysimeter. 2.0 L of water containing 7.29×10^8 *B. subtilis* endospores and 4.0 g sodium bromide were sprayed onto the soil surface. Then, the polyester cloth and sand were replaced, and the infiltrometer disk was reinstalled with 0.5 kPa suction. The leachate collection interval ranged from 30 min at the beginning to 12h near the end of leaching.

After the unsaturated leaching experiment, the suction of the infiltrometer was adjusted to 0 kPa, enabling saturated flow in the lysimeter. Then, the lysimeter was flushed with free-flowing water for 2 weeks, which also diminished the effluent concentration of *B. subtilis* and Br^- to negligible constant levels. *B. subtilis* and bromide reached *c.* 10 cfu/mL and 5 mg/L respectively at the end of the equilibration. Then, saturated leaching followed a pulse application of 8.7×10^7 *B. subtilis* and 8.0 g sodium bromide in 2 L sterilized water was continued for one week.

After completion of the saturated leaching, nine vertically drilled soil core samples were taken with a 5 cm inner-diameter hollow auger to 60 cm depth (**Figure 7**). These cores were divided into 5 cm long sections for analysis of deposited bacteria down the column. Cylindrical soil samples were collected in sterile bags and stored at 0 °C.

For measurements of soil properties, cores were taken from the same field site as the lysimeter soil. The total soil porosity was calculated from particle density and bulk density. Particle density, bulk density, and water content were measured according to the

methods by Dane and Topp (2002). Pore size distribution was measured with tension table and pressure chamber apparatus for low-suction and higher-suction ranges (Hillel 1998).

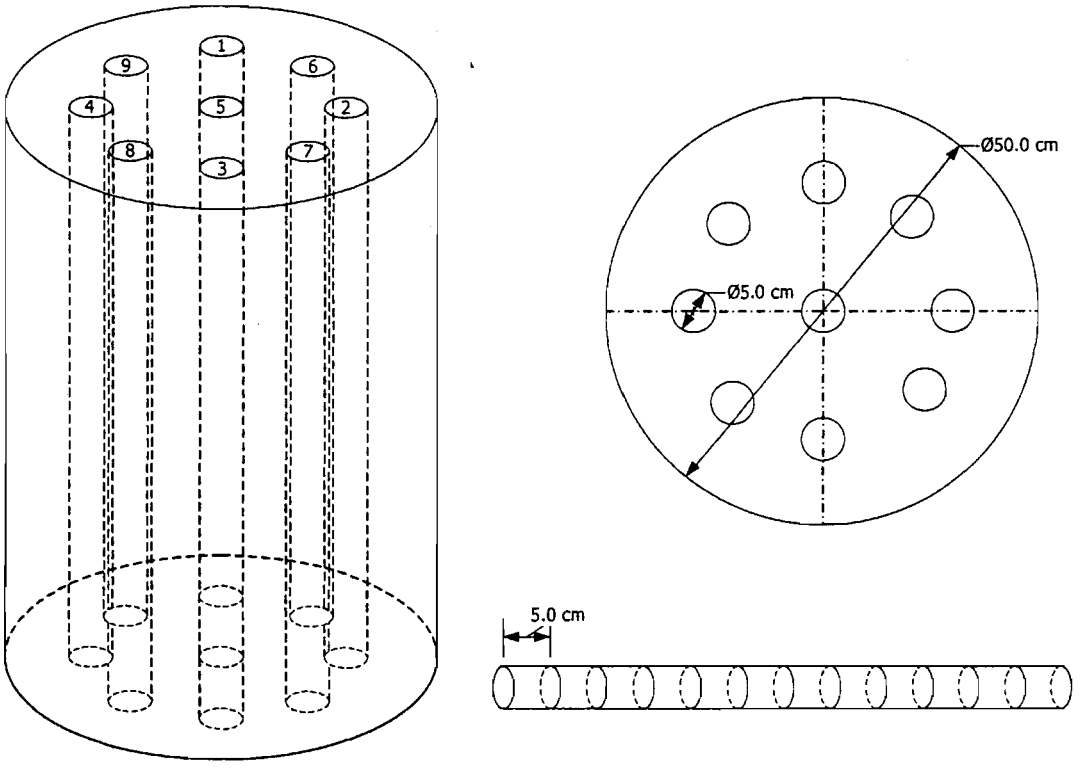

Figure 7. Sampling scheme for drilling of soil cores.

3.3. Results

3.3.1. Soil porosity and pore size distribution

Figure 8 and **Figure 9** shows total porosity, water content θ_v at 0.5 kPa suction and pore size distribution versus column depth. **Figure 8** shows that 0.5 kPa suction significantly decreased water-filled porosity within the soil column, and average soil column water content dropped from 0.45 to 0.43. The reduction of θ_v induced by suction was mainly at depths <30 cm, because below 30 cm, most soil pores had a diameter <600 μm corresponding to 0.5 kPa suction (see **Figure 9**).

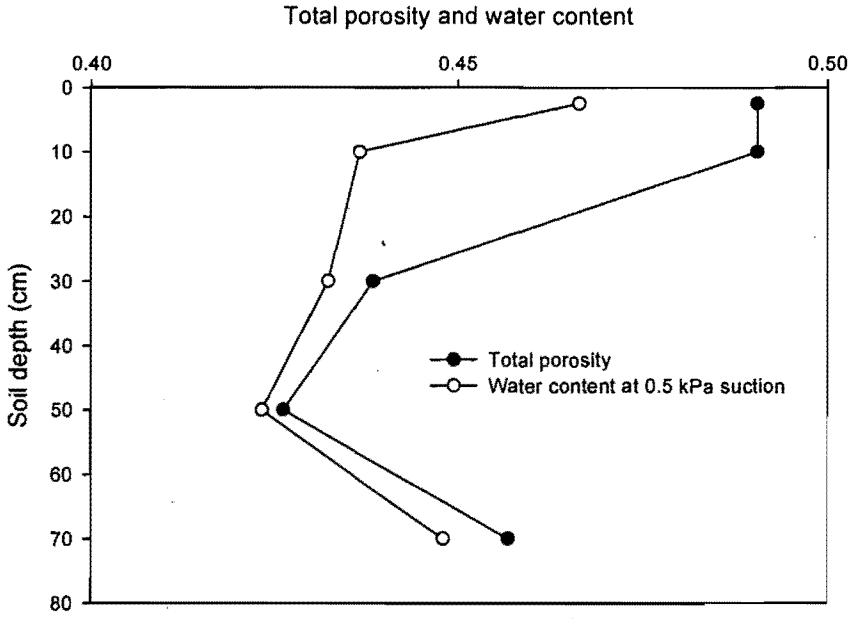

Figure 8. Total porosity and soil water content at 0.5 kPa suction.

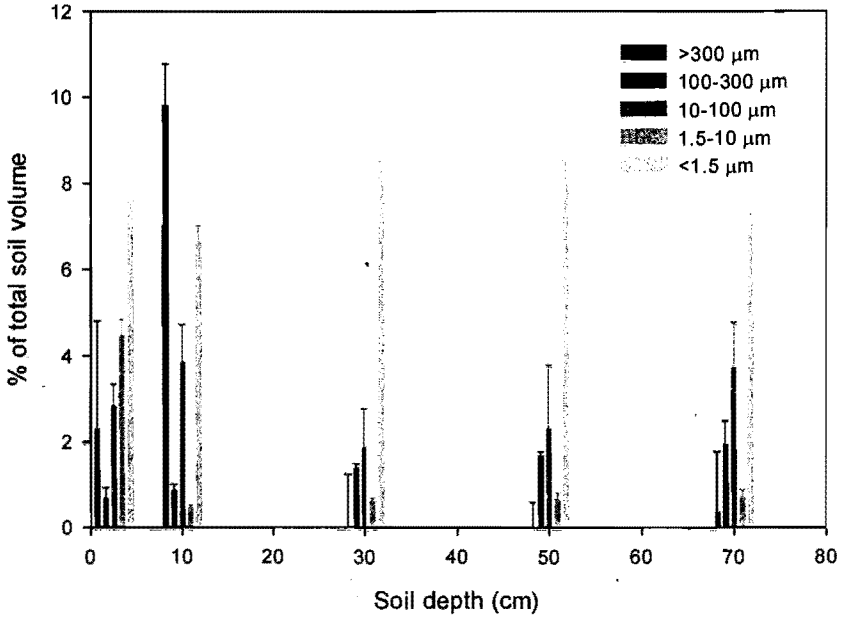

Figure 9. Soil pore size distribution at depths of 2.5, 10, 30, 50 and 70 cm.

Pores with diameter >300 μm were mainly distributed in the top 20 cm of the column and a small portion (0.36%) at depth of around 70 cm. Thus, the 0.5 kPa suction substantially reduced θ_v in the top column section, with relatively slight influence on the middle and

bottom sections. Despite few macropores at depths from 20 to 60 cm, a large variance of the pore diameters suggested possible existence of preferential flow pathways along the soil column. Also, the dense and uniform existence of pores <1.5 μm at all depths indicated a good retention ability for infiltrated bacteria.

3.3.2. Soil water suctions, effluent rate and temperature

Figure 10 shows soil matric potentials (Ψ_m) at depths of 15, 30 and 60 cm. At 0.5 kPa suction, the average values at 15 and 30 cm were –1.6 and –2.3 kPa, about 1.1 and 1.8 kPa lower than the imposed surface potential. However, Ψ_m at 60 cm was –0.35 kPa, higher than the surface applied potential. This Ψ_m distribution reflected the soil heterogeneity, seen in **Figure 8** and **Figure 9**. While vertical flow rate must be uniform, the hydraulic conductivity is not uniform with depth, and therefore matric potential will vary in a heterogeneous soil. The increase of matric potential near the column bottom was caused by the effluent collection pipe, equivalent to a water table at the bottom. Error bars show that Ψ_m was stable at 60 cm depth.

At 0 kPa suction, the column reached saturated or near-saturated flow condition and the average matric potentials were –1, –1.4, 0.03 kPa for depths of 15, 30 and 60 cm, respectively. Ψ_m at 60 cm was a little higher than 0 kPa, suggesting water perching at the bottom. There was an abrupt rise of Ψ_m for the last two days of the 0 kPa experiment (**Figure 10**), caused by the adjustment and purging of air bubbles from the infiltrometer disk.

The column outflow rate at 0 kPa averaged 3.98×10^{-6} m/s, higher than 6.95×10^{-7} m/s at 0.5 kPa by a factor of 5.7. It took 10 days to produce 1 pore volume of leachate under 0.5 kPa-suction, but only *c.* 2 days at 0 kPa suction. The flow rates at both suctions decreased gradually over the experimental period (**Figure 11**), although the 0 kPa flow rate decreased much faster than at 0.5 kPa suction. This probably resulted from the blocking of pores by colloids transported through the column. The decrease of soil temperature might be another contributing factor, as discussed below.

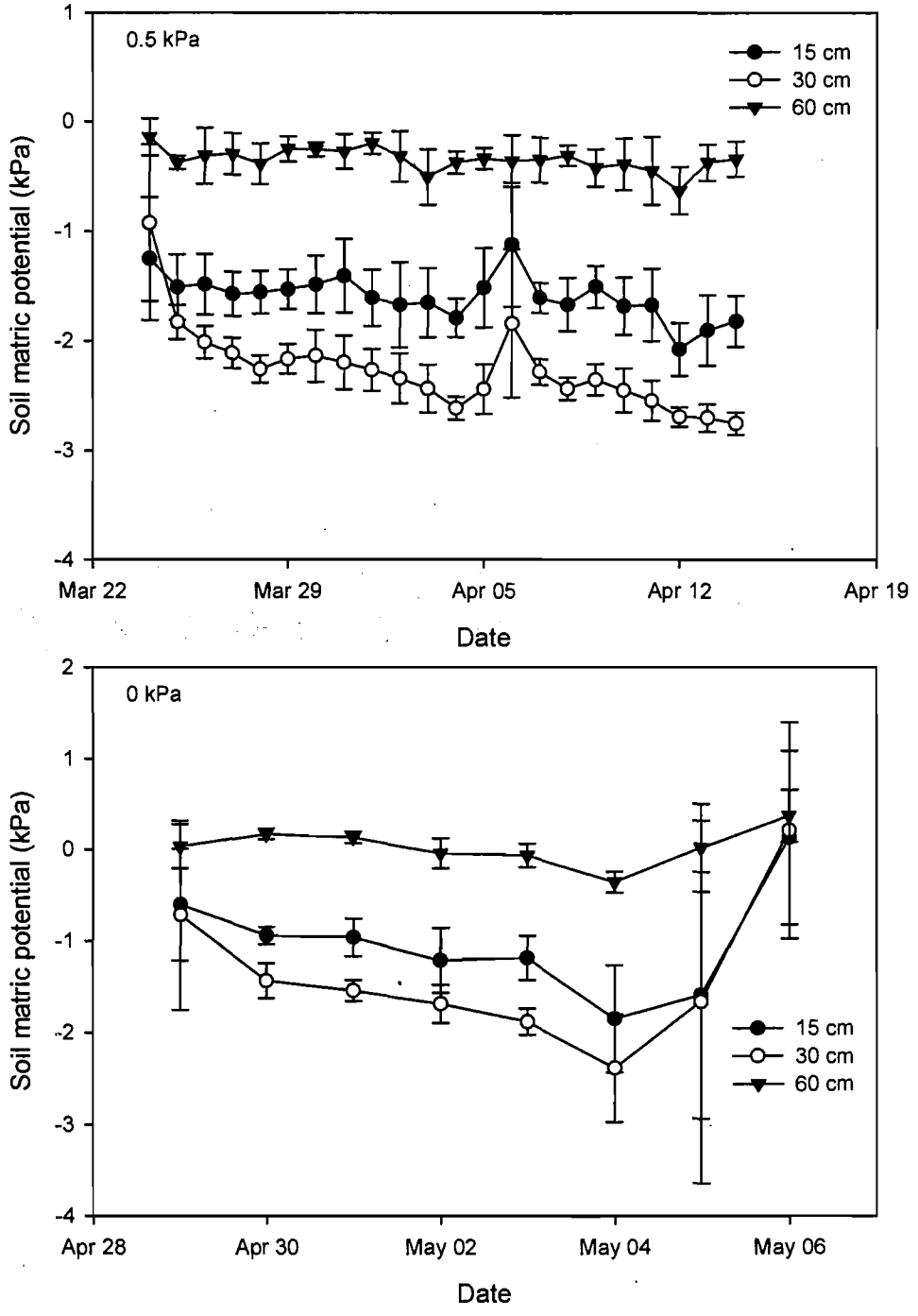

Figure 10. Soil matric potentials at different depths under 0.5 kPa and 0 kPa suctions. Error bars in the plots indicate standard deviation of 24 hours data.

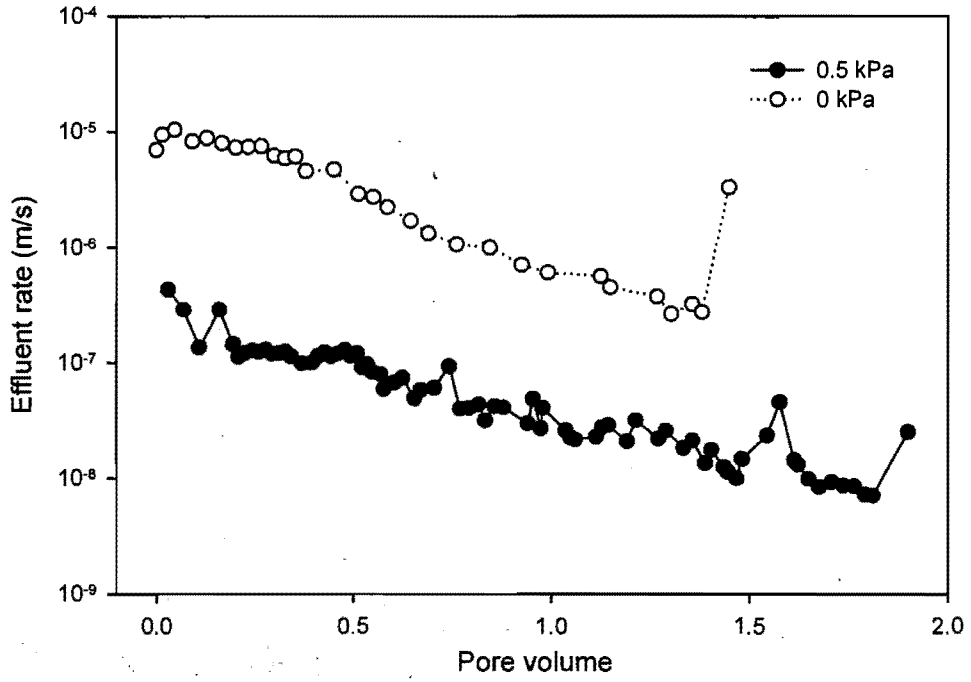

Figure 11. Column outflow rate at the two selected suctions (0.5 kPa and 0 kPa).

Figure 12 shows daily average soil temperature at 30 cm depth. For the 0.5 kPa leaching event it stayed over 13 °C during the first two weeks, rose to 18 °C and then dropped to 8 °C. At 0 kPa, it was more stable, varying between 10 °C and 14 °C. Since water viscosity is inversely related to temperature, temperature decline in the 0.5 kPa experiment was partly responsible for the diminishing flow rate. However, soil temperature cannot explain the change of flow rate during the 0 kPa experiment. It is postulated that the higher saturated flow rate mobilized more colloids from the top layer of the column, and blocked some micropores, mainly distributed in the middle of the column. Soil temperature variation would have little impact on the survival of endospores due to their resistance to low temperatures.

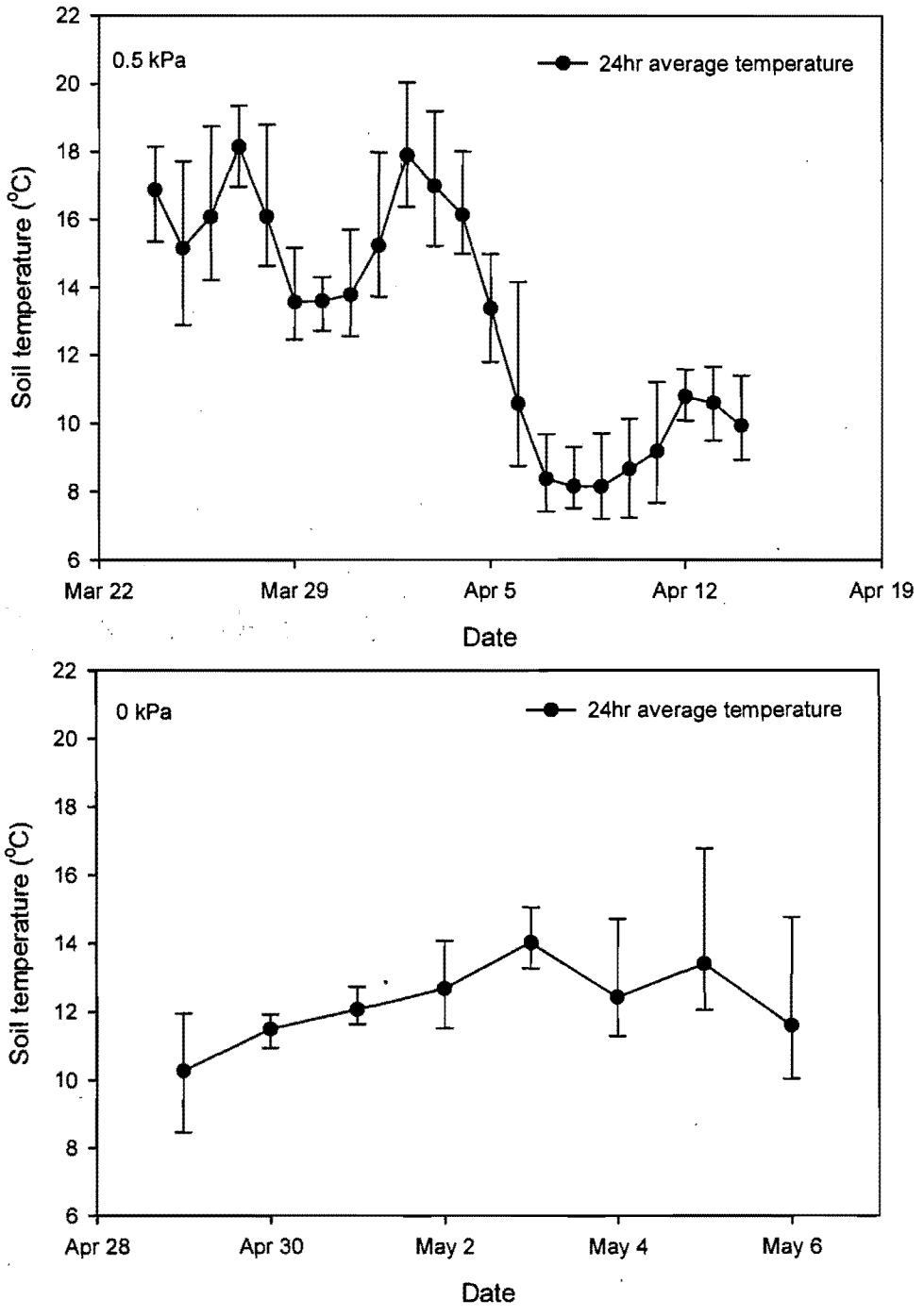

Figure 12. Soil temperature at depth of 30 cm in the soil column. Error bars indicate the daily minimum and maximum values.

3.3.3. Transport and deposition of B. subtilis and Br^-

Figure 13 shows breakthrough curves (BTCs) for *B. subtilis* and bromide at the two suctions. STANMOD version 2.2 was employed to model bromide breakthrough with the CXTFIT model included in the package. Fitted curves and parameters are indicated on the graphs. Breakthrough of *B. subtilis* occurred much earlier than the conservative chemical tracer Br^-, about 0.5 pore volume (PV) earlier at 0.5 kPa suction. The BTC of bromide at 0 kPa suction was irregularly shaped because of the preferential or by-pass flow. Another possible explanation for the plateau shaped bromide BTC is the higher concentration of sodium bromide in the pulse injection (4.0 g/L compared to 2.0 g/L at 0.5 kPa suction). But the earlier breakthrough of *B. subtilis* over bromide was still evident. On the other hand, the peak width of BTCs for *B. subtilis* at both suctions was much narrower than bromide. The effluent concentration of bacteria reached a peak, and then tailed quickly to a constant low level till the end of the experimental period. The BTC peak height for *B. subtilis* was *c.* two orders of magnitude larger under 0 kPa suction than 0.5 kPa suction. By contrast, the bromide peak height at 0 kPa was only twice that at 0.5 kPa.

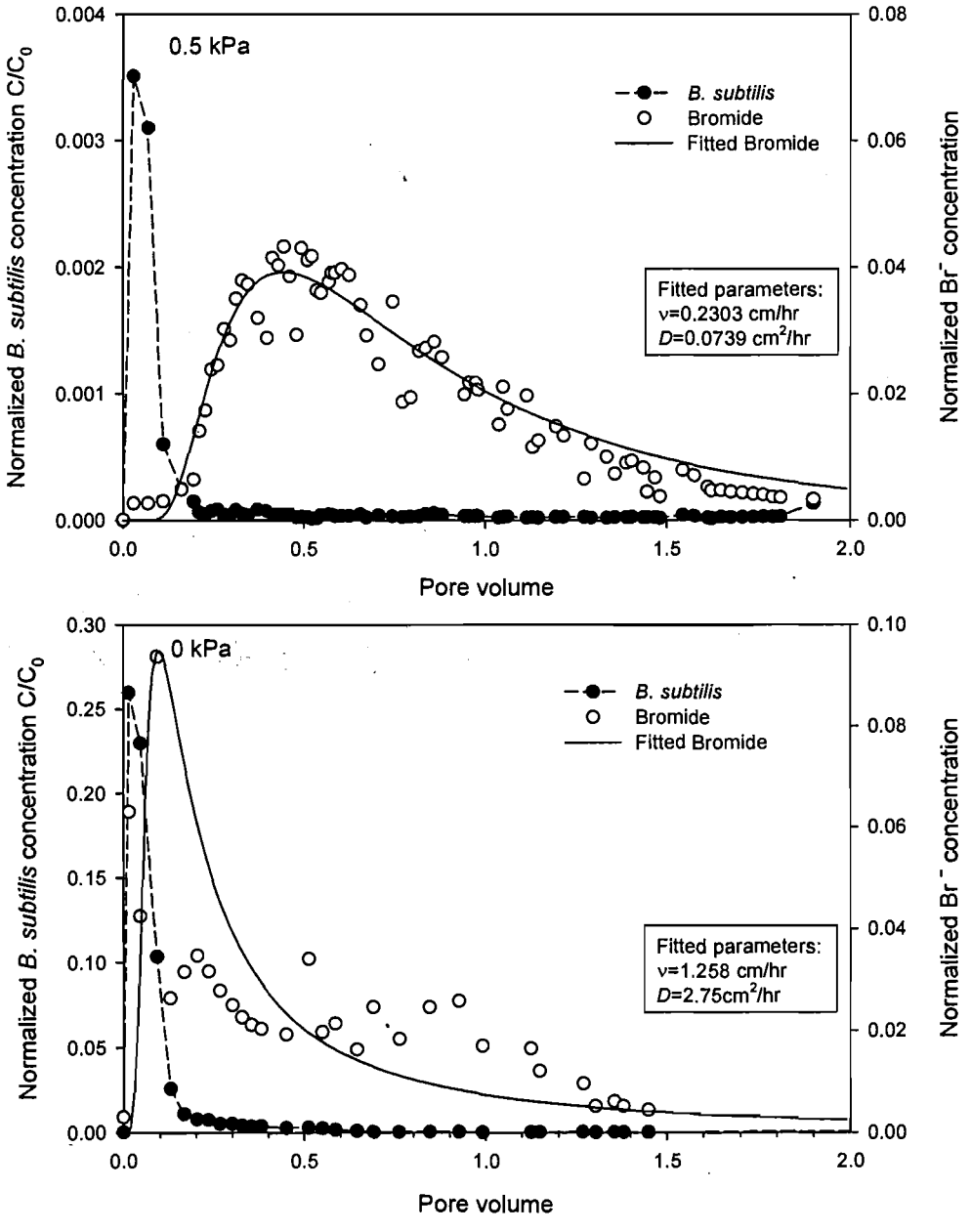

Figure 13. Breakthrough curves for *B. subtilis* and bromide at 0.5 kPa and 0 kPa suctions. The concentrations have been normalized to the initial injected concentration.

Figure 14 shows the cumulative leached bacteria and bromide. Less than 1% of applied bacterial cells were leached through the soil column at 0.5 kPa suction after about 2 effective (i.e. water-filled) PV; while *c.* 50% reached the bottom of the column at 0 kPa suction after about 1.5 PV. For bromide, the fraction of mass recovered in the effluent at both suctions reached *c.* 85% although it was about 0.5 PV earlier at 0 kPa suction. The

un-recovered bromide was possibly trapped in soils by diffusion into an immobile phase, including very fine pores of soil granules.

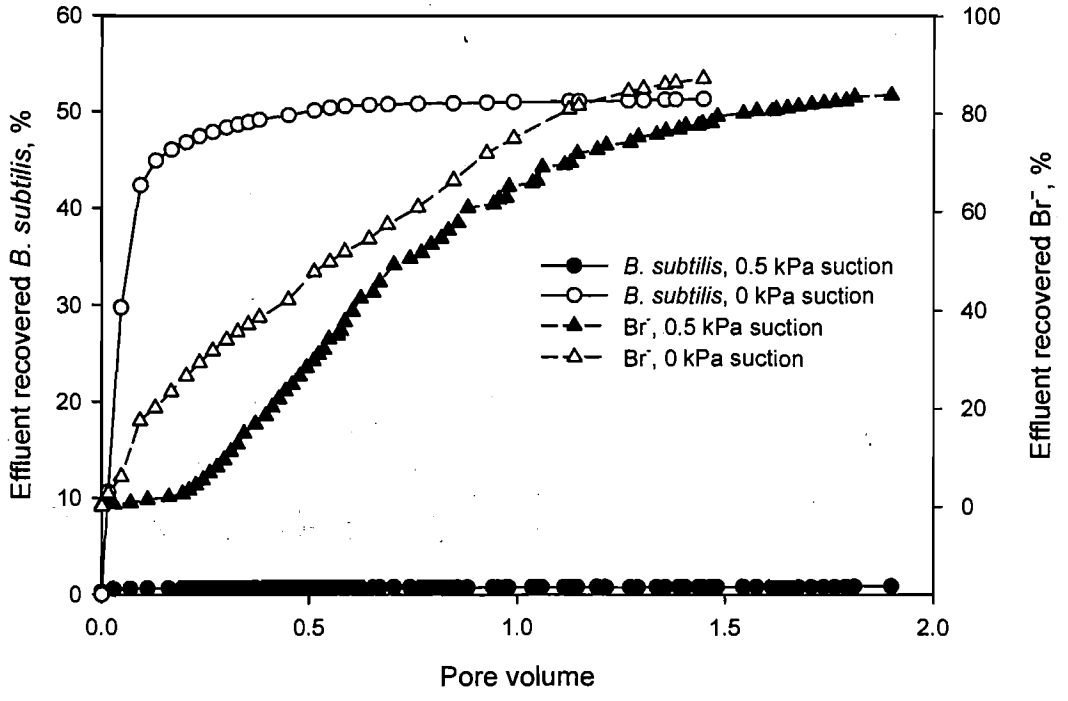

Figure 14. Cumulative leached *B. subtilis* and bromide at two suctions, as percentage of totals applied.

Figure 15 shows the distribution of deposited bacteria as a function of normalized depth (ND). Bacterial concentration decreased abruptly from the top to 0.2 ND, and then was relatively stable, although it increased a little at *c.* 0.7 ND. The transverse variance of deposited bacteria was not uniform with depth; it was higher at the top and bottom sections and lower from 10 cm to 30 cm. The highest variance occurred at the top of the column, mainly due to the relatively high fraction of macropores and presence of grass roots. Core 4 (see **Figure 7** and **Figure 15**) had exceptionally high deposited concentration from 0.6 to 0.8 ND. This might be the end of a preferential pathway such as a wormhole, or the presence of a clump of very adsorptive soil, thus a large number of bacteria were retained. The geometric mean of deposited concentration is shown in **Figure 15** with core 4 treated as an outlier and excluded.

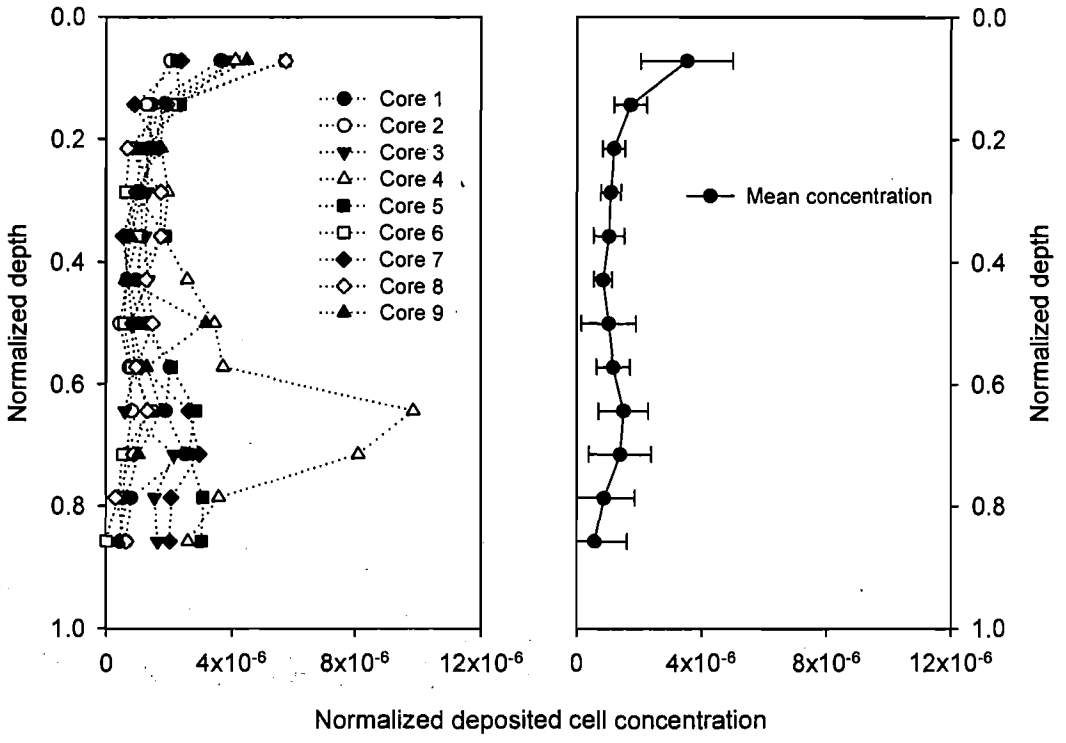

Figure 15. Distribution of deposited *B. subtilis* along the soil column after 0kPa experiment.

Although both effluent and deposited bacteria were measured in the saturated (0kPa) experiment, the mass balance of bacteria was not well conserved. About 32% of total applied bacteria were detected in the soil column and less than 7% was collected in effluent. Although there are no reports on the mass balance in bacterial transport experiments, it was postulated that the poor mass balance for bacteria is common for microbial transport in soils. Contributing factors include die-off and predation during the extended three month experimental period. The deficit could also be partly due to the detection methods, which probably did not release all deposited bacteria from soil.

3.4. Discussion

Bacteria are transported in soils via saturated or unsaturated flow. Total water flux in natural subsurface media is often dominated by macropore flow rather than matric flow under saturated or near saturated conditions (Hillel 1998; Silva 1999). In our experiment, a suction of 0.5 kPa applied on the soil surface emptied pores with diameter >600 μm. At

the same time, average θ_v down the column decreased from 0.45 to 0.43 (**Figure 8**) and water flux decreased substantially from 1.12 L/hr to 0.197 L/hr. The passive transport of bacteria by soil water flow would therefore be strongly retarded. According to the frequently used convection-dispersion equation (CDE) models, the bacteria recovered in the percolate are mainly transported by convection. The substantial decrease of water flux is therefore partly responsible for the relatively small bacterial recovery of 0.88% at 0.5 kPa suction compared to 51.3% at 0 kPa suction.

The main controlling mechanisms for bacterial retention in soil are attachment and detachment at particle surfaces (Banks, Yu *et al.* 2003; Ginn, Wood *et al.* 2002). The detachment process in natural soil happens when hydrodynamic shearing stress exceeds the attachment strength. The high pore water velocity 3.5×10^{-6} m/s at 0 kPa suction compared to 6.4×10^{-7} m/s at 0.5 kPa suction probably contributed to the higher level of leached bacterial concentration and mass recovery in percolate.

As discussed above, the surface applied 0.5 kPa suction caused only slight decrease of the average θ_v. However, the pore connectivity was probably changed greatly due to emptying of macropores (>600 μm). It is postulated that these emptied macropores acted as connecting channels for pores of different diameters (Beven and Germann 1982; Czapar and Fawcett 1992; Thomas and Phillips 1979). Because bacteria transport preferentially through macropores, macropore connectivity is crucial for transport. The loss of pore connectivity would contribute to both the increased bacterial retention and decreased soil water flux.

Pore size exclusion effects have been used widely to explain the breakthrough of bacteria relative to inert chemical tracers (Sinton, Noonan *et al.* 2000). The appearance of the bacterial concentration peak in advance of the bromide tracer is prominent in our experiment, at both suctions. At 0.5 kPa suction, the bacterial BTC peak arrived at dimensionless time of 0.03 PV, relatively later than 0.02 PV at 0 kPa suction. However, the difference is not significant and is compromised by the different sampling intervals. On the other hand, breakthrough of bromide was dramatically different between the two suctions. According to solute transport theory, more rapid water flow tends to produce a higher and narrower BTC peak. This is supported by **Figure 13**, which shows that the peak concentration arrived at 0.1 PV for 0 kPa, and 0.5 PV for 0.5 kPa, with 0.1 and 0.04 normalized concentrations, respectively. However the 0 kPa experiment also produced an

extended plateau in the bromide BTC, spanning *c.* 1 PV. This can be explained by the fact that more rapid water flow also increases dispersivity, tending to widen the BTC curve. Bromide BTCs were modeled by the CXTFIT model in STANMOD 2.2 (**Figure 13**). The fitted flow velocity and dispersion coefficients support our discussions.

The ratio of bacterial size to soil particle size also controls bacterial retention (McDowell-Boyer, Hunt *et al.* 1986). The size of *B. subtilis* endospores used in this experiment was *c.* 1 μm, and the dominance of pores with diameter <1μm in the column indicates that the straining effect was also significant in bacterial retention.

Air-water interface (AWI) trapping and film straining may also contribute to the greater bacterial attenuation at 0.5 kPa suction compared to 0 kPa. AWI adsorption is determined by cell hydrophobicity and degree of saturation, and would be greater under unsaturated conditions. However in this experiment we cannot differentiate between AWI and particle surface attachment. *B. subtilis* manifested variable hydrophobicity and might be more uncertain under natural groundwater conditions (Doyle, Nedjat-Haiem *et al.* 1984). In addition, unsaturated water flow includes water flow in films around solid surfaces. Film straining will also retard bacteria when the film thickness decreases to less than bacterial cell diameter (Wan and Tokunaga 1997). Hence, unsaturated flow favors greater bacterial retention.

In a previous experiment, a series of tension table experiments was carried out (Ratcliffe 1998), which aimed to verify the hypothesis that surface-applied bacteria under unsaturated conditions will get trapped in soil pores, and this trapping process is not easily reversible. These experimental results have recently been re-analyzed by the author with Sigmaplot 9.0. *B. subtilis* endospores (resistant to rifampicin) irrigated on the surface of intact soil cores (20 cm diameter × 8 cm length) which were equilibrated under selected suctions, i.e. 0, 0.5, 2, 5, 10 kPa, were then percolated by saturated water flow. The bacterial retention and percolation percentage were significantly correlated with the suctions. The higher retention with higher suction was explained by micropore storage, attachment to static air-water interface (AWI), and irreversible particle adsorption. The bacterial percolation was mainly controlled by replacement of pore water storage, and the reversible detachment process. Another sensitivity experiment with four replicates using lincomycin resistant strain of *B. subtilis* at 0 and 0.5 kPa suctions revealed that a small increase (0 to 0.5 kPa) in soil matric suction incurred a substantial higher level of

bacterial retention.

Only a few previous studies have quantified the number and distribution of deposited bacteria in porous media (Bolster, Mills *et al.* 1999; Bradford, Yates *et al.* 2002; Fuller, Dong *et al.* 2000; Natsch, Keel *et al.* 1996; Wollum II and Cassel 1978). In our experiment, bacterial retention was large in the first few centimeters of topsoil and decreased at 20 cm depth (Figure 10), although with a slight increase at the column bottom. When large quantities of bacterial cells were applied at the soil surface, straining retained a large fraction before pore size exclusion came into effect. Then, the pore size exclusion and detouring effects diverted bacteria into relatively large pores and attachment became the main retaining factor. The high organic matter content including grass root debris in the topsoil compared with subsoil might be a factor increasing bacterial retention in the top of the soil column.

For the saturated leaching experiment, an extended tailing of bacterial breakthrough was observed until over 4 pore volumes were sampled (data not shown). This was also observed after the 0.5 kPa experiment during the equilibration period, before the saturated experiment. (Bolster, Mills *et al.* 2000) explained the long-distance transport of bacteria as a result of intra-population variability. Microbial heterogeneity, especially of hydrophobicity has been frequently reported (Doyle, Nedjat-Haiem *et al.* 1984; Kinoshita, Bales *et al.* 1993; Wiencek, Klapes *et al.* 1991). (Fuller, Dong *et al.* 2000) reported that bacteria in their intact core experiments were composed of a range of subpopulations of cells. The existence of a non-adsorptive subpopulation of bacteria will cause longer term and longer distance transport, which jeopardizes groundwater safety.

3.5. Conclusions

In this study, an intact soil column with a tension infiltrometer was used to simulate flow in saturated conditions and unsaturated vadose zone soils. Soil matric potential, infiltration rate, and temperature were monitored. Bacterial and inert chemical tracer (Br^-) breakthrough curves under unsaturated, followed by saturated conditions were obtained during a three months leaching experiment. The soil column was destructively sampled for deposited concentration of *B. subtilis* at the end of the saturated experiment. The experimental setup allowed accurate control of suction, which empties soil pores greater than a specified diameter. This is especially important in differentiating effects of

macropore flow and matric flow.

Bacterial breakthrough occurred distinctly earlier than for conservative tracer, which is consistent with effects of pore size exclusion, preferential flow and effects of macropores. Also, saturated flow gave a higher concentration, and mass recovery ratio of effluent bacteria. Bacterial deposition in the column was large in the top few centimeters of soil. Then, it decreased markedly and kept constant along the column depth, although demonstrating some irregularity at the column bottom. Differences between saturated and unsaturated leaching results were attributed to the effects of air-water interface trapping, film straining and contrasting water flow rates. The work provides a basic framework for understanding bacterial transport through and retention in intact soils under different water contents. Studies of bacterial transport and retention at soil water contents typical of local field conditions are important to determine microbial impacts from animal waste.

Chapter Four

Design of an Experiment to Measure Transport of *Escherichia coli* through Packed Sand Columns

4.1. Introduction

The soil lysimeter experiments in Chapter 3 were designed to simulate the effects of irrigation on bacterial transport through an intact soil core, where the top layer of soils had been dried out more than the deeper layer as occurs frequently in pastures. Therefore, suction was only applied to the top of the soil column by the tension infiltrometer to make the top layers of soil within the lysimeter drier than the soils near the bottom. The pore size distribution in the intact soil column was not uniform with depth. The heterogeneity of soil pores made it difficult to determine at what depth in the soil core bacteria were being removed. Only the net removal of bacteria could be studied by determining the numbers of bacteria in the percolate. At the end of this experiment when the soil itself was sampled, the distribution of bacteria in the profile could be determined. However, this could not be conclusively attributed to either the saturated or unsaturated flow as sampling was done after both types of flow had occurred. Unfortunately, once bacteria were applied to the soil lysimeter, the soil column could not be used again with the same bacteria because of residual cells, if no effective method of sterilization was applied without destruction of the soil structure. One way to circumvent this problem is to use bacteria with minor differences in properties, such as resistance to different antibiotics.

To be able to study the phenomenon of bacterial movement under more controlled conditions, a new experimental approach was designed. Uniform suctions and a uniform pore size distribution throughout the whole column were needed. Also, it was necessary to sterilize the system (kill residual bacteria) without changing the properties of the porous medium. This system needed to be designed so that the effects of macropores (>30 μm) on the movement of bacteria through micropores could be studied by changing the suction. Lastly, the adsorption of bacteria to the particles needed to be studied.

4.2. Objectives of the experiments

This second experiment was designed to study controlled bacterial transport through sand columns with steady-state saturated and unsaturated flow. The aim of this experiment was to investigate the role of pore space properties (via mechanisms of air-water interface trapping, film straining, and attachment to solid-water interfaces) on bacterial transport and retention. The adjustable experimental parameters include grain size, water content, matric suction, total porosity, and pore size distribution. The experimental setup needed to be capable of reproducible tests with different sands, water saturation (suction), and column length. The objectives were to:

1) Develop an experimental design to maintain constant suction and steady-state flow rate in sand columns. This system needed to be able to apply bacteria on top of sand column without interfering with the suction and water flow.

2) Measure the grain and pore size distribution, moisture characteristics, and bacterial adsorption for the sand.

3) Determine the differences in bacterial transport and retention under saturated and unsaturated flow.

4) Measure the effect of suctions up to 4.9 kPa (higher than the 0.5 kPa in the first experiment above) on bacterial transport and retention with various water saturations.

5) Determine the recovery of bacteria in percolate and removal efficiency of bacteria in sand columns after transport under various suctions.

6) Demonstrate quantitatively the effects of air-water interface trapping (adsorption) and film straining. Test whether bacterial transport can be simulated using two-site (equilibrium and first-order kinetic adsorption sites) adsorption processes from the BTCs.

7) Verify the usefulness of CXTFIT 2.1 models to describe unsaturated bacterial transport. If CXTFIT 2.1 is not sufficient, to develop a mathematical model to describe the breakthrough of bacteria from unsaturated sand columns.

4.3. Rationale and literature review

4.3.1. Physical principles

The relationship between water content θ_v and the largest diameter d (cm) of water-filled pores can be expressed via the relationship between suction s (cm) and d. This latter relationship is described by the capillary rise equation. Assuming water has a zero contact angle with the capillary tube, then

$$h = \frac{2\sigma}{\rho_w g r} \tag{9}$$

Where h (m) is the height of water rise in a capillary tube, r is the radius of the tube (m), σ is the surface tension of water (kg s^{-2}), ρ_w is the water density (kg m^{-3}), and g is gravitational acceleration (m s^{-2}). For water at 10 °C, σ = 0.0727 kg s^{-2}, ρ_w = 1000 kg m^{-3}, g = 9.81 m s^{-2}. Thus

$$h = 15 \times 10^{-6} / r \ \text{(m)} \tag{10}$$

This equation is adapted in terms of the suction and largest water-filled pore diameter as:

$$d = 0.3/s \ \text{(cm)} \tag{11}$$

Where, $d = 2 \cdot r$ in cm. Therefore, the sand column water potential (or suction) should be measured and used to calculate the corresponding pore diameter.

The water flow rate (water flux) in a tube is usually described by Poiseuille's law:

$$Q = \frac{\pi r^4 \Delta P}{8 L \mu} \tag{12}$$

Here Q is water flux (m^3 s^{-1}), ΔP is the pressure difference (Pa), r is the tube radius (m), L is the tube length (m), and μ is the water dynamic viscosity (Pa s). For water at 10 °C, μ = 1.312 × 10^{-3} Pa s. Thus, the mean flow velocity in m s^{-1} through the tube can be derived as:

$$\bar{u} = Q/A = \left(\frac{\pi r^4 \Delta P}{8L\mu}\right) \Big/ \left(\pi r^2\right) = \frac{r^2 \Delta P}{8L\mu} \tag{13}$$

To achieve a steady-state unsaturated flow, a constant suction through the column should be maintained during the experimental period. Assuming that flow is purely gravity-driven and neglecting hysteresis effects, for any given suction and water content, there will be only one possible flow rate to keep the sand column at a stable water content.

For constant water content, $dS_w/dz=0$. For a unit hydraulic gradient, $dh_t/dz=1$, which means the hydraulic head h_t should be equal to the column length. When the inflow rate equals the outflow rate, i.e. $v_i = v_o$, the water saturation should not change. Water saturation is $S_w = \theta_v/\theta_{v,s}$ (where $\theta_{v,s}$ is saturated water content), so the SMC relationship can be elucidated by simultaneous measurement of water suctions and water contents along the sand column.

4.3.2. Unsaturated experimental setups in the literature

Table 1 shows the grain sizes of sand and the column dimensions used by previous researchers. The ratio of column length to inner diameter is within a range from 2 to 4.

Table 1. Dimensions of experimental sand columns and grain sizes reported in the literature.

Column Diameter (cm)	*Column Length (cm)*	*Sand Grain size (μm)*	*Reference*
12.7	32.8	300-355	(Lenhart and Saiers 2002; Saiers and Lenhart 2003)
5.34	20	250-500	(Schafer, Ustohal *et al.* 1998)
2.6	12.5	50-250	(Jewett, Logan *et al.* 1999)
2.5	5	300-420	(Bai, Brusseau *et al.* 1997)
7.6	25.4	354-710	(Powelson and Mills 2001)
5	20	Sediment	(Cherrey, Flury *et al.* 2003)
2.2	8	354-710	(Powelson and Mills 1996)

Also, sands with diameters from 50-710 μm have generally been used. The internal diameter of columns ranges from 2.5 to 12.7 cm, and length from 5 to 32.8 cm.

Table 2 summarizes values of flow rate, pore volume, degree of saturation and porosity used in the literature.

Table 2. Values of experimental parameters used in previous research

Column volume (mL)	*Porosity*	*Flow rate (mL/min)*	*Degree of saturation*	*Time (PV)*[†]	*Suction (kPa)*	*Reference*
392.7	0.1~0.4	3.14-809	0.16~1	8	0.5~1.5	(Cherrey, Flury *et al.* 2003)
66.3	0.36	-	0.48~1	1+3	4.05~6.68	(Jewett, Logan *et al.* 1999)
6226	0.39	8.4-12.2	0.6~0.86	8.3+4	1.5	(Schafer, Ustohal *et al.* 1998)
3141.3	0.384	391-193	0.226~1	6~10	1.85~2.92	(Lenhart and Saiers 2002)
3141.3	0.335	83.6	0.355, 1	12	2.85	(Saiers and Lenhart 2003)

[†] The plus sign indicates reported experiments had two leaching events.

4.4. Devices, dimensions and installation

Experiments reported in the literature usually used a hanging tube to control the suction at the bottom of columns. The experiment in chapter 3 used a tension infiltrometer to control the suction at the top of the soil lysimeter. This experiment used both methods to achieve more even suctions throughout the sand column. The tension infiltrometer at the top and a hanging tube at the bottom of the sand column help to keep a constant flow rate and stable suction. To make the installation of tensiometers easy, our design used a column with a total length of 45 cm (or 23 cm) and an inner diameter of 22.5 cm.

The sand column casing consisted of four or two short PVC rings, which were connected and glued with Siliaflex sealant. This enabled the column length to be increased by using more sections. The column base consisted of one layer of stainless steel mesh, two layers of polyester mesh, and one layer of 23 μm nylon membrane. Table 3 lists the devices and quantities needed in the experiment.

Table 3. Devices used in the experiment

Device	*Number*	*Requirements*
Electronic balance	1	Accuracy of 0.5 g.
Tension infiltrometer	2	20 cm diameter.
Tensiometer and pressure transducer	10	Measuring range up to 1 m-H_2O.
Data logger	2	Campbell Scientific Instruments, CR10
Water reservoir	2	Storage of bacterial suspension and cell-free water.
Sand column	1	Plastic column, 23/45 cm length and 22.5 cm diameter, cut into three 11 cm long and one 12 cm long sections.
Bottom membrane	2	Polyester cloth with pore size of 24 μm, allowing suctions up to 7 kPa.
Metal mesh	2	Stainless steel mesh with 1mm diameter pores.
Computer	1	Data collection and processing.

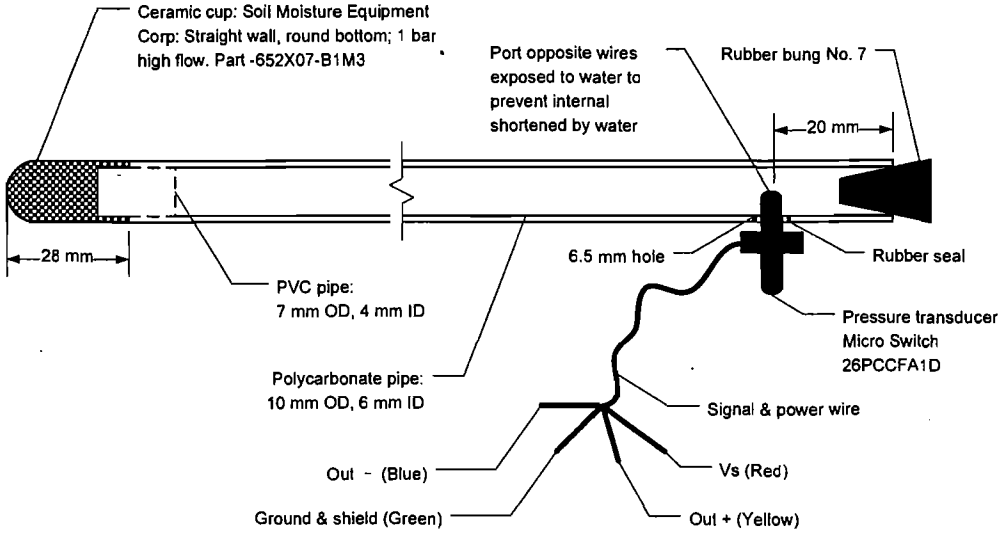

Figure 16. Schematic of the tensiometer and pressure transducer.

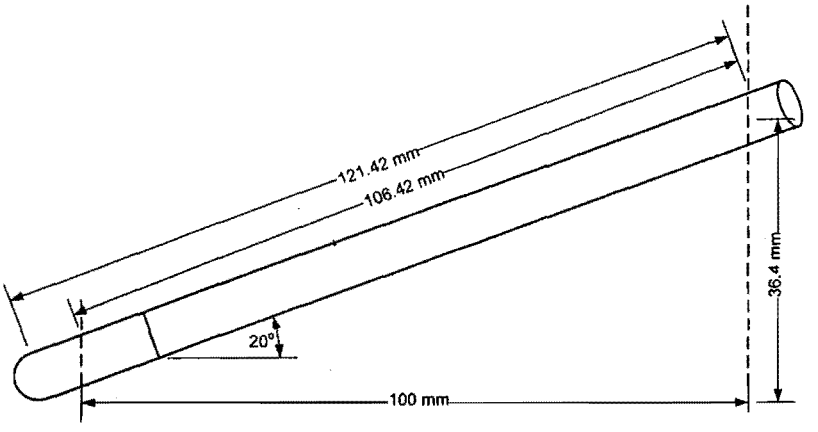

Figure 17. Tensiometer insertion geometry.

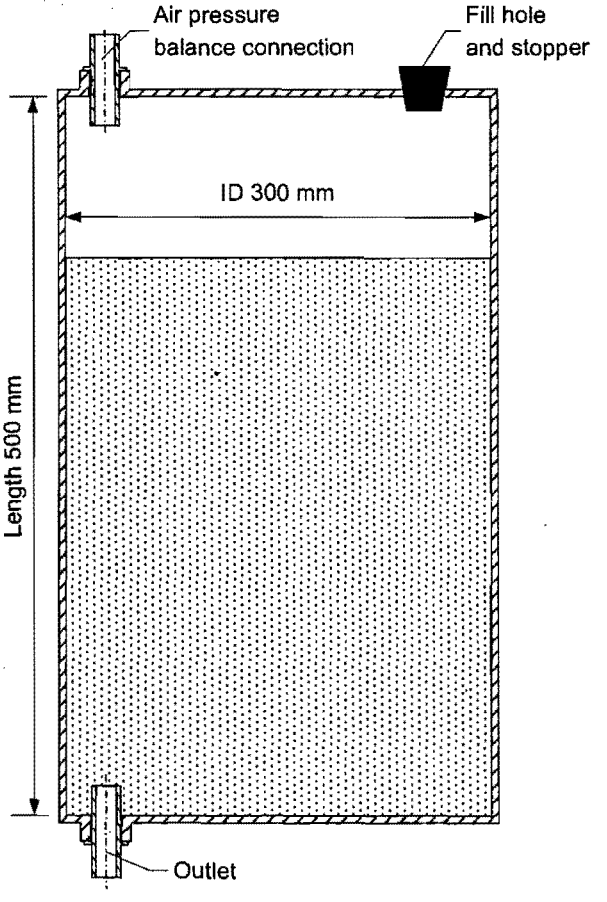

Figure 18. Schematic and dimensions of water reservoir.

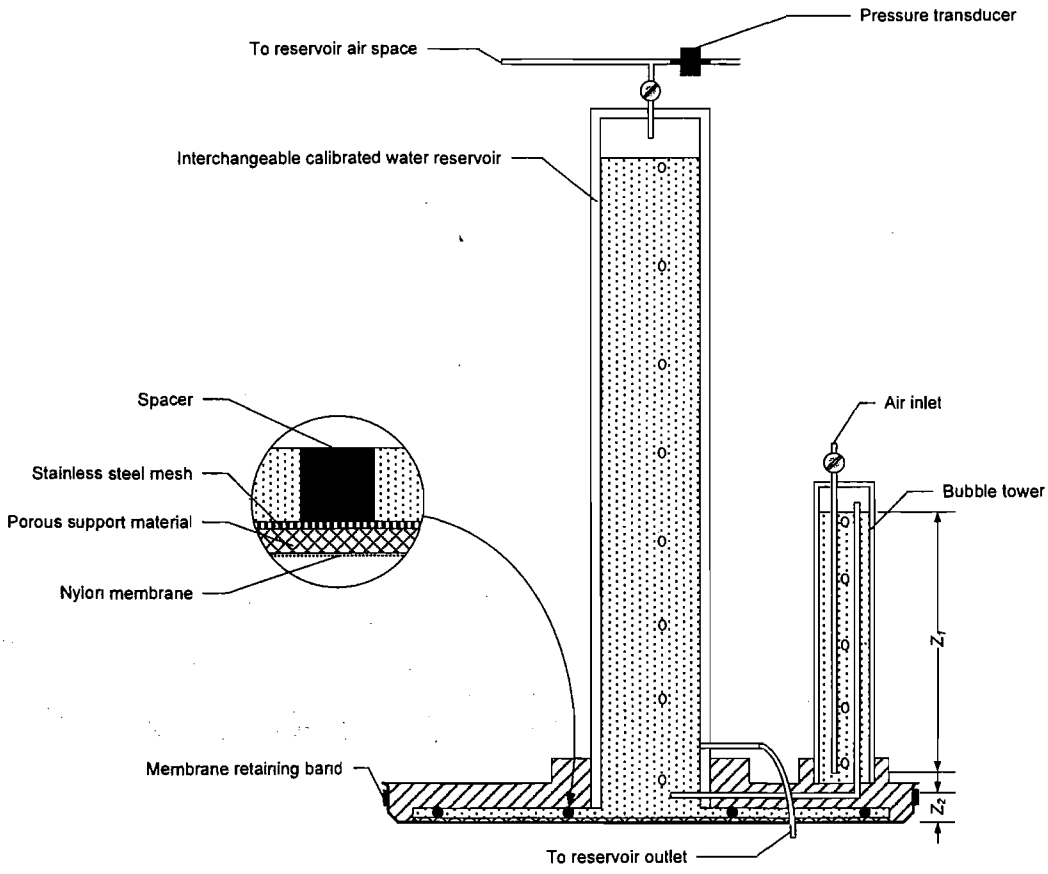

Figure 19. Schematic of disk permeater for unsaturated experiments.

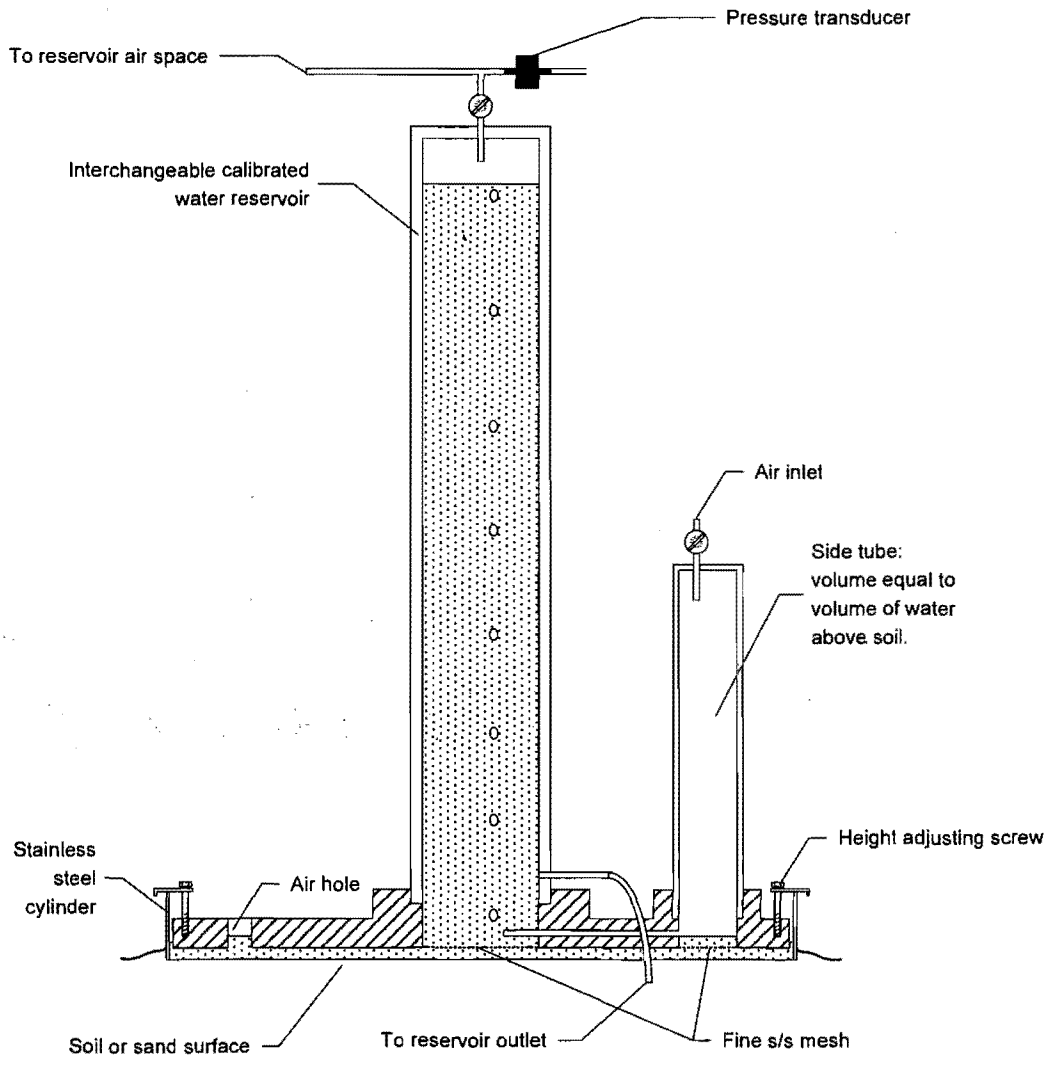

Figure 20. Disk permeater for saturated experiments.

To calculate the volume and weight of the sand column, the bulk density and particle density of the sand used was assumed to be 1.7 and 2.65 g cm^{-3}, respectively. The porosity of the sand column was assumed to be 0.36 ($\varepsilon = 1 - \rho_b/\rho_p = 1 - 1.7/2.65 = 1 - 0.642 = 0.36$). The volume of the water container was designed to hold a volume equal to 4 pore volumes of fully saturated sand column.

Table 4. Volumes and weights of the sand column and water container.

Instrument	*Volume (L)*	*Weight (Kg)*
Sand column (full size)	17.5	~29.7
Water container	35	35

4.5. Experimental parameters

In the experiments, the effects of various values of suction S (corresponding to water content θ_v, largest water-filled pore size d, water saturation S_w) were investigated. The suction values used were 0~5 kPa. These suctions were determined using tensiometers, and the water content was calculated according to the measured SMC. Bacterial concentrations of *c.* 5×10^8 cfu/mL were sprayed onto the sand surface as a pulse input. Also, inert and reactive sands were used to find the relative importance of bacterial adsorption at the AWI compared with the SWI.

Table 5. Experimental parameters

Factors	*Abbreviation*	*Methods*
Inlet bacterial concentration	c	Serial dilution, membrane filtration, and plate counts.
Outlet bacterial concentration	c_0	Same as above.
Inlet/outlet bromide concentration	$c^{'}, c_0^{'}$	Ion exchange chromatography
Inflow/outflow rate	v_i, v_o	Pressure transducer on water reservoir; leachate collection and weighing.
Matric suction	S	Tensiometer and pressure transducers
Total porosity	ε	Measurement of ρ_b and ρ_p, $\varepsilon = 1 - \rho_b / \rho_p$. Effective porosity equals to water content.
Ambient temperature	T	Thermometer.
Grain sizes of sand		Sieving, weighting.
Pore size distribution and moisture characteristics		Buchner funnel setup, capillary equation was used to calculate the equivalent pore size distribution.

4.6. Chemicals

Because tap water was shown to be free from *E. coli*, the water used in the experiment

was not autoclaved before infiltration through the sand columns. Sodium bromide (NaBr) was used as a conservative chemical tracer and analysed by Ion Exchange Chromatography (IEC) and Flow Injection Analysis (FIA) methods. All pipes, valves, columns were autoclaved or sterilized with 75% ethanol before and after experimental runs. Sterile plastic bags and 1 L autoclaved bottles were used to collect and store leachate and sand samples. Chemicals used in this experiment are summarized in **Table 6**.

Table 6. Chemicals used for sand treatment and substrates for bacterial enumeration.

	Name	*Equation*	*Concentration*
Sand treatment	Nitric acid	HNO_3	10%
	Sodium hydroxide	NaOH	0.5 M, 40 g/L
Bacterial enumeration	mFC agar	-	20.8 g/ 400 mL
	Sodium hydroxide	NaOH	0.2M, 8 g/L
	Rosolic acid	-	0.04g/ 400 mL
	Nutrient broth	-	8g/ L

Chapter Five

Measurement and Modeling of Transport of *Escherichia coli* through Sand Columns

5.1. Introduction

The interactions and mechanisms controlling bacterial transport under unsaturated flow are much more complicated than those under saturated flow (Chu, Jin *et al.* 2001; Keller and Sirivithayapakorn 2004; Lenhart and Saiers 2002; Schafer, Ustohal *et al.* 1998; Wan and Tokunaga 1997; Wan, Wilson *et al.* 1994). In addition to traditionally recognized advection, dispersion and mineral-grain attachment, air-water interfaces (AWI) and film straining affect the transport and retention of bacteria through an unsaturated sand column. Experimental evidence for the importance of the mechanisms on bacterial transport under unsaturated flow is still lacking. Previous research has not focused on the effects of pore properties (total or water-filled porosity, pore size distribution) and adsorption at phase interfaces. Because suction, water content and pore size distribution are all correlated, the grain surface and pore space properties are the fundamental determinants of the above effects.

In this chapter, results from unsaturated and saturated bacterial transport through coarse and fine sand columns. The main objectives were to investigate effects of water saturation (matric suction), particle size, and length of column on bacterial transport and retention, and to model the pattern of bacterial transport under unsaturated flow by mechanistic models, which had separate terms accounting for bacterial attachment to solid-water interface and air-water interface. The modeling approaches were polished based on the experimental results and analysis of bacterial adsorption processes. Silica sand columns with tension infiltrometer and flow-controlled irrigation were employed to produce bacterial transport with various water saturations. Water flow and matric potential in the sand columns were well-controlled in order to establish a steady unsaturated condition. The concentrations of bacteria and an inert chemical tracer (sodium bromide) in the

drainage water were continuously monitored. To model the transport of bacteria in unsaturated flow, traditional convection dispersion equation (CDE) model was modified by including a first-order kinetic term to account for the attachment of bacteria to air-water interfaces, and terms for the equilibrium/first-order adsorption to sand surfaces. Also, we compared the performances of one-site first order kinetic model and two-site model with and without effects of air-water interface. Whenever it was possible, equilibrium and equilibrium + AWI models were also employed to fit experimental data.

5.2. Materials and Methods

5.2.1. Sand, treatment and characterization

The silica sands were obtained from Fulton Hogan Ltd., Christchurch, New Zealand. The original bulk Oamaru sands were sieved into coarse (COS) and fine (FOS) fractions by a sieve (Endecotts Ltd. London, England) with aperture of 500 μm, brass frame, and S/S mesh. Surface treatment was used to remove trace organic matter and clay particles from the commercial silica sand, and thus to increase the experimental reproducibility. The treatment method was modified from what described by Chu et al. (2001), Kunze and Dixon (1986), and Powelson and Mills (1998). The sand was first soaked in 10% HNO_3 (nitric acid) for 24 h and then rinsed with deionized water; then soaked in 0.5 mol/L NaOH (sodium hydroxide) for 2 h and rinsed with deionized water again.

The sand bulk density and particle density were measured to calculate porosity, $\varepsilon = 1 - \rho_b / \rho_p$, where ρ_b is bulk density and ρ_p is particle density. Bulk density on oven-dry (105 °C) basis was calculated using $\rho_b = M_s / V_t$, where M_s is the mass of dry sand and V_t is the sand volume. A measuring cylinder was used to record the volume of sand with three replicates. Particle density measurement was determined in three replicates using air-dried sand (Silva 1999). Fifty grams of sand was weighed into 100 mL volumetric flasks. The flasks were filled with distilled water and de-aired by gently boiling the water for several minutes without losing any sand. The flasks were cooled in a water bath and filled up with boiled, and cooled distilled water, then weighed (W_{sw}). The contents of flasks were removed, thoroughly

cleaned, then weights of flasks with boiled cooled distilled water were recorded (W_w). Finally the weights of cleaned empty flasks W_a were recorded and particle density were calculated using the following equation:

$$\rho_p = \rho_w(W_s - W_a)/[(W_s - W_a) - (W_{sw} - W_w)] \quad (14)$$

Where, ρ_w is water density (kg m^{-3}) at the experimental temperature, W_s is the weight of flask plus soil (corrected to 105 °C oven dry water content).

Sand moisture characteristics (relationship between water potential and water content) were determined by a Buchner funnel connected with manometer tube and burette. Both water release (drying) and imbibing (wetting) processes were measured. Water content function was fitted to the observed data by van Genuchten model and relative hydraulic conductivity was calculated with fitted parameters as a function of suction (van Genuchten 1980). The van Genuchten function uses the parameters of θ_r residual water content, θ_{sat} saturated water content, α (equivalent to the inverse of air entry suction), n ($n = 1 + \lambda$, λ is pore size index), and m, which is in most cases assumed to be $m = 1 - 1/n$. h is matric suction (kPa), which is positive.

$$\theta = \theta_r + \frac{(\theta_{sat} - \theta_r)}{[1 + (\alpha h)^n]^m} \quad (15)$$

$$K_r(S) = \frac{1 - (\alpha h)^{n-2}[1 + (\alpha h)^n]^{-m}}{[1 + (\alpha h)^n]^{2m}} \quad (16)$$

Because the unsaturated flow in our experiments was developed by gradually decreasing the water content, only water release curves were reported.

5.2.2. Bacteria and adsorption to Oamaru silica sand

Escherichia coli strain D was used as the tracer bacterium. *E. coli* is a member of the family *Enterobacteriaceae* of facultatively anaerobic, gram-negative, non-sporing rods, often motile organisms (Bell and Kyriakides 1998). The cell dimensions of *E. coli* are about 2 μm long and 0.7 μm in diameter (Smith-Keary 1988). A single colony of *E. coli* was inoculated into nutrient broth (Life Technologies, Paisley, Scotland) and incubated in a rotary shaker (120 rpm) at 37 °C for 48 hr. The final concentration of *E.*

coli reached about 1×10^9 cfu/mL. Then bacteria suspension in nutrient broth was stored in a fridge at 4 °C before being used in the column transport experiments.

The methods used to measure bacterial adsorption to the sands were modified from Ling *et al.* (2002) and Huysman and Verstraete (1993b). Adsorption of *E. coli* at concentrations ranging 10^4, 10^5, 10^6, and 10^7 cfu/mL to Oamaru coarse (>500μm) and fine (<500μm) sands was measured in 50 mL conical vials. First, bacteria in nutrient broth were centrifuged at 4000 rpm (Heraeus Varifuge 3.0R, rotor radius 21.1 cm) for 10 min and washed twice with deionised water. The strains were re-suspended in deionised water and adjusted to concentrations of 10^5 and 10^6 cfu mL^{-1}. Bacterial suspension 20 mL and 2 g fine- or coarse-grained Oamaru sand were added in a 50 mL conical tube (Labserv, Biolab Ltd. NZ). The conical tube was vortexed vigorously for 10 s, and mixed for 1 h on a rotary shaker at 100 rpm. The tubes were subsequently centrifuged at 120 *g* rcf (700 rpm) for 30 s with brake off in centrifuge (Heraeus Varifuge 3.0R). The bacterial concentration in the supernatant was determined by serial dilution and plate counting in Difco™ mFC agar (Becton, Dickinson and Company, Sparks, USA). All tests were done in triplicate. The mathematical relationships for bacterial adsorption were expressed as:

$$K_d = C_s / C_w \tag{17}$$

$$C_s = (N_t - N_s)/W \tag{18}$$

$$C_w = N_s / V \tag{19}$$

$$P_a = [(N_t - N_s)/N_t] \times 100 \tag{20}$$

Where C_s and C_w are bacterial concentrations on solid (cells g^{-1}) and in liquid (cells mL^{-1}), respectively. K_d is a distribution coefficient (mL g^{-1}). N_t and N_s are the total number of bacteria added to the sand (cfu) and in the supernatant (cfu). W is the mass of sand used in the mixture (g), and V is the volume of water in the mixture (mL). P_a is the percentage of adsorption (%).

5.2.3. Sand columns

Figure 21 is a schematic diagram of the sand column (45 cm long). The sand column

consisted of four or two PVC rings with 22.5 cm inner diameter, which were fitted together by sealant and adhesive waterproof sealing tape. Two lengths of column, 45 cm and 23 cm, were set up by using four or two rings. The base of the sand column had one layer of nylon mesh (60 μm pores), two layers of polyester mesh (23 μm pores, Universal Screen Supplies Ltd., NZ), stainless steel mesh, which were all assembled over an 8 mm thick PVC sheet. This combination of meshes was designed to sustain the required suction up to 5 kPa without air bubbling through. A test of bacterial passage through the membrane and mesh showed that they wouldn't capture *E. coli* at various concentrations ($10^3 \sim 10^9$ CFU/mL).

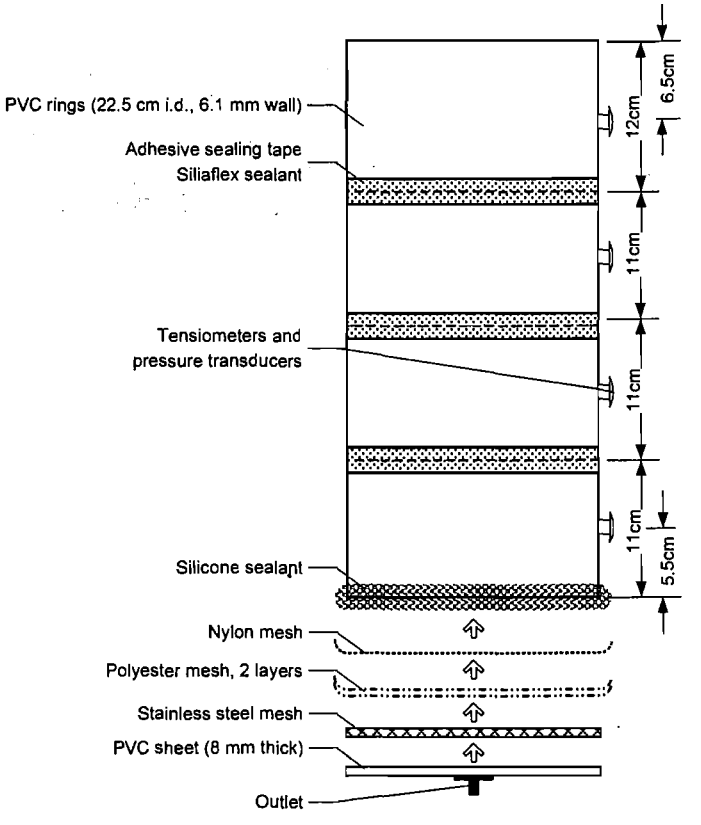

Figure 21. Schematic diagram of sand column setup.

Tensiometers (Fabricated from Soil Moisture Equipment Corp Ceramic Cups - Part 652X07B1M03) were installed at the middle of each ring with 20° downward angle. Honeywell 26PC pressure transducers were connected to a datalogger (CR10, Campbell Scientific Instruments) and calibrated. Real-time matric suctions recorded by the transducers were displayed in numerical and graphic format on a laptop computer. Water flow rate, suction of the tension infiltrometer, and position of outlet

pipe were adjusted according to the tensiometer readings.

5.2.4. Transport experiment

Figure 22 shows the experimental system for the controlled bacterial transport through sand columns. To avoid edge flow effects, sand columns were packed according to a modified method from Lenhart and Saiers (2002). For each transport experiment, a fresh column was packed by pouring sand in about 2000 g increments into the column, which always had a small volume of water standing over the sand. After each increment of the sand, the contents of the column were stirred gently with a stirring-rod. The wall of the column was tapped a certain number of times (i.e. 30). The fill-stir-tap steps were repeated until the sand reached the specified height. This packing procedure was believed to be capable of removing entrapped air and producing a fully saturated condition.

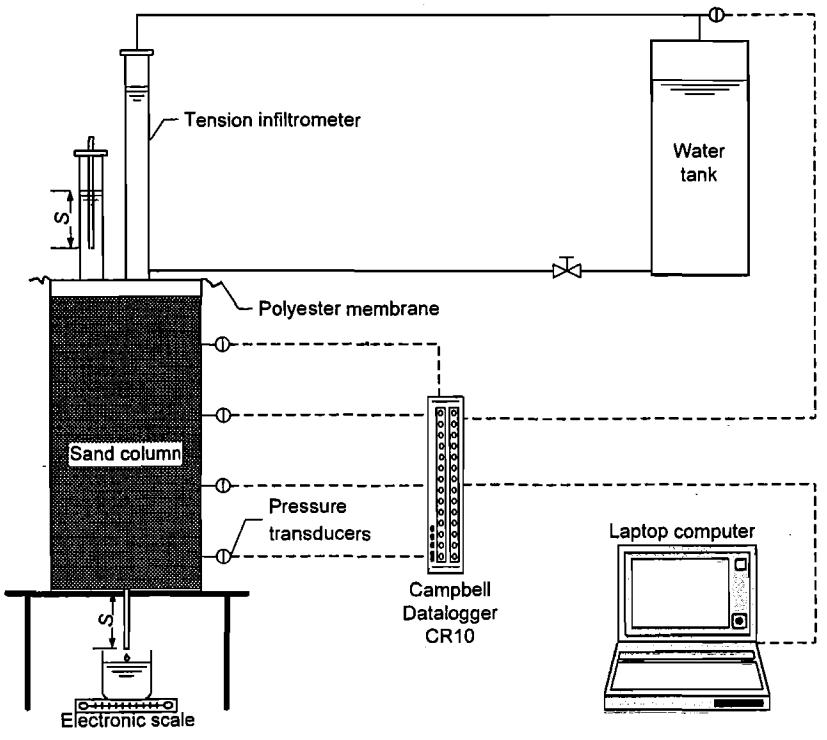

Figure 22. The experimental setup for bacterial transport through sand columns.

To diminish influences from the potential growth or die-off of *E. coli*, experiments were carried out in a dark room at 7 ± 1 °C. At the beginning of the experiments, silica

sand (Industrial Sands Ltd., NZ) of particle size 75-297 μm was poured on top of the polyester cloth under the infiltrometer to a thickness of about 10-15 mm, and was flattened for maximum contact with the infiltrometer disk. The tension infiltrometer and a hanging tube at the bottom of the sand columns were adjusted to control the water suction. For unsaturated flow, the suction S was adjusted until the sand water potentials displayed on the computer reached stable.

Table 7. Transport experiments and parameters

Run[†]	*Sand*[*]	*Length (cm)*	*Suction (kPa)*	*Degree of saturation*	*Bacterial C_0 (cfu/mL)*	*Flow rate (mL/min)*[♠]
CA♦	COS	44	0	1	4.15×10^8	776.9
CB◊	COS	44	1.0	0.67	4.01×10^8	172.7
CC♦	COS	22	0	1	9.25×10^8	255.8
CD◊	COS	22	1.2	0.49	5.08×10^7	209.2
FA♦	FOS	44	0.1	1	5.55×10^8	50.9
FB◊	FOS	44	1.3	0.9996	3.74×10^8	63.0
FC♦	FOS	22	0	1	4.80×10^8	146.7
FD◊	FOS	22	1.5	0.9991	4.21×10^8	118.9

[†] Runs under saturated conditions are indicated by filled diamonds ♦; unsaturated runs are labeled by empty diamonds ◊.

[*] COS: Coarse Oamaru Sand; FOS: Fine Oamaru Sand.

[♠] Flow rate was calculated based on sample weight and sampling intervals.

Bacteria in the nutrient broth were centrifuged at 4000 rpm for 10 min and washed twice with deionised water. The strains were re-suspended in deionised water and adjusted to the initial concentration of c. 10^8 cfu mL^{-1}. Two subsamples (1 mL bacterial suspension into 9 mL peptone water) were collected to determine the initial bacterial concentration. 0.2 g sodium bromide (NaBr) was added to the suspension to reach a concentration of 0.01 g mL^{-1}. Once the sand column equilibrated, the polyester cloth and contact sand were removed and the bacterial suspension was

sprayed uniformly to the sand surface by a sprayer (Tamiya spraywork Air brush and compressor, Tamiya Inc., Japan). Then, the polyester cloth and sand were replaced, and the infiltrometer disk was reinstalled. The leachate collection was about 1 L every sample, with time interval ranging from 2 min for the COS column to 30 min for the FOS columns.

After each transport experiment, sand was emptied from the columns and autoclaved at 121 °C to remove all retained bacteria. The column and infiltrometer were sterilized by 75% ethanol solution. Before the start of new runs with the system, the initial leachate was checked to ensure no remaining bacteria from the last run. Experimental parameters for each run are listed in Table 7.

5.2.5. Sampling and assay

The leachate samples from each run of bacterial transport were collected in sterilized 1 L bottles or sterile plastic sample bags. Samples were stored at the cold room (7 °C) for no more than 12 hr. Bacterial concentration was measured by membrane filtration, serial dilution and plate counting in m FC agar. Weight of samples was measured for the calculation of dimensionless transport time i.e. pore volume. Subsamples were collected from each sample into 30 mL vials for the analysis of bromide concentration. Bromide in the effluent was analyzed using a Dionex DX–120 Ion Exchange Chromatograph fitted with a Dionex AS 50 Autosampler and integrated by Chromeleon Peaknet 6.0.

5.2.6. Mathematical models

5.2.6.1. Equilibrium, one-site, and one-site + AWI kinetic models

To identify factors affecting on bacterial transport, mechanistic models have generally been employed to model the breakthrough curves to get important process parameters. Saturated bacterial transport through homogeneous porous media under steady water flow has been widely modeled by the convection-dispersion equation supplemented by a sink term accounting for attachment (Corapcioglu and Haridas 1985; Harvey and Garabedian 1991; Hornberger, Mills *et al.* 1992; Lenhart and Saiers 2002; Lindqvist, Cho *et al.* 1994; Tan, Gannon *et al.* 1994).

$$\frac{\partial c}{\partial t} = D\frac{\partial^2 c}{\partial z^2} - v\frac{\partial c}{\partial z} - k_1 c \tag{21}$$

Where c is bacterial concentration in water (cfu/mL), s is attached bacteria at solid-water interfaces in porous media (cfu/g), D is the dispersion coefficients (cm^2/min), v is pore water velocity (cm/min), k_1 is an adsorption rate constant (min^{-1}), t is time (min) and z is distance from the inlet (cm). If bacterial attachment to particle surfaces is considered as a relatively fast reaction and assumed to be an equilibrium process, it can be described as a linear isotherm.

$$s = K_d c \tag{22}$$

$$\frac{\partial s}{\partial t} = K_d \frac{\partial c}{\partial t} \tag{23}$$

Where K_d is a distribution coefficient (mL/g). The other type of reversible adsorption assumes a first-order kinetic reaction for the rates of adsorption and desorption from solid-water interfaces.

$$\frac{\rho_b}{\theta}\frac{\partial s}{\partial t} = k_1 c - \frac{\rho_b}{\theta} k_2 s \tag{24}$$

Where k_2 is a desorption rate constants (min^{-1}). This model is called the nonequilibrium one-site kinetic model. For bacterial transport under unsaturated conditions, another sink term must be added to the equation: the adsorption of bacteria at air-water interfaces. Because of the strong affinity of bacteria to AWI, this term can be modeled as an irreversible adsorption (Lewis, Pao *et al.* 2004; Schafer, Ustohal *et al.* 1998).

$$\frac{\partial c}{\partial t} = D\frac{\partial^2 c}{\partial z^2} - v\frac{\partial c}{\partial z} - k_1 c + k_2 \frac{\rho_b}{\theta} s - k_0 c \tag{25}$$

Where, k_0 indicates the rate constant of sorption at AWI (min^{-1}). Thus, the governing partial differential equation for one-dimensional bacterial transport in homogeneous, unsaturated porous media with first-order kinetic adsorption (or filtration) is

$$\frac{\partial c}{\partial t} + \frac{\rho_b}{\theta}\frac{\partial s}{\partial t} = D\frac{\partial^2 c}{\partial z^2} - v\frac{\partial c}{\partial z} - k_0 c \tag{26}$$

This one-site AWI model can be applied to experimental data by STANMOD 2.2 (U. S. Salinity Laboratory), by assuming the k_0 in this model to be μ (first-order decay coefficient) and f=0 (fraction of adsorption sites at equilibrium assumed to be zero) in the two-site nonequilibrium model (Toride, Leij *et al.* 1999). For the inert tracer (bromide) used in this study, the BTCs were fitted by the equilibrium model assuming no adsorption to sand particles.

5.2.6.2 Two-site, and two-site + AWI kinetic models

Fuller *et al.* (2000) reported that bacteria in intact core experiments were composed of a range of subpopulations of cells. The subpopulations of the same bacteria might have different adsorption affinities. Besides, sand particle surface might not be homogenous for bacterial adsorption. Considering the heterogeneity of cells and sand surface, it is better to include both equilibrium and kinetic bacterial adsorption in the CDE model. Thus, a two-site model which includes both equilibrium and first-order kinetic adsorption processes was developed to model unsaturated bacterial transport. The attachment of bacteria to air-water interfaces was still modeled as a first-order irreversible adsorption.

$$\frac{\partial c}{\partial t}+\frac{\rho_b}{\theta}\left(\frac{\partial s_1}{\partial t}+\frac{\partial s_2}{\partial t}\right)=D\frac{\partial^2 c}{\partial z^2}-v\frac{\partial c}{\partial z}-k_0 c \qquad (27)$$

Where c is bacterial concentration in water (cfu/mL), s_1 and s_2 is attached bacteria on porous media surfaces by equilibrium or kinetic adsorption, respectively (cfu/g), D is the dispersion coefficients (cm^2/min), v is the pore water velocity (cm/min), k_1 is the adsorption rate constant for adsorption at particle surfaces (min^{-1}), k_0 is adsorption coefficient at air-water interfaces, t is time (min) and z is distance from inlet (cm).

$$\frac{\partial s_1}{\partial t}=f\cdot K_d\frac{\partial c}{\partial t} \qquad (28)$$

The first-type adsorption sites were modeled as an equilibrium process. f is the fraction of exchange sites assumed to be at equilibrium adsorption.

$$\frac{\partial s_2}{\partial t}=(1-f)\frac{\theta}{\rho_b}k_1 c-k_2 s_2 \qquad (29)$$

The second-type adsorption sites were modeled as a first-order kinetic process. This model could be modeled by STANMOD 2.2 by assuming k_0 to be the first-order decay coefficient. The attachment coefficients are calculated as follows.

$$\begin{aligned} k_1 &= \alpha(R-1) \\ k_2 &= \alpha \end{aligned} \tag{30}$$

Where α is the first-order kinetic coefficient in CXTFIT, and R is the retardation factor. Modeling results from one-site and one-site + AWI models were compared with the two-site models. Also, Equilibrium and equilibrium + AWI models were used if STANMOD suggested the potential applicability.

5.2.6.3. Model evaluation and sensitivity analysis

The efficiency of the mathematical models to fit the experimental data is usually described by coefficient of determination, which is a dimensionless sum of squared errors (Hendry, Lawrence *et al.* 1999; Hornberger, Mills *et al.* 1992; Reddy and R. M. 1996). This coefficient is defined as

$$E = 1 - \frac{\sum_{i=1}^{N} (C_{fit}^{i} - C_{obs}^{i})^2}{\sum_{i=1}^{N} (C_{fit}^{i} - C_{avg})^2} \tag{31}$$

$$C_{avg} = \sum_{i=1}^{N} C_{obs}^{i} \Big/ N \tag{32}$$

Where, C_{fit}^{i} and C_{obs}^{i} are the fitted and observed bacterial concentration at time t_i, C_{avg} is the mean value of all N observed bacterial concentrations, and N is the number of observations. An E value close to unity indicates a good fit of the model to observed concentrations, whereas a value close to zero indicates a lack of fitness of the observed data by the selected model. The drawback of this method is that the larger concentration values were more heavily weighted in the expression. Therefore, the E value is combined with visual inspection analysis together to evaluate the goodness of fit.

To examine the effects of three fitting parameters (k_1, k_2, and k_0) in one-site kinetic

CDE model (or four parameters including k_1, k_2, k_0, and f in two-site model) on the predicted breakthrough curves, one selected key parameter varied while other parameters were kept constant. The range of parameter values generally covered possible bacterial transport in our sand column experiments. In CXTFIT 2.1, the input parameters β and ϖ for one-site + AWI model were calculated as:

$$\beta = \frac{1}{R} \tag{33}$$

$$\varpi = k_2 (R-1)\frac{L}{v} \tag{34}$$

Where β is a dimensionless partitioning variable; and ϖ is a dimensionless mass transfer coefficient. For two-site + AWI model, these two input parameters were calculated as:

$$\beta = \frac{1}{R} + f\left(1-\frac{1}{R}\right) \tag{35}$$

$$\varpi = k_2 R\frac{L}{v}(1-\beta) \tag{36}$$

To predict the bacterial concentration in leachate from sand columns, it was assumed that bacteria were introduced at the column top as a pulse injection with duration of 0.2 pore volume; the length of sand column was 40 cm; water flow rate was 10 cm min^{-1}; dispersion coefficient D was 3 cm^2 min^{-1}. Breakthrough curves using one-site and two-site models were employed to analysis effects of key parameters on the model prediction.

5.3. Results

5.3.1. Characteristics of Oamaru sand

The physical and surface properties of Oamaru sands used are listed in **Table 8**. Coarse Oamaru sand (COS) has a grain size ranging 500 to 2400 μm, while fine Oamaru sand (FOS) ranges from 75 to 500 μm. Though both COS and FOS have very similar value of particle density, porosity, and bulk density, their specific surface area differed by a factor of about seven.

Table 8. Characteristics of Oamaru sand COS and FOS.

Sand	*COS*	*FOS*
Grain size	500 ~ 2360	75 ~ 500
Specific surface area (cm^2/g)	26.2	182.7
Bulk density (g/cm^3)	1.61	1.63
Particle density (g/cm^3)	2.67	2.65
Porosity θ	0.398	0.384

Figure 23 shows the particle and pore size distributions of Oamaru sands. The particles of COS are distributed mainly around diameter of 1.18 mm, namely above 70%, and about 15% at 0.6 and 2.36 mm, respectively. FOS has a much wider distribution of particle sizes, concentrated in the range from 0.2 to 0.4 mm. Only 10% of FOS sand particles have size less than 0.2 mm and greater than 0.4 mm. The pore size for COS was distributed mainly between 200 and 600 μm, with about 10% at 30 μm, and 5% greater than 600 μm. Pores of other sizes accounted for less than 2%. By contrast, FOS has most pores in the range 30 μm to 60 μm. About 7% of pores for FOS were around diameters of 40, 70, 90, 110 μm. The majority of FOS pores has diameters about one log of magnitude smaller than COS.

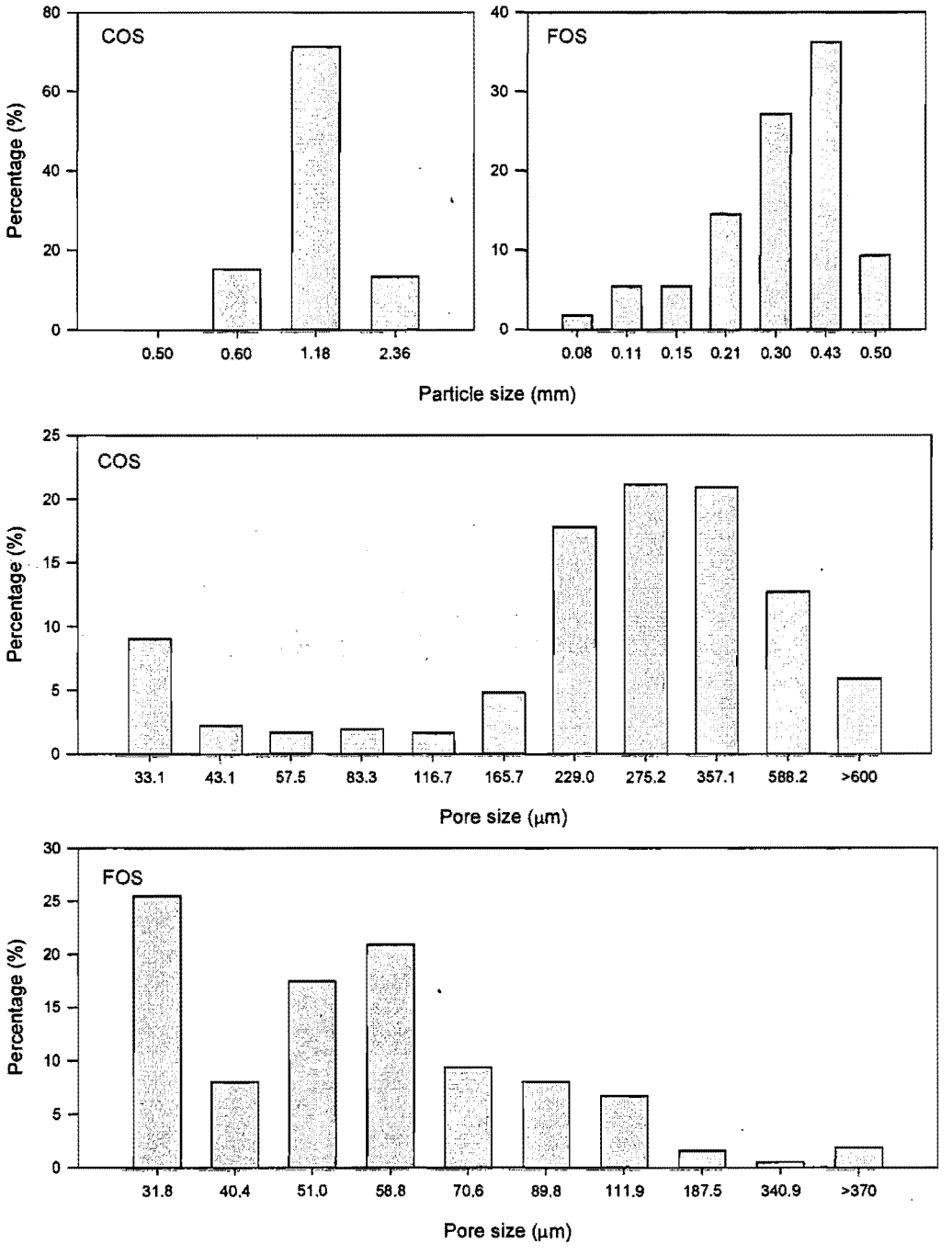

Figure 23. Particle and pore size distributions for the Oamaru sands.

Figure 24 shows the measured moisture characteristics (water content θ vs. matric suction) of coarse and fine Oamaru sand. Van Genuchten models (van Genuchten 1980) for water content was used to fit the observed data and calculate the relative conductivity. The water content and conductivity of COS decreased abruptly from a suction of 0 kPa (saturated) to 1 kPa. However, the θ and conductivity of a FOS didn't

change significantly as matric suction increased from 0 to 2 kPa. This difference of moisture release characteristics was determined by the disparity of their pore size distributions. As observed in the different runs of experiment, different suctions (water content) for FOS sometimes gave no big difference of water flow rate. This could be explained by the fact that no obvious change of conductivity exists for FOS from suctions of 0 to 2 kPa. The fitted parameters were used to calculate water content and saturation in the experiment from measured values of matric suction by tensiometers.

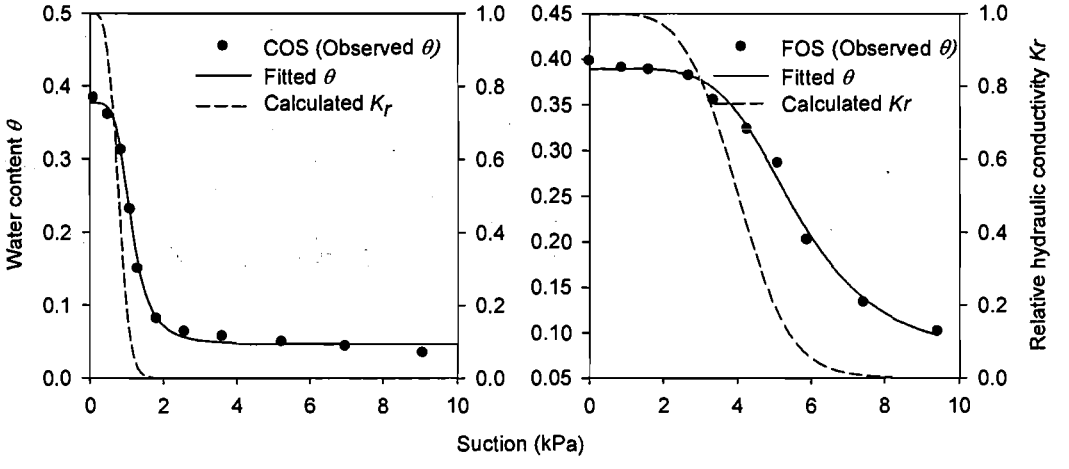

Figure 24. Moisture characteristics for coarse and fine Oamaru sand (COS and FOS).

5.3.2. Saturation, and matric suction

Figure 25 and **Figure 26** show the degree of saturation with the column depth for bacterial transport through COS and FOS experiments. For the saturated COS experiments, both 44 cm and 22 cm sand columns had very uniform saturation of unity, i.e. a fully saturated condition. However, unsaturated experiments $CB^{\Diamond}$ and $CD^{\Diamond}$ didn't have such uniform water saturation. $CB^{\Diamond}$ had a large variation of saturation, varying from 0.53 to 0.8 at four depths. Experiment $CD^{\Diamond}$ had 0.3 and 0.77 saturation degree at top and bottom. This nonuniformity resulted from the moisture release characteristics of the COS, as shown in **Figure 24**. Although water saturation was not uniform in the sand columns, the suctions at different depths and water flow rate during the trial period were stable. The average saturation and water flow rate were employed in the mathematical modeling.

For both saturated and unsaturated FOS experiments, the saturation was uniform in the columns, as shown in **Figure 26**. When suctions are less than 2 kPa, the water content and conductivity is not so sensitive to suction changes for FOS. $FB^{\diamond}$ and $FD^{\diamond}$ applied only 1.3 and 1.5 kPa suction, which fell in the insensitive moisture range. Thus, FOS experiments were expected to have similar degree of saturation in columns and water flow rate. As shown in Table 7, unsaturated experiment $FB^{\diamond}$ had a similar flow rate as saturated $FA^{\blacklozenge}$.

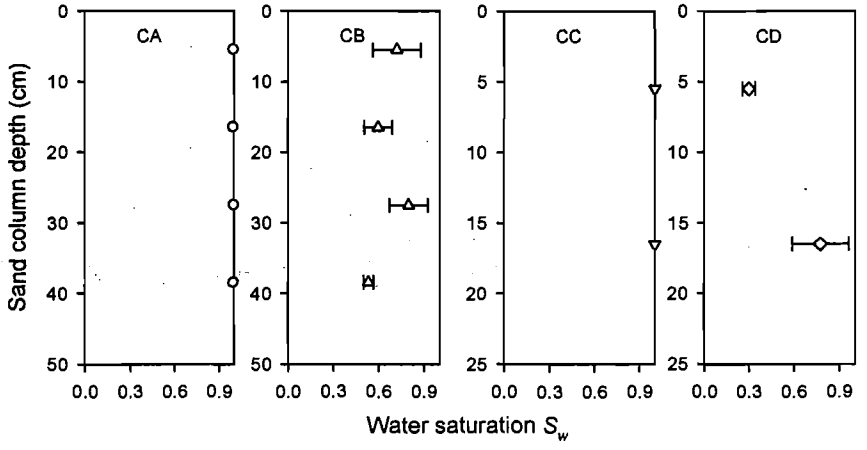

Figure 25. Distribution of degree of saturation in COS sand columns. Error bars are standard deviations for saturation variance during the whole leaching event.

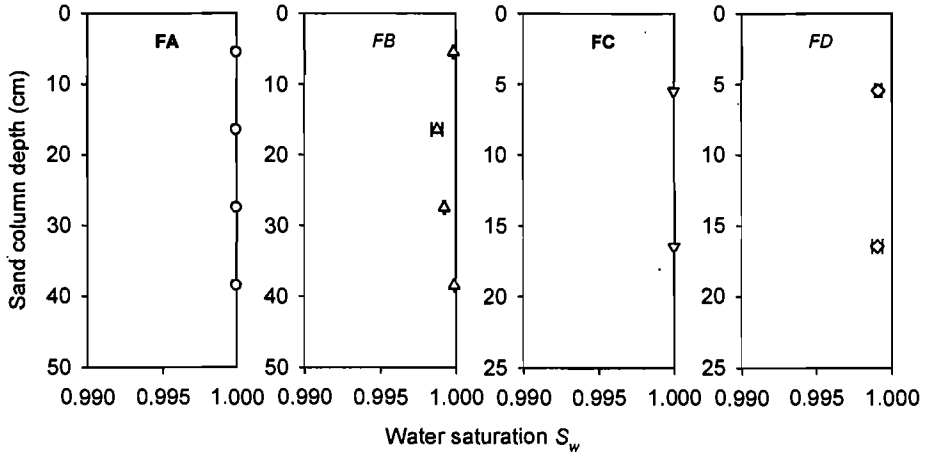

Figure 26. Distribution of degree of saturation in FOS sand columns. Error bars are standard deviation for saturation variance during the whole leaching event.

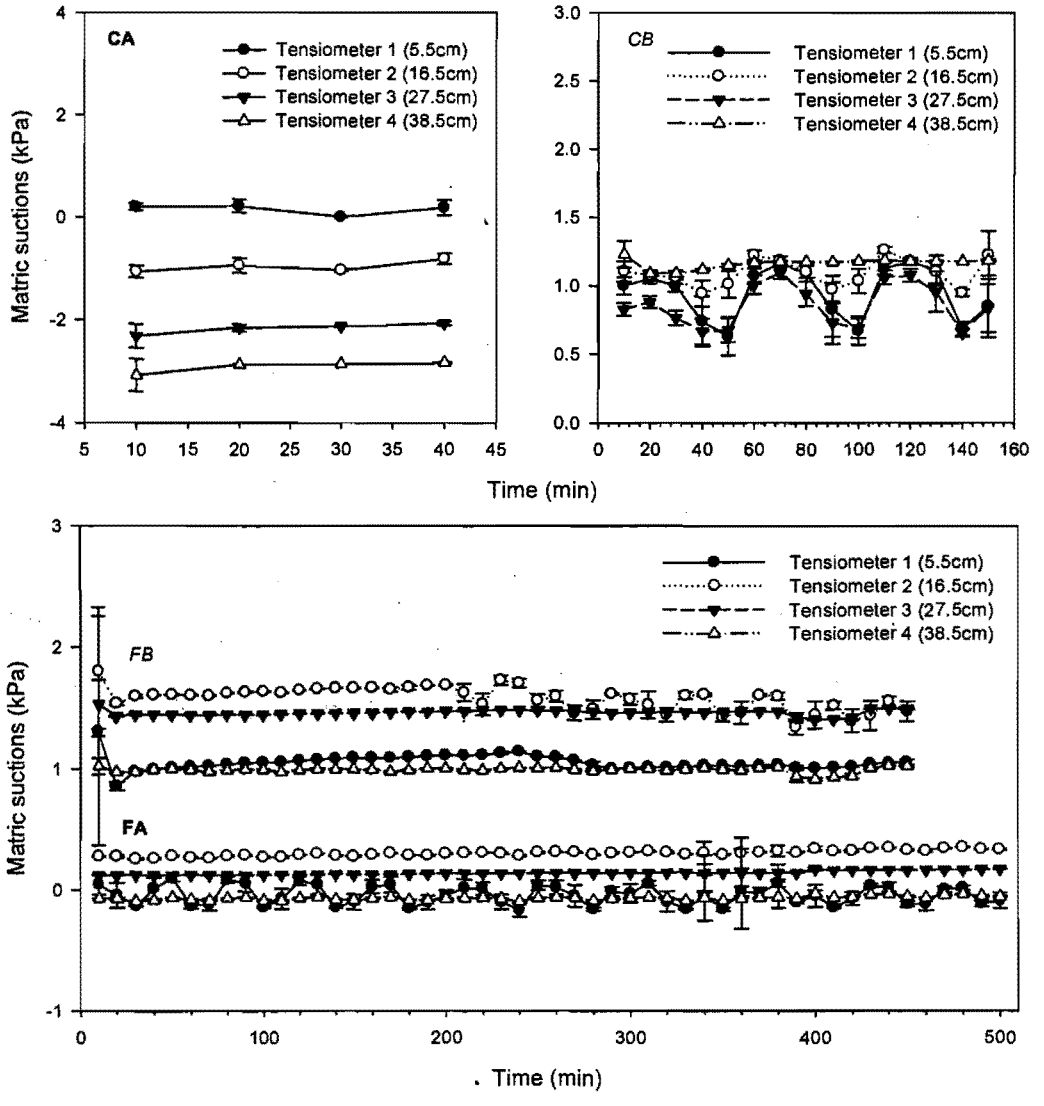

Figure 27. Matric suctions for COS experiments CA$^{\blacklozenge}$, CB$^{\lozenge}$ and FOS experiments FA$^{\blacklozenge}$, FB$^{\lozenge}$. Error bars indicate standard deviation of measured suctions in 10 min.

Figure 27 shows the variations of matric suctions for selected transport experiments CA$^{\blacklozenge}$, CB$^{\lozenge}$, FA$^{\blacklozenge}$, and FB$^{\lozenge}$. For COS experiments, suction always had greater variation for both saturated and unsaturated sand columns. This is probably caused by the bigger pore sizes and higher flow rate. The water phase (and air phase if unsaturated) in COS sand columns could be changed more rapidly with small changes of environmental factors. FOS experiments had better uniformity of suctions. It is noticed that tensiometer 1 (top) and tensiometer 4 (bottom) coincide with each other for FA$^{\blacklozenge}$ and FB$^{\lozenge}$. This is because the tension infiltrometer and hanging siphon tube controlled the matric suction at the top and bottom respectively, which resulted in the

water potential being close to the imposed values. The scattering nature of matric suction values indicates a slightly nonuniformity of column packing. Especially for coarse sand columns, more precautions should be exercised because of its hydrodynamic properties.

5.3.3. Bacterial adsorption to Oamaru sand

The adsorption of *E. coli* at surfaces of the Oamaru sands was fitted by Langmuir and Freundlich isotherms (**Figure 28**). The Langmuir and Freundlich equations are expressed as:

$$C_s = \frac{S_{\max} K_L C_w}{1 + K_L C_w} \tag{37}$$

$$C_s = K_d C_w^{\,m} \tag{38}$$

Where C_s is the concentration of adsorbed bacteria (cfu/g) and C_w is the concentration of bacteria in supernatant after equilibrium has been reached (cfu/mL). S_{max} is the maximum adsorption sites per gram of sand (cfu/g); K_L is a constant related to binding energy (mL/cfu); K_d is a distribution (partition) coefficient (mL/g). The fitted S_{max} for COS and FOS is 1.45×10^{11} and 8.58×10^{12} cfu/g, which is not proportional to the specific sand surface area 26.16 and 182.71 cm^2/g. This observation suggested that bacterial adsorption to particles was not pure surface interactions. The size ratio between bacteria and adsorptive particles also contributed to the observed adsorption. According to fitted value of K_L, affinity of *E. coli* to FOS was higher than COS, namely 6.65×10^{-11} vs. 3.67×10^{-11} mL/cfu.

Simulation by Freundlich isotherm indicates that the partition coefficient K_d for FOS was about three orders of magnitude higher than COS, while the exponents m had no significant difference, i.e. 1.3 and 1.37. **Figure 29** shows that percent adsorption (PA) of *E. coli* to Oamaru sand was not correlated to the initial cell concentration from 10^4 to 10^8 cfu/mL. The average percent of adsorption for COS and FOS is 45.9 ± 7.8 % and 96.9 ± 3.2 %, respectively. The P_a values were also not proportional to the specific surface area.

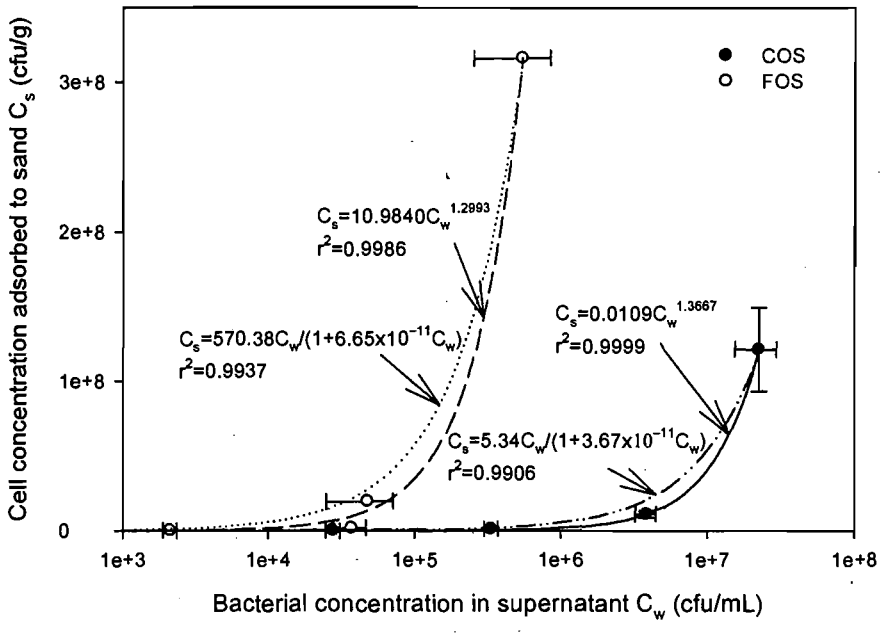

Figure 28. Adsorption of E. coli to COS and FOS in batch experiments, fitted by Langmuir and Freundlich isotherms. Horizontal and vertical error bars are standard deviation for C_w and C_s respectively.

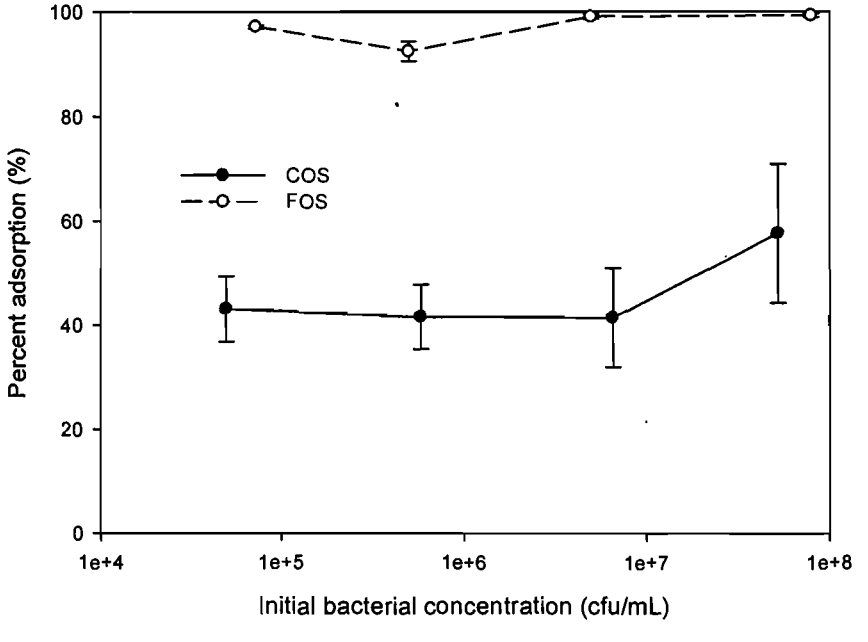

Figure 29. Percent adsorption vs. initial concentration of *E. coli*. Error bars are standard deviation of three replicates.

5.3.4. Model sensitivity analysis

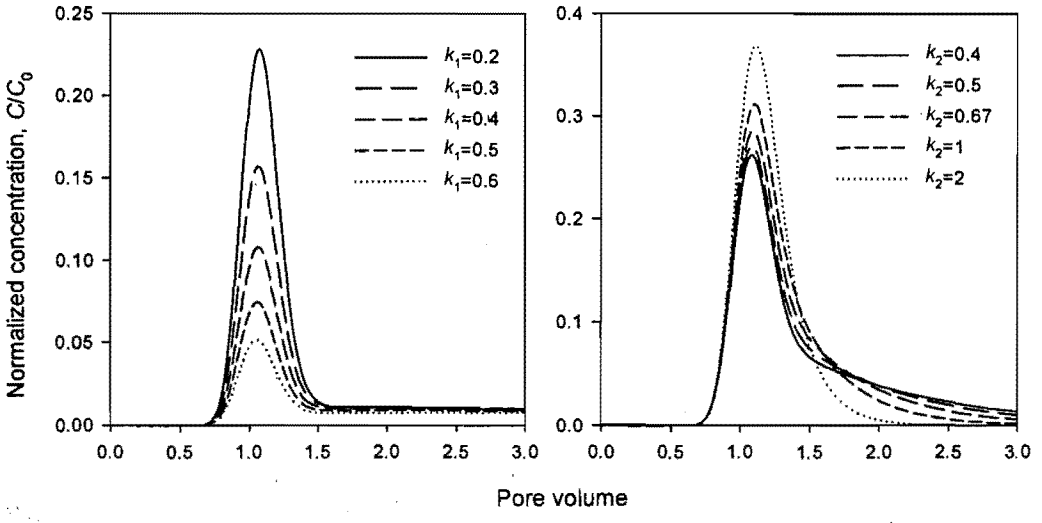

Figure 30. Effect of key model parameters (k_1 and k_2) on bacterial transport in sand columns, simulated by one-site + AWI model.

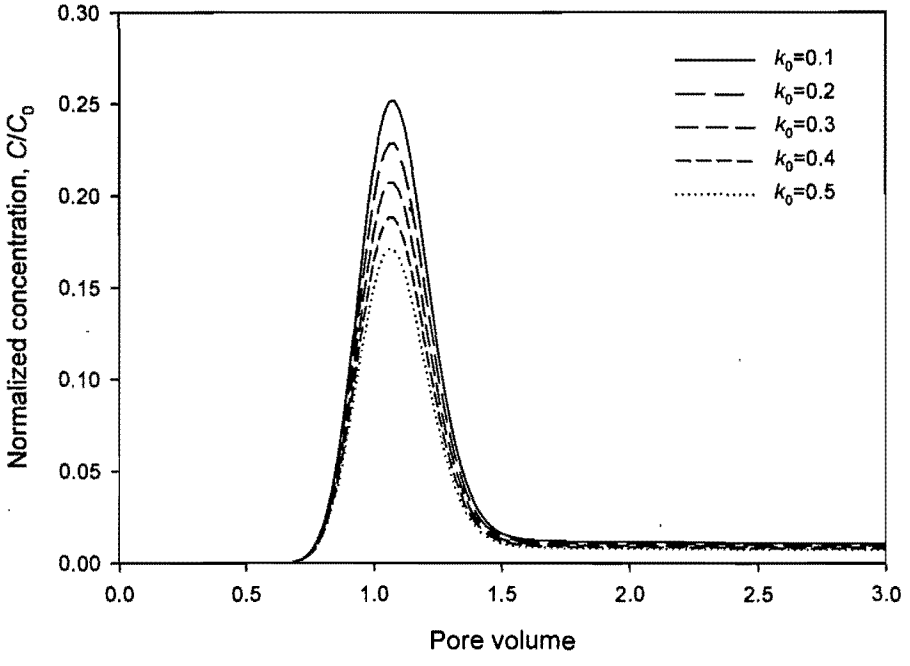

Figure 31. Effect of model parameter k_0 on bacterial transport in sand columns, simulated by one-site + AWI model.

For one-site + AWI model under the examined conditions (as specified in 2.6.3), an increase in k_1 resulted in decreased bacterial transport, which was obvious by comparing the peak height of BTCs. This has an implication that when bacterial affinity to porous media increases, the leached bacteria concentration will decrease significantly (**Figure 30**). An increased k_2 value cause the leached bacterial concentration to rise up, and tails of BTCs to move forward and disappear rapidly. As shown in **Figure 31**, the value of k_0 only affects the peak breakthrough concentration, without effects on the peak timing and tails of BTCs. In a word, the leached peak concentration is determined by all three parameters, while the tails of BTCs are influenced significantly by k_2.

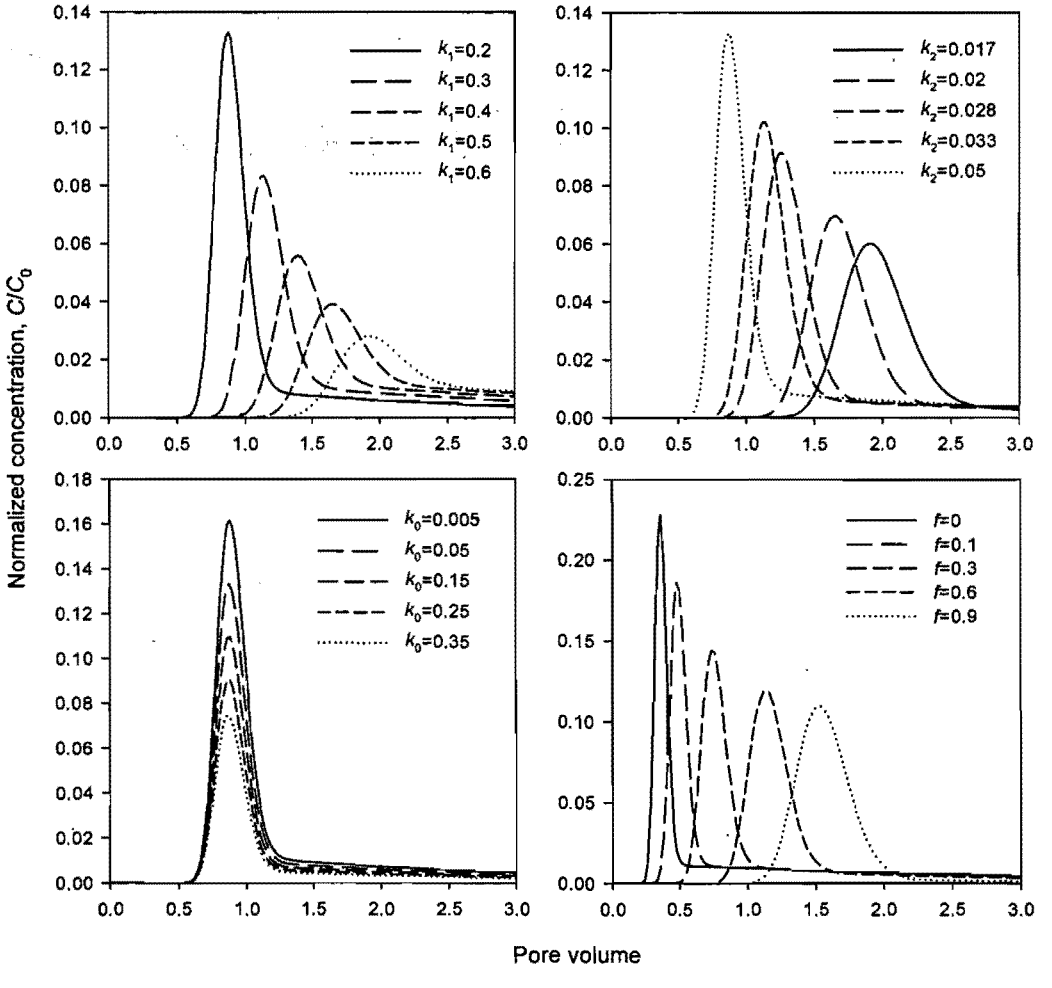

Figure 32. Effect of model parameter k_1, k_2, k_0, and f on bacterial transport in sand columns, simulated by two-site + AWI model.

Effects of four key model parameters on BTC prediction using two-site + AWI model was shown in **Figure 32**. The value of k_0 only impacts the peak concentration, which was the same as for one-site model. However, the peak timing of BTCs were dramatically affected by k_1, k_2, and f. Increased values of k_1 and f shifted the BTC peaks to bigger pore volumes, and resulted in lower peak concentrations. Whereas increased k_2 was just the opposite for predicted BTCs. Besides, k_1 had strong effect on the BTC tails in two-site model as k_2 in one-site model.

5.3.5. Bacterial breakthrough curves and modeling results

Recovery of bacteria and bromide after each leaching experiments (25 L leachate collected) is shown in Table 9. For the COS experiments, saturated runs $CA^{\blacklozenge}$ and $CC^{\blacklozenge}$ recovered over 80% of applied bacteria, roughly double the recovery of unsaturated runs $CB^{\lozenge}$ and $CD^{\lozenge}$. The recovery in the FOS long column experiments ($FA^{\blacklozenge}$ and $FB^{\lozenge}$) didn't show the same pattern. The saturated long column (44cm) $FA^{\blacklozenge}$ recovered ten times less of the total bacteria added than unsaturated $FB^{\lozenge}$. This is expected when considering that $FA^{\blacklozenge}$ had lower flow rate compared to $FB^{\lozenge}$ (see Table 7). $FC^{\blacklozenge}$ (22 cm short column) recovered 17.5% of injected bacteria, i.e. more than ten times higher than unsaturated $FD^{\lozenge}$. Column length showed no significant effects on bacterial recovery in the COS experiments. However, short columns with FOS recovered significantly more bacteria (1~2 log of magnitude) than long columns. Recovery of bromide reached about 70 % for both COS and FOS sand columns. Generally, saturated sand columns recovered slightly more bromide in leachate than unsaturated columns. However, the difference of bromide recovery between saturated and unsaturated columns was not as significant as bacterial recovery.

Bacterial concentration in the leachate of $CA^{\blacklozenge}$ was two times that of $CB^{\lozenge}$, which can be attributed to unsaturated flow of $CB^{\lozenge}$. $CC^{\blacklozenge}$ and $CD^{\lozenge}$ showed the same type of concentration ratio. However, the peak bacterial concentration for short columns $CC^{\blacklozenge}$ and $CD^{\lozenge}$ reached only half of $CA^{\blacklozenge}$ and $CB^{\lozenge}$. Considering the variance of bacterial enumeration, this difference was probably not significant. The exceptional lower leached concentration of $FA^{\blacklozenge}$ compared to $FB^{\lozenge}$ was caused by the lower flow rate of $FA^{\blacklozenge}$ (see Table 1). The ratio of concentrations between $FC^{\blacklozenge}$ and $FD^{\lozenge}$ is about 30, which indicates the strong effects of water saturation on bacterial transport through

fine sands.

Table 9. Recovery of bacteria and bromide after about 25 L of leachate collected.

Run ▲	*CA*♦	*CB*◊	*CC*♦	*CD*◊	*FA*♦	*FB*◊	*FC*♦	*FD*◊
Leachate volume (L)	25.64	25.90	28.14	27.82	26.96	27.73	25.23	25.33
Bacterial recovery (%)	89.00	54.36	80.71	44.25	0.002	0.03	17.45	1.42
Bromide recovery (%)	74.34	71.45	73.03	69.01	66.64	67.98	73.31	73.09

▲ Saturated and unsaturated sand columns are indicated by filled ♦ and empty diamonds ◊, respectively.

Fitted BTCs are shown in Figure 33 and **Figure 34**. For both COS and FOS, degree of saturation did not cause significant delay of bacterial breakthrough through sand columns except for CD◊ (Figure 33). Powelson and Mills (1998) also observed that unsaturated conditions delayed bacterial breakthrough. This is noticeable when comparing the model estimates of k_1/k_2 to that of Powelson and Mills (1998). Though effects of air-water interfaces and film straining could reduce the transport of bacteria (which might cause artifacts of relative breakthrough because of attachment, see (Zhang, Johnson *et al.* 2001a)), the stable interstitial water velocity could diminish this difference. We argue that change of water flow rate and sizes of water-filled pores with degree of saturation would not produce strong effects on breakthrough timing (normalized time, PV). Column length did not show any relationship to the timing of bacterial breakthrough. There was also no significant difference of the peak timing of bacterial breakthrough between COS and FOS experiments.

The Peclet number (Pe = vL/D, the ratio of advection to dispersion processes) for bacterial transport was calculated from estimated values of D and measured water flow velocity (see Table 11). We found that for all COS columns (short and long, saturated and unsaturated), the relative effect of advection increased when the AWI effect was added into the model. However, this change was not observed in fine sand columns FA, FC, and FD, probably due to the relatively weak effect of advection due to slow flow velocity. Nevertheless, advection is a much more dominant process in fine sand than coarse sand columns, i.e. higher Pe values for FOS. This is supported by low values of D in FOS columns, which suggests both advection and dispersion

decreased with slower water flow velocity. Pe values in Table 11 decreased with column length, which implies that the dispersion effect on bacterial transport was attenuated in longer columns.

Table 11 also shows that FOS had a higher AWI attachment rate, indicated by much higher values of k_0 compared to COS experiments. The bacterial adsorption rate at AWI was regarded as proportional to the area of AWI, which for saturation degree > 0.5, was assumed to be linearly proportional to the air content $(1-\theta)$ (Lewis, Pao *et al.* 2004; Schafer, Ustohal *et al.* 1998). Estimated values of k_0 from our experiments were not proportional to air content in sand column. This suggested that bacterial deposition at AWI might also depend on the contact time and degree of AWI scattering. Slow flow rate in FOS provides more contact time and opportunity for bacteria to adsorb at AWI. Also, air bubbles in FOS were distributed in smaller sizes than in COS, when the same air content was achieved. Another explanation of this observation was that air-water interfaces were more stable in FOS than COS columns.

The saturated sand could probably have some trapped air-bubbles, forming air-water interfaces for bacterial attachment. Though this might be not as significant as in unsaturated experiments, it would lead to part of bacterial retention in sand columns. Model estimated values of k_0 in Table 11 indicated that the ratio of saturated to unsaturated AWI adsorption coefficient was about 1/2 ($FC^{\blacklozenge}/FD^{\Diamond}$), 1/3 ($CA^{\blacklozenge}/CB^{\Diamond}$), and 1/5 ($CC^{\blacklozenge}/CD^{\Diamond}$). Exceptionally, no significant difference was observed for k_0 between saturated $FA^{\blacklozenge}$ and unsaturated $FB^{\Diamond}$. This suggested that $FA^{\blacklozenge}$ had more air-water interfaces than unsaturated $FB^{\Diamond}$. This unexpected higher AWI area might be caused by trapped air bubbles during the sand column packing. Also, trapped air in FOS columns was stable because of slow flow velocity and low hydrodynamic dispersion in fine sand.

When AWI adsorption was integrated into the two-site model, f value was increased at least ten times for all sand columns except $CA^{\blacklozenge}$. As can be seen from the model sensitivity analysis, bacterial adsorption at air-water interfaces was relatively irreversible and thus better modeled by first-order kinetic process. In two-site model, this part of bacterial retention was accounted for by bacterial adsorption at particle surfaces. Also, two-site model resulted in extremely large R, e.g. 575 and 321 for $FA^{\blacklozenge}$ and $FB^{\Diamond}$ respectively. The AWI amended two-site model could fit the observed data

and get more reasonable R values (see **Table 17**). This observation was also consistent with the results of one-site models.

One-site kinetic model could fit the bacterial breakthrough in saturated COS columns with as high performance as one-site + AWI model. However, the fitting capability of one-site model decreased for unsaturated COS columns. It was shown that one-site model failed to fit experimental data in both saturated and unsaturated FOS columns. By contrast, one-site + AWI model always fit bacterial breakthrough in both saturated and unsaturated, COS and FOS columns. Also, the descending limbs and tailing of BTCs were fitted better by one-site + AWI model compared to one-site model. Two-site and two-site + AWI models always fit well for both coarse and fine, saturated and unsaturated sand columns. Besides, equilibrium + AWI model also fit well to coarse sand column experiments. When comparing the model efficiency E listed in **Table 11**, **Table 17**, and **Table 18**, it is evident that two-site + AWI had the highest goodness of fitting.

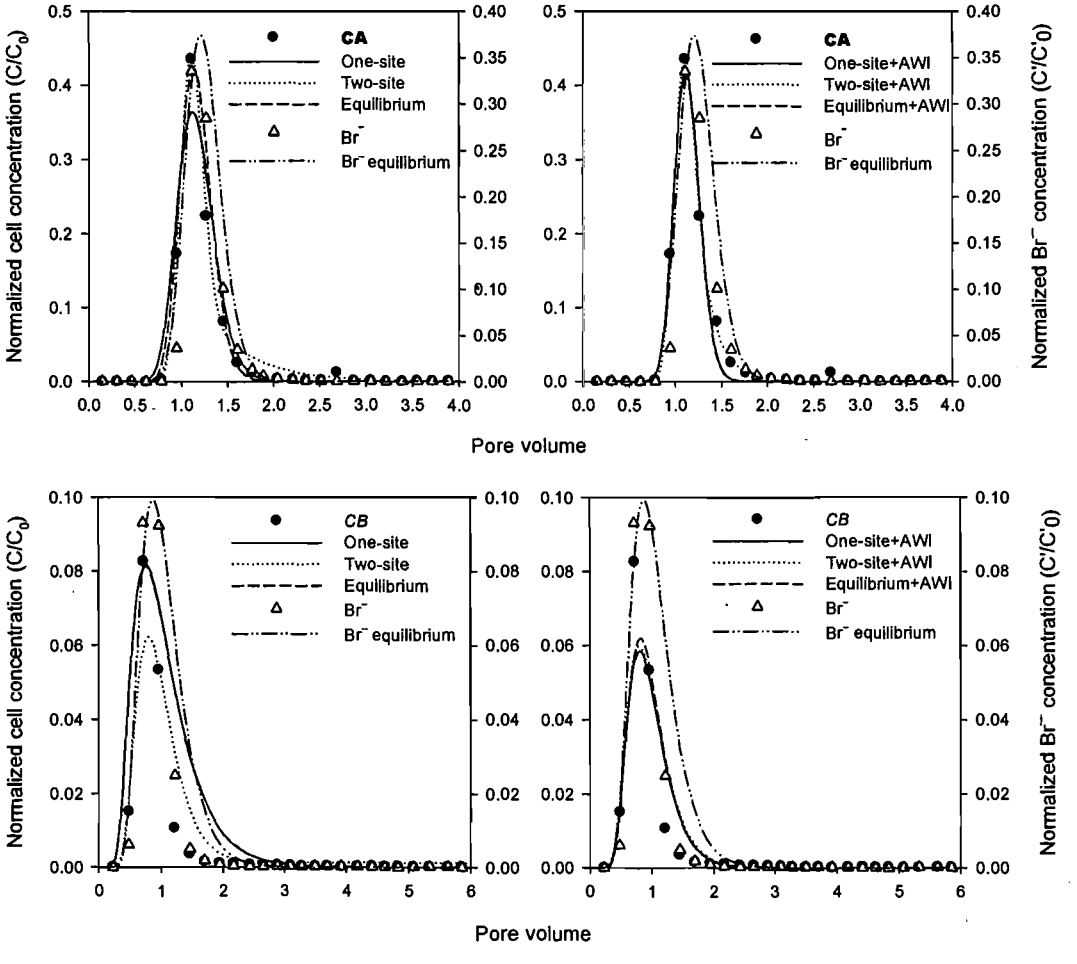

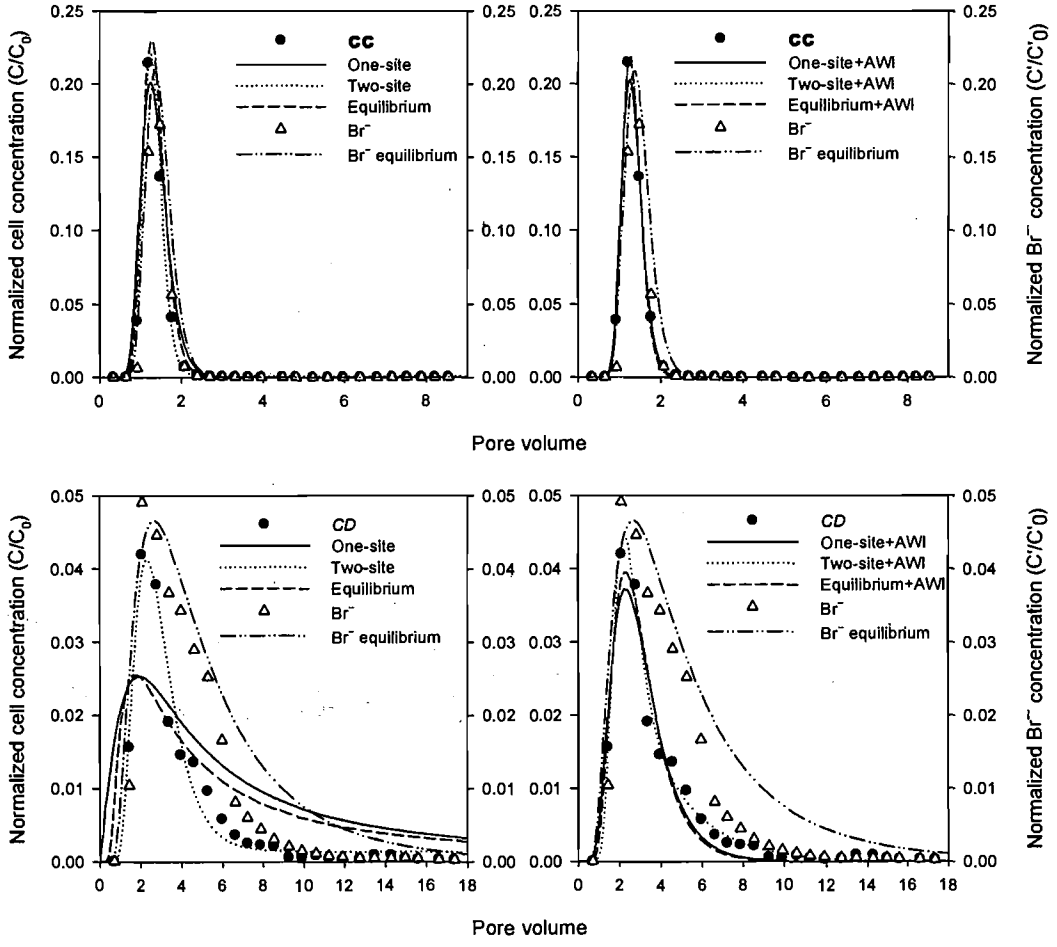

Figure 33. Bromide and bacterial breakthrough curves for COS experiments (CA$^{\blacklozenge}$, CB$^{\lozenge}$, CC$^{\blacklozenge}$, and CD$^{\lozenge}$), fitted by equilibrium, one-site, and one-site + AWI kinetic models. Saturated and unsaturated sand columns are labeled by bold and italic fonts, respectively.

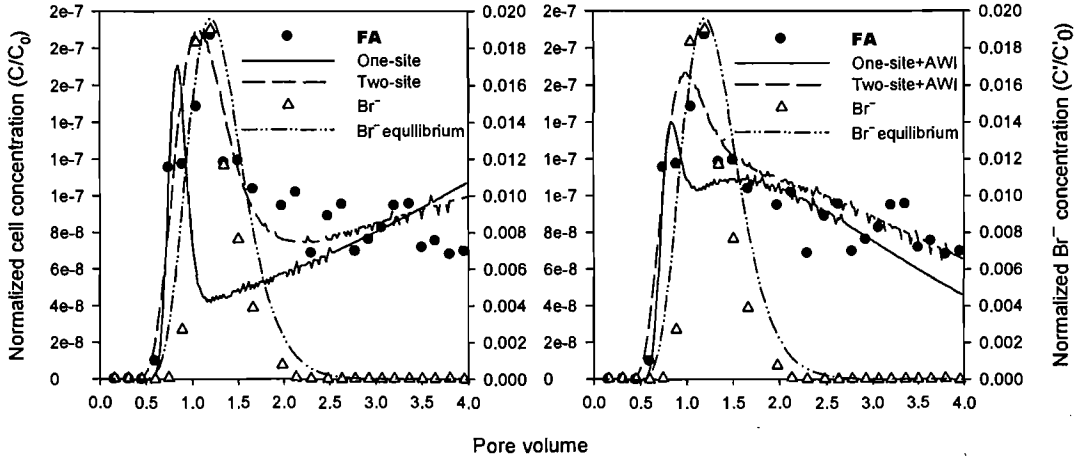

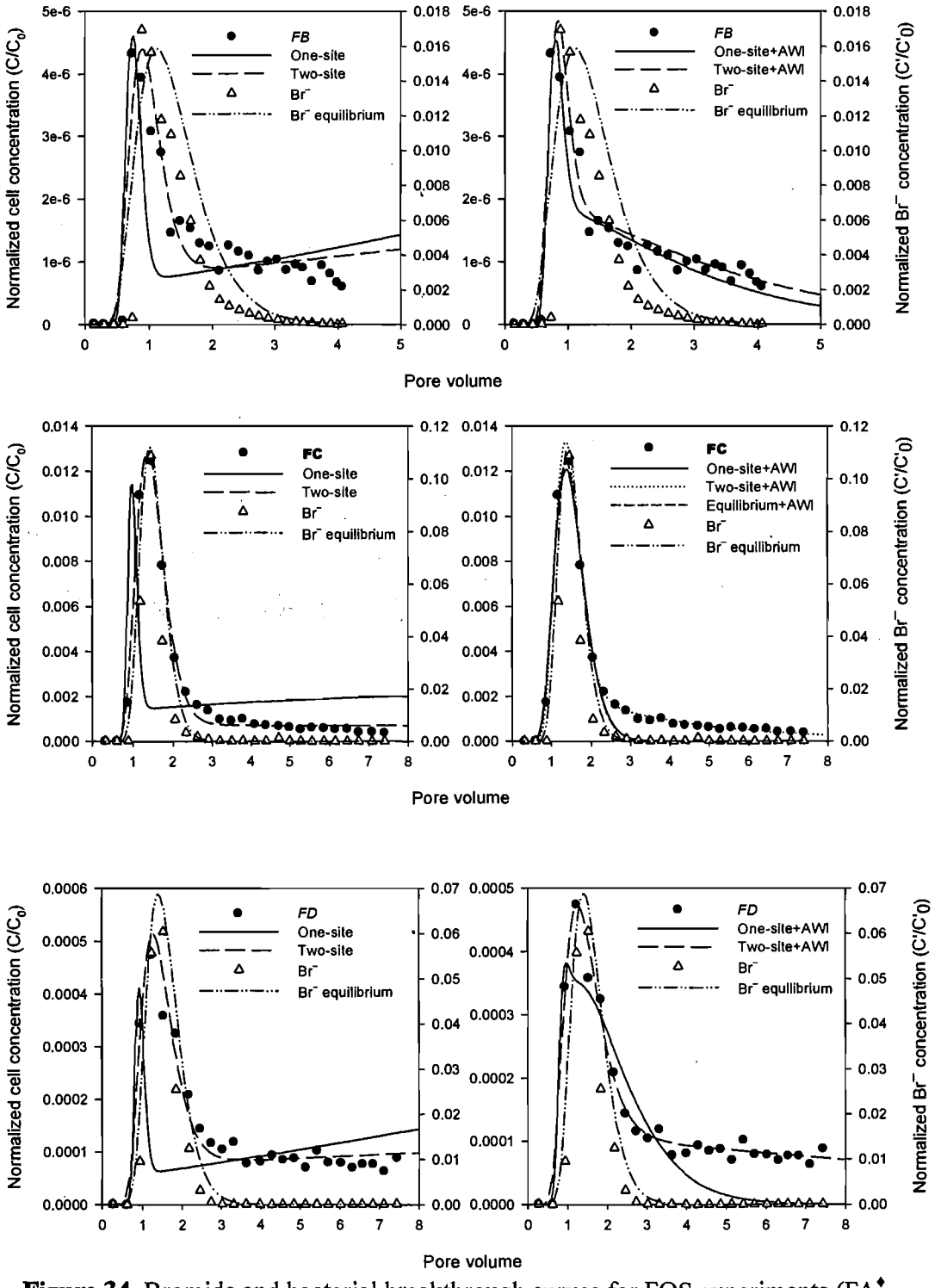

Figure 34. Bromide and bacterial breakthrough curves for FOS experiments (FA$^{\blacklozenge}$, FB$^{\lozenge}$, FC$^{\blacklozenge}$, and FD$^{\lozenge}$), fitted by equilibrium, one site, and one site + AWI kinetic models. Saturated and unsaturated sand columns are labeled by bold and italic fonts, respectively.

Table 10. Percent adsorption and distribution coefficient of *E. coli* with untreated and treated COS and FOS Oamaru sands.

Bacterial concentration level (cfu/mL)	*Adsorption (%)*		*Distribution coefficient (mL/g)*	
	COS	FOS	COS	FOS
10^4	43.1 ± 6.3	97.1 ± 0.3	0.34 ± 0.08	0.01 ± 0.00
10^5	41.6 ± 6.2	92.4 ± 1.9	0.36 ± 0.09	0.02 ± 0.01
10^6	41.4 ± 9.5	99.0 ± 0.5	0.38 ± 0.17	0.003 ± 0.001
10^7	57.5 ± 13.3	99.3 ± 0.4	0.20 ± 0.10	0.002 ± 0.001

Table 11. Estimates of parameters for one-site and one-site + AWI kinetic models[†].

Run[▲]	*Model*	k_0	k_1	k_2	k_1/k_2	*D*	*R*	*Pe*	*E*
CA[♦]	OS		11.79	155.1	0.076	3.68	1.08	62	0.9324
	OSA	0.21	11.79	240.5	0.049	1.72	1.05	132.5	0.9827
CB[◊]	OS		3.91	217	0.018	8.95	1.02	8.5	0.5817
	OSA	0.62	3.91	390.6	0.01	5.27	1.01	14.3	0.8677
CC[♦]	OS		7.76	26:7	0.29	1.18	1.29	31.8	0.9317
	OSA	0.23	7.76	30.1	0.26	0.73	1.26	51.8	0.9916
CD[◊]	OS		13.06	0.65	20.1	125.6	21.2	0.5	0.5323
	OSA	1.04	13.06	5.02	2.6	7.84	3.6	8.1	0.9496
FA[♦]	OS		0.11	0	164.3	0.11	165.3	131.4	0.0195
	OSA	11.51	0.03	0.01	2.22	0.13	3.2	112.4	0.7574
FB[◊]	OS		0.10	0	173.5	0.3	174.5	59.7	0.5282
	OSA	8.85	0.02	0.01	1.84	0.23	2.8	78.5	0.9260
FC[♦]	OS		0.15	0.01	24	0.15	25	138.9	0.0074

	OSA	2.16	4.30	5.87	0.73	0.86	1.73	24.4	0.9556
FD◊	OS		0.24	0	79.4	0.15	80.4	112.7	0.0841
	OSA	4.77	0.10	0.08	1.24	0.22	2.2	77.8	0.7386

† The first row represents estimates of one-site kinetic model (OS), the second row is estimates of one-site + AWI model (OSA).

▲ Saturated and unsaturated sand columns are indicated by filled and empty diamonds, respectively.

Table 12. Estimated model coefficients by two-site and two-site + AWI models †

Run▲	*Model*	k_0	k_1	k_2	k_1/k_2	K_d	f	D	R	Pe	E
CA♦	TS		0.05	0.25	0.19	0.044	0.13	1.28	1.19	178.5	0.9901
	TSA	0.14	0.08	0.88	0.089	0.021	0	1.72	1.05	242.0	0.9987
CB◊	TS		0.02	0.00	8.87	1.39	0	5.42	9.87	13.9	0.8706
	TSA	0.58	3.91	390.59	0.01	0.0016	0.56	5.68	1.01	13.3	0.8722
CC♦	TS		0.02	0.00	6.69	1.567	0.037	0.62	7.69	60.4	0.9971
	TSA	0.234	7.76	30.80	0.25	0.059	0.999	0.64	1.25	59.1	0.9969
CD◊	TS		0.14	0.00	67.3	7.667	0.034	6.29	68.29	10.1	0.9775
	TSA	4.77	0.10	0.04	2.76	0.314	0.58	3.24	3.76	19.5	0.9986
FA♦	TS		0.33	0.00	573.9	136.98	0.011	3.35	574.9	4.3	0.8394
	TSA	21.99	0.05	0.01	9.67	2.31	0.26	1.57	10.67	9.2	0.8716
FB◊	TS		0.16	0.00	319.6	76.25	0.005	1.10	320.6	16.3	0.8562
	TSA	9.58	0.02	0.01	2.89	0.69	0.094	0.47	3.89	38.1	0.9300
FC♦	TS		0.10	0.00	65.7	15.68	0.01	0.80	66.7	26.0	0.9917

	TSA	1.78	0.02	0.01	1.91	0.46	0.312	0.63	2.9	33.1	0.9990
FD$^{\diamond}$	TS		0.26	0.00	176.2	42.02	0.01	1.65	177.2	10.2	0.9470
	TSA	5.95	0.11	0.01	20.45	4.88	0.14	2.89	21.5	5.9	0.9748

† The first row of data was estimates from two-site model (TS); the second row was estimates from two-site + AWI models (TSA).

▲ Saturated and unsaturated columns are indicated by $^{\blacklozenge}$ and $^{\diamond}$, respectively.

Table 13. Estimated model coefficients by adsorption equilibrium (EQ) and equilibrium + AWI models (EQ + AWI).

Run[♦◊]	*Model*	*D*	*R*	K_d	k_0	*E*
CA[♦]	EQ	2.61	1.06	0.015	–	0.9516
	EQ + AWI	1.67	1.05	0.011	0.22	0.9829
CB[◊]	EQ	8.95	1.02	0.003	–	0.5817
	EQ + AWI	4.86	1.00	0.589	0.0002	0.8737
CC[♦]	EQ	0.89	1.27	0.064	–	0.9518
	EQ + AWI	0.63	1.25	0.059	0.24	0.9969
CD[◊]	EQ	1190	180.5	20.45	–	0.6608
	EQ + AWI	7.36	3.52	0.287	1.04	0.9572
FC[♦]	EQ + AWI	0.87	1.74	0.176	2.17	0.9582

[♦◊] Saturated and unsaturated columns are indicated by [♦] and [◊], respectively.

5.4. Discussion

5.4.1. Experimental design

Former soil lysimeter experiments (Jiang, Noonan *et al.* 2005) were designed to simulate the effects of irrigation on bacterial transport in an intact soil core, where the top layer of soils had been dried out more than the deeper layer as occurs frequently in pastures. The heterogeneity of soil pores made it difficult to determine at what depth in the soil core bacteria were being removed. Only the net removal of bacteria could be studied by determining the numbers of bacteria in the percolate. Unfortunately, once bacteria were applied to the soil lysimeter, the soil column could not be used again with the same bacteria because of the residual cells, if no effective method of sterilization was applied without destruction of the soil structure. One way to circumvent this problem is to use bacteria with minor differences in properties, such as resistance to different antibiotics.

To be able to study the phenomenon of bacterial movement under more controlled conditions, a new experimental approach was designed in this paper. Stable suctions and uniform pore size distribution throughout the whole column were needed. Also, it was necessary to sterilize the system (kill residual bacteria) without changing the properties of porous media. This system needed to be designed so that effects of macropores (>30 μm) on the movement of bacteria compared to micropores could be studied by changing the suction.

Experiments reported in the literature usually used a hanging tube to control the suction at the bottom of columns (Jewett, Logan *et al.* 1999; Saiers and Lenhart 2003; Schafer, Ustohal *et al.* 1998). The disadvantage associated with the hanging tubes was the mixing and dispersion of bacterial concentration in siphon. The former experiment used a tension infiltrometer to control the suction at the top of the soil lysimeter (Jiang, Noonan *et al.* 2005). This experiment used both methods to achieve more even suctions throughout the sand column. The tension infiltrometer at the top and a hanging tube at the bottom of the sand column help to keep a constant flow rate and stable suction.

The virtues of our experimental setup are well-controlled water flow and suctions, continuously-monitored water potential and infiltration rate, capable of reproducible tests. These features are especially useful for studies of bacterial transport. However, some

shortcomings of the system were also realized. The inserted tensiometers might interfere with the water flow in sands. Even with uniform packing of sands, the system could not reach uniform water content with the column depth. Also, it was found that autoclaving sands at 121 °C possibly reduced sand particle sizes. It was recommended new sands were used to pack sand columns for different tests. The packing procedure also produced big influence on the hydraulic conductivity, and therefore bacterial transport. A constant packing procedure must be employed throughout for a series of tests.

5.4.2. Bacterial adsorption

The adsorption of *E. coli* strain D to coarse and fine silica sands measured by batch experiments showed that both the adsorption percentage and fitted maximum adsorption sites per surface area were not correlated with specific surface area. The maximum adsorption sites for FOS were about 10 times of that for COS, which suggests that bacterial adsorption is not linearly related to the contact surfaces. It has been reported that the sorption coefficient of bacteria to soil particles (K_d) measured by batch sorption experiments and that predicted by transport models were contrary, with one being directly proportional to the specific surface area and one not (Bengtsson and Ekere 2001). Also, our batch adsorption experiments determined the particle sizes as important factors affecting adsorption coefficient. This was not consistent to the findings of Bengtsson (2001). The relative importance between cell surface hydrophobicity and sand surface charge might account for the discrepancy. We also postulated that bacterial adsorption is not just related to specific surface area, but also different interactions (e.g. abrasion of solid phase surfaces, compression of the hydrodynamic boundary layer, and suspension degree of the particles) between cells and particle surface in COS and FOS. Thus, the applicability of results from batch adsorption experiments to bacterial transport was limited because of the dynamic feature of bacteria in sand columns.

Though some work reported that bacterial adsorption to soil mainly occurred in the first few minutes of contact and reached equilibrium very swiftly, i.e. from 15 to 20 minutes (Huysman and Verstraete 1993a). The conditions for batch adsorption were so different from bacterial adsorption processes in sand columns with flowing water. However, the measured percent of adsorption could be used as an indicator to estimate the recovery of bacteria in leachate. The PA for COS was 45.9%, and bacterial recovery for $CB^{\diamond}$ and $CD^{\diamond}$

was very close to the percentage of suspended bacteria (100 – 45.9 = 54.1%), i.e. 54.4% and 44.3%, respectively. However, $CA^{\blacklozenge}$ and $CC^{\blacklozenge}$ recovered much higher percentage of bacteria, which indicated that many bacteria reached the outlet pipe before they reached equilibrated adsorption. $FC^{\blacklozenge}$ and $FD^{\lozenge}$ showed the same trend as coarse sand columns, though $FA^{\blacklozenge}$ and $FB^{\lozenge}$ were exceptions because of its flow rate and hydraulic properties of fine sand, as discussed in 3.5 and 3.1.

For bacterial transport in sand columns, in addition to the effects of hydraulic properties, bacterial retention was mainly attributed to bacterial adsorption to particle surfaces and air-water interfaces. Cells attachment to fine sands was assumed to be easier and produced less detachment due to lower hydrodynamic shearing force. In a similar manner, bacterial adsorption to AWI increased with more unsaturated conditions (higher air-water interface area). Taking all these factors into consideration, unsaturated fine sand columns retained bacteria more than coarse sand columns because of slower water flow rate, greater particle surface area, and more scattered air-water interfaces.

5.4.3. BTCs

As shown in **Table 9**, recovery of bromide was not correlated with the length of column, sand particle sizes, and water content. This had an implication that bromide was a good inert tracer for water flow in porous media, and the leachate concentration of bromide could be used to determine changing ranges of important bacterial transport parameters, such as water flow rate and dispersion coefficient. The early breakthrough of bacteria relatively to conservative chemical tracers (e.g. bromide) has been reported frequently and pore size exclusion was the applicable explanation (Sinton, Noonan *et al.* 2000). For coarse sand columns, the early breakthrough of *E. coli* relative to bromide was evident for saturated and unsaturated flow conditions, namely 0.15, 0.11, 0.3, 0.3 pore volume for $CA^{\blacklozenge}$, $CB^{\lozenge}$, $CC^{\blacklozenge}$, and $CD^{\lozenge}$ respectively. The early breakthrough for fine sand columns was also discriminable except for $FA^{\blacklozenge}$. However, the early breakthrough for $FA^{\blacklozenge}$ can still be observed from the simulated BTCs. *E. coli* reached peak concentration *c.* 0.15, 0.3, 0.15 pore volume earlier than bromide for $FB^{\lozenge}$, $FC^{\blacklozenge}$, and $FD^{\lozenge}$ respectively.

For coarse sand columns, the ratio of *E. coli* peak concentration between saturated and unsaturated columns with the same length was *c.* 5 ($CA^{\blacklozenge}/CB^{\lozenge}$=5.5, $CC^{\blacklozenge}/CD^{\lozenge}$=5). This

ratio for FA$^{\blacklozenge}$/FB$^{\lozenge}$ and FC$^{\blacklozenge}$/FD$^{\lozenge}$ was 0.04 and 25.5, respectively. This suggested that bacterial retention in fine sands was more prominent than coarse sands even by decreasing the same degree of water content. This was supported by the fact that fine sands had higher adsorption affinity for bacteria and smaller pores with slower water flow, when compared with coarse sands.

The column length was showed to have no clear effects on the *E. coli* peak concentration. It was reported that *Bacillus subtilis* concentrated in top 10 cm of soils when applied to the soil lysimeter (Jiang, Noonan *et al.* 2005). Therefore, the differences observed between the 44 cm and 22 cm sand columns were mainly because of the different water flow rate. *E. coli* peak concentration for fine sand columns was at least ten times lower than coarse sand columns. Thus, sand particle size was a significant factor affecting bacterial transport and retention in porous media.

The tailing of breakthrough curves was observed in fine sand columns, as shown in **Figure 34**. The tailing of BTCs was mainly caused by bacterial adsorption and following reversible desorption from media surfaces. Another explanation was that some of applied bacteria was stored in pore water at suspended state, and was gradually replaced by flowing water.

5.4.4. Effects of matric suction

The relationship between matric suction and the biggest water-filled pore diameter can be described by capillary rise equation (Hillel 1998). The largest water-filled pore diameter for the experimental suctions of 1, 1.2, 1.3, 1.5 kPa was 300, 250, 230, 200 μm, respectively. The pores with diameter greater than these critical values will be emptied by suction, while smaller pores will be water-filled. The bacteria applied to sand columns with various suctions thus entered different sized pores. Under higher suctions, bacteria were trapped in smaller pores. Also, it has been reported that the smallest ratio of pore size to cell size T/C was 1.5 for bacteria entering a pore (Sirivithayapakorn and Keller 2003). From pore size distributions shown in Figure 23, both COS and FOS have pores well above the threshold value. Thus, bacterial entrapment into small pores was not significant in our experiments.

Water flow rate (water flux in a pore) is proportional to the fourth power of pore size, as

described by Poiseuille's law. Thus, the majority of water flow through a sand column is through bigger pores. Because of the difficulty in replacing water in small pores, the storage of initial applied bacterial suspension in pores with extremely slow flow velocity was a possible explanation of the greater bacterial retention observed in FOS compared to COS, and unsaturated compared to saturated columns. Thus, it is arguable that the matric suction, along with water content provides the best indicator of bacterial retention.

5.4.5. Modeling approaches

Bacteria will tend not to enter smaller pores because of extremely slow flow in these regions, thus irreversible attachment must have occurred considering the low recovery percent of bacteria in leachate after substantial volume of leachate collected (Sirivithayapakorn and Keller 2003). In unsaturated sand, this irreversible attachment was mainly due to adsorption to AWI and partly to sand grains. Thus, mechanistic models were developed by incorporating adsorption terms into traditional CDE model to simulate bacterial transport in saturated/unsaturated porous media.

In literature, bacterial adsorption has been previously modeled as an equilibrium or a kinetic term in CDE models (Corapcioglu and Haridas 1984; Harvey and Garabedian 1991; Lindqvist, Cho *et al.* 1994; Reddy and R. M. 1996). Equilibrium adsorption usually had to assume the adsorption reached equilibrium almost instantaneously. One-site kinetic could approach equilibrium process when the rates of attachment and detachment were the same. When only the total bacterial recovery in leachate was concerned, discrimination between equilibrium and kinetic adsorption may not be critical. In addition, bacterial concentrations are relatively low in nature compared with adsorption sites available in subsurfaces, so there is no need to include blocking or ripening effects in the model for bacterial transport in sand columns (Schafer, Ustohal *et al.* 1998).

However, for monitoring bacterial concentration in leachate and predicting bacterial spreading in large-scale field applications, more comprehended two-site models and two-site + AWI models were proposed to be more appropriate for complex field-scale applications. The proposed model could cope with variable water content, different porous media (coarse and fine media in our experiments) and water flow rate. It was obvious that two-site + AWI model had the highest model efficiency among all model approaches examined in this paper. Based upon discussion above, this model was

suggested as the most appropriate model for modeling bacterial transport in sand columns. However, f in two-site model could not be physically measured and the fitted value might just be an artifact. Although the intrinsic flaw associated with two-site + AWI model, it is still a simple and effective modeling approach.

5.5. Conclusion

A sand column leaching system with well-controlled water saturation and flow rate was built to investigate the effects of water saturation, particle size, and column length on leaching bacterial concentration. The special virtue of the experimental setup was well-controlled water flow and suctions (by both top tension infiltrometer and bottom hanging siphon tube), continuously-monitored water potential and infiltration rate, capable of reproducible tests. The adsorption of *E. coli* to silica sands was measured in batch adsorption experiments. Percent adsorption (P_a) of *E. coli* strain D to sands was not correlated with the initial cell concentration. The applicability of batch adsorption data to transport experiments was limited.

The breakthrough curves were fitted by modified one-site/two-site and AWI adsorption amended convection-dispersion kinetic model. The early breakthrough of *E. coli* relative to bromide was clear for all sand column transport experiments. The column length had no evident effects on the *E. coli* peak concentration, which support the observation that bacteria were retained in top ten centimeters of porous media. Because of stronger bacterial adsorption in fine sands, tailing of BTCs was prominent for all fine sand columns. Bacterial recovery in leachate from COS was significantly higher than FOS sand columns. Thus, particle size was a significant factor influencing bacterial transport and retention. Saturated columns with either COS or FOS also recovered more bacteria from the percolate than corresponding unsaturated columns.

Equilibrium, one-site, two-site and their AWI adsorption amended models were fitted to experimental data. Two-site + AWI model achieved constant high model efficiency for both coarse and fine sands, under either saturated or unsaturated flow conditions. Although this model had some intrinsic flaws, its goodness of fit, simplicity, and well-established mechanisms supported it as the most applicable modeling approach to the observed data.

Chapter Six
Conclusions and Suggestion on Future Research Directions

6.1. Conclusions

Understanding and knowledge of microbial transport in soils is crucial in addressing groundwater contamination, subsurface bioremediation, and agronomic use of GEMs. Bacterial transport in unsaturated soils is much less well understood than in saturated conditions, especially for intact soils. Though the effects of air-water interfaces and film straining have been proposed to explain the increased retention of bacteria, the effects of soil heterogeneity and pore size distribution on unsaturated bacterial transport are still unclear in the literature. Also, no appropriate mathematical models have previously been developed and verified rigorously. Our study aimed to clarify soil macropores, matric suction, pore size distribution, and column length on bacterial transport in unsaturated water flow. A mechanistic mathematical model for unsaturated bacterial transport was also developed to model bacterial transport in sand columns. Based on the experimental and modeling results, mechanisms of unsaturated bacterial transport were identified and an improved model was put forward.

The first experiment aimed to investigate the fate and transport of bacteria (endospores) in intact soils with different water saturations, and particularly the effect of low suction (and hence removal of water flow in the largest macropores). An intact soil column (50 cm diameter × 70 cm depth) with a tension infiltrometer was used to investigate the transport and deposition of *Bacillus subtilis* endospores (i.e. dormant and persistent bacteria) during saturated and unsaturated flows. Soil porosity and pore size distribution were measured. Porosity decreased with depth and macropores were concentrated in the topsoil. Three tensiometers and a temperature sensor were installed along the soil column to monitor matric suction and temperature. One particularly attractive feature of the experiment is that the tension infiltrometer empties pores greater than a specified diameter. This is especially important in differentiating effects of macropore flow and matric flow.

Breakthrough curves for bacteria and chemical tracer Br^- at 0 kPa and 0.5 kPa suction were obtained during the three-month leaching experiment. Bacterial breakthrough occurred earlier than the inert chemical tracer, which is consistent with effects of pore size exclusion. Also, saturated flow gave a significantly higher concentration and recovery ratio of leached bacteria than unsaturated flow, i.e. 51% vs. 0.88%. Recovery of Br^- in leachate at both suctions reached above 85%. The column was destructively sampled for deposited endospores at the completion of leaching. Bacterial deposition was concentrated in the top ten centimeters, then decreased abruptly, and then was relatively constant with column depth, although showing some irregularity at the bottom of the column.

To more fully investigate the factors which influence bacterial transport in porous media, a sand column leaching system with well-controlled water contents was built. Results for bacterial transport through silica sand columns under water saturated and unsaturated conditions are presented. The objective was to investigate the effects of water saturation, particle size, and column length on bacterial concentration in drainage, and to model the breakthrough curves by a modified traditional one site convection-dispersion kinetic model.

Bacterial recovery in leachate from COS columns were significantly higher than FOS sand columns after the same volume of leachate was collected. This was explained as FOS has slower water flow rate, higher particle surface area, and more scattered air-water interfaces. However, grain size did not show any effects on the timing of bacterial breakthrough. Although FOS sand had a much higher specific surface area, its affinity for bacteria was compromised by slow water velocity and weak dispersion effects in fine sand columns. Modeling by a one site + AWI approach also revealed that bacterial affinity to AWI is higher in FOS than COS. Also, bacterial adsorption at air-water interfaces was not just proportional to air content in porous media as suggested in literature. It is more likely that AWI adsorption is sensitive to the size of air bubbles and water flow velocity in the porous media.

Saturated columns with either COS or FOS also gave more bacterial recovery in leachate than corresponding unsaturated columns, except for columns FA (saturated) and FB (unsaturated). This is because saturation of FOS was very insensitive to change of matric suction under 2 kPa. Also, FOS usually trapped trace air more firmly which makes it very

difficult to reach fully saturated condition. Model estimated values of k_0 indicate that the ratio of adsorption coefficient to AWI between saturated and unsaturated is about 1/2 (columns FC/FD), 1/3 (columns CA/CB), and 1/5 (columns CC/CD). This is not directly proportional to the increases of air content in sand columns. Thus, the degree of saturation must be coupled with grain size to characterize unsaturated bacterial transport.

Column length had a nonsignificant effect on bacterial recovery, which suggests that bacterial retention mainly happens in the top layers of sand column. However, dispersion rather than advection effects are more prominent in short columns. The short residence time for bacteria in short columns also suggests that some adsorption processes were completed in a very short time, which could be simplified as an equilibrium, instantaneous process. This phenomenon could also act as a cornerstone for the development of a two-site + AWI model to supplement equilibrium adsorption.

6.2. Suggestions for future research

It is well-known that microbial transport shows different phenomena and outcomes at different scales: pore scale, column scale, and field scale (Ginn, Wood *et al.* 2002). This thesis mainly focused on the column scale. However, pore scale observations will help to construct a sound and comprehensive picture of mechanisms for bacterial transport in porous media. Field scale experiments are extremely useful for application of column scale experimental results or to acquire data for setting up regulations. In the sand column experiments, it was found that bacterial deposition at air-water interface was not proportional to air content. The extent of dispersion of the air content in porous media may also play an important role in AWI adsorption. Thus, it is useful to conduct some observations of the air-water interface in microscale, especially effect of air-bubbles sizes and water flow rate on the affinity for bacteria.

Regarding field scale experiments of bacterial transport, there are some technical problems associated with monitoring long-distance and long-term transport. In this case, other environmental factors, such as soil temperature, precipitation, sunlight etc. will all contribute to a certain degree to the fate and transport of microbes. Understanding of bacterial regrowth and die-off is becoming more important in field scale experiments. It is also conceivable that mathematical modeling of field bacterial transport will become more complicated. Field models must also consider heterogeneity of subsurface media,

and fluctuations of water flow velocity and water content. Thus, stochastic models may be better than traditional CDE analytical models.

There is also another field which has been overlooked. Early literature mainly focused on saturated transport of microbes. Later, unsaturated transport of bacteria gained more interest. However, the change of water content from saturated to unsaturated, and vice versa, might have some special features that need to be explored. Preliminary tension table experiments with small intact soil cores leads in this direction (Noonan *et al.*, personal communication). Other research was also found in the literature dealing with sand columns with fluctuating water content during experiments (Powelson and Mills 2001). The combination of changing water content with timing of bacterial application will provide useful information in respect of using animal waste as a fertilizer. In addition, bacterial transport in the natural subsurface involves passage through the unsaturated-saturated transition layer. How will the bacteria transport through this zone? Or, how will the fluctuation of water table influence the transport (and retention) of bacteria? The exploration of these effects will also contribute to the improvement of current bioremediation technology.

References

Bai G, Brusseau ML, Miller RM (1997) Influence of a Rhamnolipid biosurfactant on the transport of bacteria through a sandy soil. *Applied and Environmental Microbiology* **63**, 1866-1873.

Banks MK, Yu W, Govindaraju RS (2003) Bacterial adsorption and transport in saturated soil columns. *Journal of Environmental Science and Health Part a-Toxic/Hazardous Substances & Environmental Engineering* **38**, 2749-2758.

Becker MW, Collins SA, Metge DW, Harvey RW, Shapiro AM (2004) Effect of cell physicochemical characteristics and motility on bacterial transport in groundwater. *Journal of Contaminant Hydrology* **69**, 195-213.

Bell C, Kyriakides A (1998) 'E. coli A practical approach to the organism and its control in foods.' (Blackie Academic & Professional: London)

Bengtsson G, Ekere L (2001) Predicting sorption of groundwater bacteria from size distribution, surface area, and magnetic susceptibility of soil particles. *Water Resources Research* **37**, 1795-1812.

Benyahia F (2000) Bioremediation of soils contaminated by oil spills in the UAE: an engineering solution approach. In 'The Fourth Annual U.A.E. University Research Conference'. U.A.E. University pp. 6-8

Beven K, Germann P (1982) Macropores and water flow in soils. *Water Resources Research* **18**, 1311-1325.

Bitton G, Harvey RW (1992) Transport of pathogens through soils and aquifers. In 'Environmental Microbiology'. (Ed. R Mitchell) pp. 103-124. (Wiley-Liss)

Bolster CH, Mills AL, Hornberger GM, Herman JS (1999) Spatial distribution of deposited bacteria following miscible displacement experiments in intact cores. *Water Resources Research* **35**, 1797-1807.

Bolster CH, Mills AL, Hornberger GM, Herman JS (2000) Effect of intra-population variability on the long-distance transport of bacteria. *Ground Water* **38**, 370-375.

Bouma J (1991) Influence of soil macroporosity on environmental quality. In 'Advances in Agronomy' pp. 1-37. (Academic Press, Inc.)

Bouwer EJ, Rittmann BE (1992) Comment on "Use of colloid filtration theory in modeling movement of bacteria through contaminated sandy aquifer". *Environmental Science and Technology* **26**, 400-401.

Bradford SA, Yates SR, Bettahar M, Simunek J (2002) Physical factors affecting the transport and fate of colloids in saturated porous media. *Water Resources Research* **38**, 63.01-63.12.

Cameron KC, Smith NP, Mclay C, Fraser PM, McPherson RJ, Harrison DF, Harbottle P (1992) Lysimeter without edge flow: an improved design and sampling procedure. *Soil Science Society of America Journal* **56**, 1625-1628.

Camesano TA, Unice KM, Logan BE (1999) Blocking and ripening of colloids in porous media and their implications for bacterial transport. *Colloids and Surfaces A: Physicochemical and Engineering Aspects* **160**, 291-308.

Caron J, Banton O, Angers DA, Villeneuve JP (1996) Preferential bromide transport through a clay loam under alfalfa and corn. *Geoderma* **69**, 175-191.

Chapelle FH (1999) Bioremediation of petroleum hydrocarbon-contaminated ground water: the perspectives of history and hydrology. *Ground Water* **37**, 122-132.

Cherrey KD, Flury M, Harsh JB (2003) Nitrate and colloid transport through coarse Hanford sediments under steady state, variably saturated flow. *Water Resources Research* **39**, SWC4.1-SWC4.10.

Chu Y, Jin Y, Baumann T, Marylynn VY (2003) Effect of soil properties on saturated and unsaturated virus transport through columns. *Journal of Environmental Quality* **32**, 2017-2025.

Chu Y, Jin Y, Markus F, Marylynn VY (2001) Mechanisms of virus removal during transport in unsaturated porous media. *Water Resources Research* **37**, 253-263.

Corapcioglu MY, Choi KH (1996) Modeling colloid transport in unsaturated porous media and validation with laboratory column data. *Water Resources Research* **32**, 3437-3449.

Corapcioglu MY, Haridas A (1984) Transport and fate of microorganisms in porous media: A theoretical investigation. *Journal of Hydrology* **72**, 149-169.

Corapcioglu MY, Haridas A (1985) Microbial transport in soils and groundwater: A numerical model. *Advances in Water Resources* **8**, 188-200.

Czapar GF, Fawcett RS (1992) Herbicide and tracer movement in soil columns containing an artificial macropore. *Journal of Environmental Quality* **21**, 110-115.

Dane JH, Topp CG (2002) 'Methods of Soil Analysis Part 4 Physical Methods.' (Soil Science Society of America, Inc: Madison, Wisconsin, USA)

Dong H, Rothmel RK, Onstott TC, Fuller ME, DeFlaun MF, Streger SH, Dunlap R, Fletcher M (2000) Simultaneous transport of two bacterial strains in intact cores from Oyster, Virginia: Biological effects and numerical modeling. *Applied and Environmental Microbiology* **68**, 2120-2132.

Doyle RJ, Nedjat-Haiem F, Singh JS (1984) Hydrophobic characteristics of *Bacillus* spores. *Current Microbiology* **10**, 329-332.

Dunsmore BC, Bass CJ, Lappin-Scott HM (2004) A novel approach to investigate biofilm accumulation and bacterial transport in porous matrices. *Environmental Microbiology* **6**, 183-187.

Edmonds RL (1976) Survival of coliform bacteria in sewage sludge applied to a clearcut forest and potential movement into groundwater. *Applied and Environmental Microbiology* **32**, 537-546.

El-Farhan YH, Denovio NM, Herman JS, Hornberger GM (2000) Mobilization and transport of soil particles during infiltration experiments in an agriculture field, Shenandoah Valley, Virginia. *Environmental Science and Technology* **34**, 3555-3559.

Finneran KT, Housewright ME, Lovley DR (2002) Multiple influences of nitrate on

uranium solubility during bioremediation of uranium contaminated subsurface sediments. *Environmental Microbiology* **4**, 510-516.

Fontes DE, Mills AL, Hornberger GM, Herman JS (1991) Physical and chemical factors influencing transport of microorganisms through porous media. *Applied and Environmental Microbiology* **57**, 2473-2481.

Fuller ME, Dong H, Mailloux BJ, Onstott TC, DeFlaun MF (2000) Examining bacterial transport in intact cores from Oyster, Virginia: Effect of sedimentary facies type on bacterial breakthrough and retention. *Water Resources Research* **36**, 2417-2431.

Gannon JT, Manilal VB, Alexander M (1991) Relationship between cell surface properties and transport of bacteria through soil. *Applied and Environmental Microbiology* **57**, 190-193.

Gerba CP (1985) Microbial contamination of the subsurface. In. (Eds CH Ward, W Giqer and PL McCarty) pp. 53-67. (Willey Interscience)

Gerba CP, Smith JE (2005) Sources of pathogenic microorganisms and their fate during land application of wastes. *Journal of Environmental Quality* **34**, 42-48.

Germann PF, Alaoui A (2002) Drag force approach to the transport of colloids in unsaturated soils. *Water Resources Research* **38**, 18.01-18.15.

Ginn TR (2002) A travel time approach to exclusion on transport in porous media. *Water Resources Research* **38**, 12.01-12.12.

Ginn TR, Wood BD, Nelson KE, Scheibe TD, Murphy EM, Clement TP (2002) Processes in microbial transport in the natural subsurface. *Advances in Water Resources* **25**, 1017-1042.

Grolimund D, Elimelech M, Borkovec M, Barmettler K, Kretzschmar R, Sticher H (1998) Transport of in situ mobilized colloidal particles in packed soil columns. *Environmental Science and Technology* **32**, 3562-3569.

Hagedorn C, Hansen DT, Simonson GH (1978) Survival and movement of fecal indicator bacteria in soil under conditions of saturated flow. *Journal of Environmental Quality* **7**, 54-59.

Harvey RW, Garabedian SP (1991) Use of colloid filtration theory in modeling movement of bacteria through a contaminated sandy aquifer. *Environmental Science and Technology* **25**, 178-185.

Hekman WE, Heijnen CE, Trevors JT, van Elsas JD (1994) Water flow induced transport of *Pseudomonas fluorescens* cells through soil columns as affected by inoculant treatment. *FEMS Microbiology Ecology* **13**, 313-324.

Hendry MJ, Lawrence JR, Maloszewski P (1999) Effects of velocity on the transport of two bacteria through saturated sand. *Ground Water* **37**, 103-112.

Hermansson M (1999) The DLVO theory in microbial adhesion. *Colloids and Surfaces B: Biointerfaces* **14**, 105-119.

Hillel D (1998) 'Environmental Soil Physics.' (Academic Press: San Diego, CA, USA)

Hornberger GM, Mills AL, Herman JS (1992) Bacterial transport in porous media: Evaluation of a model using laboratory observations. *Water Resources Research* **28**, 915-938.

Houston J, Learner MA, Dancer BN (1989) Selection of an antibiotic-resistant strain of *Bacillus subtilis* var. *niger* (*B. globigii*) for use as a tracer in microbially rich waters. *Water Research* **23**, 387-388.

Huysman F, Verstraete W (1993a) Water-facilitated transport of bacteria in unsaturated soil columns: Influence of cell surface hydrophobicity and soil properties. *Soil Biology and Biochemistry* **25**, 83-90.

Huysman F, Verstraete W (1993b) Water-facilitated transport of bacteria in unsaturated soil columns: influence of inoculation and irrigation methods. *Soil Biology and Biochemistry* **25**, 91-97.

Jabro JD, Lotse EG, Simmons KE, Baker DE (1991) A field study of macropore flow under saturated conditions using a bromide tracer. *Journal of Soil and Water Conservation*, 376-380.

Jackson A, Roy D, Breitenbeck G (1994) Transport of a bacterial suspension through a soil matrix using water and an anionic surfactant. *Water Research* **28**, 943-949.

Jewett DG, Logan BE, Arnold RG, Bales RC (1999) Transport of *Pseudomonas fluorescens* strain P17 through quartz sand columns as a function of water content. *Journal of Contaminant Hydrology* **36**, 73-89.

Jiang GM, Noonan MJ, Buchan GD, Smith NP (2005) Transport and deposition of *Bacillus subtilis* through an intact soil column. *Australian Journal of Soil Research* **43**, 695-703.

Jin Y, Flury M (2002) Fate and transport of viruses in porous media. *Advances in Agronomy* **77**, 39-102.

Keller AA, Sirivithayapakorn S (2004) Transport of colloids in unsaturated porous media: Explaining large-scale behavior based on pore-scale mechanisms. *Water Resources Research* **40**, W12403.

Kinoshita T, Bales RC, Yahya MT, Gerba CP (1993) Bacteria transport in a porous medium: retention of *Bacillus* and *Pseudomonas* on silica surfaces. *Water Resources* **27**, 1295-1301.

Kunze GW, Dixon JB (1986) Pretreatment for mineralogical analysis. In 'Methods of Soil Analysis, Part 1'. (Ed. A Klute). (ASA and SSSA: Madison, WI)

Lance JC, Gerba CP (1984) Virus movement in soil during saturated and unsaturated flow. *Applied and Environmental Microbiology* **47**, 335-337.

Lenhart JJ, Saiers JE (2002) Transport of silica colloids through unsaturated porous media: experimental results and model comparisons. *Environmental Science and Technology* **36**, 769-777.

Lewis RW, Pao WKS, Yang X-S (2004) Instability and reaction-diffusion transport of bacteria. *Communications in Numerical Methods in Engineering* **20**, 777-787.

Li Q, Logan BE (1999) Enhancing bacterial transport for bioaugmentation of aquifers using low ionic strength solutions and surfactants. *Water Research* **33**, 1090-1100.

Lindqvist R, Cho JS, Enfield CG (1994) A kinetic model for cell density dependent bacterial transport in porous media. *Water Resources Research* **30**, 3291-3299.

Ling TY, Achberger EC, Drapcho CM, Bengtson RL (2002) Quantifying adsorption of an indicator bacteria in a soil-water system. *Transactions of the ASAE* **45**, 669-674.

Liu CX, Gorby YA, Zachara JM, Fredrickson JK, Brown CF (2002) Reduction kinetics of Fe(III), Co(III), U(VI), Cr(VI), and Tc(VII) in cultures of dissimilatory metal-reducing bacteria. *Biotechnology and Bioengineering* **80**, 637-649.

Loosdrecht MCMv, Lyklema J, Norde W, Schraa G, Zehnder AJB (1987) The role of bacterial cell wall hydrophobicity in adhesion. *Applied and Environmental Microbiology* **53**, 1893-1897.

Lorch HJ, Benckieser G, Ottow JCG (1995) Basic methods for counting microorganisms in soil and water. In 'Methods in Applied Soil Microbiology and Biochemistry'. (Eds K Alef and P Nannipieri). (Academic Press)

Mailloux BJ, *et al.* (2003) The role of physical, chemical, and microbial heterogeneity on the field-scale transport and attachment of bacteria. *Water Resources Research* **39**, SBH2.1-SBH2.17.

Martin GN, Noonan MJ (1977) 'Effects of domestic wastewater disposal by land irrigation on groundwater quality of the central Canterbury plains.' Ministry of Works and Development, Christchurch, New Zealand; Department of Agricultural Microbiology, Lincoln College, Canterbury, New Zealand, Water & Soil Technical Publication No. 7, Wellington.

Matthess G, Pekdeger A (1985) Survival and transport of pathogenic bacteria and viruses in ground water. In 'Ground Water Quality'. (Eds CH Ward, W Giger and PL McCarthy) pp. 477-482. (John Wiley and Sons Inc.: New York)

McCaulou DR, Bales RC (1995) Effect of temperature-controlled motility on transport of bacteria and microspheres through saturated sediment. *Water Resources Research* **31**, 271-280.

McDowell-Boyer LM, Hunt JR, Sitar N (1986) Particle transport through porous media. *Water Resources Research* **22**, 1901-1921.

McGechan MB (2002) Transport of particulate and colloid-sorbed contaminants through

soil, part 2: trapping processes and soil pore geometry. *Biosystems Engineering* **83**, 387-395.

McGechan MB, Lewis DR (2002) Transport of particulate and colloid-sorbed contaminants through soil, part 1: general principles. *Biosystems Engineering* **83**, 255-273.

McLeod M, Aislabie J, Ryburn J, McGill A, Taylor M (2003) Microbial and chemical tracer movement through two Southland soils, New Zealand. *Australian Journal of Soil Research* **41**, 1163-1169.

Mills AL, Herman JS, Hornberger GM, DeJesus TH (1994) Effect of solution ionic strength and iron coatings on mineral grains on the sorpiton of bacterial cells to quartz sand. *Applied and Environmental Microbiology* **60**, 3300-3306.

Morris BL, Foster SSD (2000) Cryptosporidium contamination hazard assessment and risk management for British groundwater sources. *Water Science and Technology* **41**, 67-77.

Munyankusi E, Gupta SC, Moncrief JF, Berry EC (1994) Earthworm macropores and preferential transport in a long-term manure applied typic Hapludalf. *Journal of Environmental Quality* **23**, 773-784.

Natsch A, Keel C, Troxler J, Zala M, Albertini NV, Defago G (1996) Importance of preferential flow and soil management in vertical transport of a biocontrol strain of *Pseudomonas fluorescens* in structured field soil. *Applied and Environmental Microbiology* **62**, 33-40.

Nelson BN, Cellan R, Mudder T, Whitlock J, Waterland R (2002) In situ, anaerobic, biological immobilization of uranium, molybdenum and selenium in an alluvial aquifer. *SME annual meeting, Feb. 25-27, 2002, Phoenix, AZ*, 6.

Nicosia LA, Rose JB, Stark L, Stewart MT (2001) A field study of virus removal in septic tank drainfields. *Journal of Environmental Quality* **30**, 1933-1939.

Payne RB, Gentry DA, Rapp-Giles BJ, Casalot L, Wall JD (2002) Uranium reduction by *Desulfovibrio desulfuricans* strain G20 and a cytochrome c3 mutant. *Applied and*

Environmental Microbiology **68**, 3129-3132.

Pierzynski SV (2000) Remediation of soil and groundwater. In 'Soils and Environmental Quality'. (Ed. B Raton) pp. 377-395. (CRC press Inc.: USA)

Powelson DK, Mills AL (1996) Bacterial enrichment at the gas-water interface of a laboratory apparatus. *Applied and Environmental Microbiology* **62**, 2593-2597.

Powelson DK, Mills AL (1998) Water saturation and surfactant effects on bacterial transport in sand columns. *Soil Science* **163**, 694-704.

Powelson DK, Mills AL (2001) Transport of *Escherichia coli* in sand columns with constant and changing water contents. *Journal of Environmental Quality* **30**, 238-245.

Ratcliffe T (1998) Research notes on tension infiltrometer and tension table experiments. In. (Christchurch)

Reddy HL, R. M. F (1996) Analysis of biodegradation and bacterial transport: Comparison of models with kinetic and equilibrium bacterial adsorption. *Journal of Contaminant Hydrology* **22**, 271-287.

Reddy KR, Khaleel R, Overcash MR (1981) Behavior and transport of microbial pathogens and indicator organisms in soils treated with organic wastes. *Journal of Environmental Quality* **10**, 255-266.

Rijnaarts HHM, Norde W, Bouwer EJ, Lyklema J, Zehnder AJB (1996) Bacterial deposition in porous media related to the clean bed collision efficiency and to substratum blocking by attached cells. *Environmental Science and Technology* **30**, 2869-2876.

Robert M, Chenu C (1992) Interactions between soil minerals and microorganisms. In 'Soil Biochemistry'. (Eds G Stotzky and J Bollag) pp. 307-379)

Saiers JE, Lenhart JJ (2003) Ionic-strength effects on colloid transport and interfacial reactions in partially saturated porous media. *Water Resources Research* **39**, SBH8.1-SBH8.13.

Schafer A, Ustohal P, Harms H, Stauffer F, Dracos T, Zehnder AJB (1998) Transport of bacteria in unsaturated porous media. *Journal of Contaminant Hydrology* **33**, 149-169.

Scheibe TD, Wood BD (2003) A particle-based model of size or anion exclusion with application to microbial transport in porous media. *Water Resources Research* **39**, SBH3.01-SBH3.10.

Schijven JF, Hassanizadeh SM (2000) Removal of viruses by soil passage: Overview of modeling, processes, and parameters. *Critical Reviews in Environmental Science and Technology* **30**, 49.

Schijven JF, Medema G, Vogelaar AJ, Hassanizadeh SM (2000) Removal of microorganisms by deep well injection. *Journal of Contaminant Hydrology* **44**, 301-327.

Shein EV, Polyanskaya LM, Devin BA (2002) Transport of microorganisms in soils: Physicochemical approach and mathematical modeling. *Eurasian Soil Science* **35**, 500-508.

Silliman SE, Fletcher M, Dunlap R, Schneegurt MA (2001) Bacterial transport in heterogeneous porous media: Observations from laboratory experiments. *Water Resources Research* **37**, 2699-2707.

Silva RG (1999) Effect of urinary nitrogen, dairy shed effluent and nitrogen fertiliser on nitrate leaching from a pasture soil. PhD thesis, Lincoln University.

Silva RG, Cameron KC, Di HJ, Smith NP, Buchan GD (2000) Effect of macropore flow on the transport of surface-applied cow urine through a soil profile. *Australian Journal of Soil Research* **38**, 13-23.

Singh P, Kanwar RS (1991) Preferential solute transport through macropores in large undisturbed saturated soil columns. *Journal of environmental quality* **20**, 295-300.

Sinton LW, Noonan MJ, Finlay RK, Pang L, Close ME (2000) Transport and attenuation of bacteria and bacteriophages in an alluvial gravel aquifer. *New Zealand Journal of Marine and Freshwater Research* **34**, 175-186.

Sirivithayapakorn S, Keller A (2003) Transport of colloids in saturated porous media: A pore-scale observation of the size exclusion effect and colloid acceleration. *Water Resources Research* **39**, SBH11.01-SBH11.11.

Slepecky RA, Hemphill HE (1992) The genus *Bacillus* - Nonmedical. In 'In the Prokaryotes'. (Eds A Balows, HG Truper, M Dworkin, W Harder and KH Schleifer). (Springer-Verlag.: NewYork.)

Smith-Keary PF (1988) 'Genetic Elements in *Escherichia coli.*' (Macmillan Education Ltd: Houndmills, Basingstoke, Hampshire)

Smith MS, Thomas GW, White RE, Ritonga D (1985) Transport of *Escherichia coli* through intact and disturbed soil columns. *Journal of Environmental Quality* **14**, 87-91.

Stenstrom TA (1989) Bacterial hydrophobicity, an overall parameter for the measurement of adhesion potential to soil particles. *Applied and Environmental Microbiology* **55**, 142-147.

Suzuki Y, Kelly SD, Kemner KA, Banfield JF (2003) Microbial populations stimulated for hexavalent uranium reduction in uranium mine sediment. *Applied and Environmental Microbiology* **69**, 1337-1346.

Sylvia DM, Fuhrmann JJ, Hartel PG, Zukerer DA (1998) 'Principles and applications of soil microbiology.' (Prentice Hall: Upper Saddle River, New Jersey 07458)

Tan Y, Bond WJ, Griffin DM (1992) Transport of bacteria during unsteady unsaturated soil water flow. *Soil Science Society of America Journal* **56**, 1331-1340.

Tan Y, Gannon JT, Baveye PC, Alexander M (1994) Transport of bacteria in an aquifer sand: Experiments and model simulations. *Water Resources Research* **30**, 3243-3252.

Thomas GW, Phillips RE (1979) Consequences of water movement in macropores. *Journal of Environmental Quality* **8**, 149-152.

Thompson SS, Flury M, Yates MV, Jury WA (1998) Role of the air-water-solid interface in bacteriophage sorption experiments. *Applied and Environmental Microbiology* **64**,

304-309.

Thompson SS, Yates MV (1999) Bacteriophage inactivation at the air-water-solid interface in dynamic batch systems. *Applied and Environmental Microbiology* **65**, 1186-1190.

Toride N, Leij FJ, van Genuchten MT (1999) 'The CXTFIT code for estimating transport parameters from laboratory or field tracer experiments Version 2.1.' U. S. Salinity Laboratory, Research Report No. 137, Riverside, CA.

Unc A, Goss MJ (2003) Movement of faecal bacteria through the vadose zone. *Water, Air and Soil Pollution* **149**, 327-337.

Unc A, Goss MJ (2004) Transport of bacteria from manure and protection of water resources. *Applied Soil Ecology* **25**, 1-18.

van Genuchten MT (1980) A closed-form equation for predicting the hydraulic conductivity of unsaturated soils. *Soil Science Society of America Journal* **44**, 892-898.

Wallach R (1994) Groundwater contamination by sewage irrigation. In 'Groundwater Contamination and Control'. (Ed. V Zoller) pp. 189-202)

Wan J, Tokunaga TK (1997) Film straining of colloids in unsaturated porous media: conceptual model and experimental testing. *Environmental Science and Technology* **31**, 2413-2420.

Wan J, Wilson JL (1994) Visualization of the role of the gas-water interface on the fate and transport of colloids in porous media. *Water Resources Research* **30**, 11-23.

Wan J, Wilson JL, Kieft TL (1994) Influence of the gas-water interface on transport of microorganisms through unsaturated porous media. *Applied and Environmental Microbiology* **60**, 509-516.

Weiss TH, Mills AL, Hornberger GM, Herman JS (1995) Effect of bacterial cell shape on transport of bacteria in porous media. *Environmental Science and Technology* **29**, 1737-1740.

Wiencek KM, Klapes NA, Foegeding PM (1991) Adhesion of *Bacillus* spores to inanimate materials: effects of substratum and spore hydrophobicity. *Biofouling* **3**, 139-149.

Williams JP, Vepraskas MJ (1994) Solute movement through quartz-diorite saprolite containing quartz veins and biological macropores. *Journal of Environmental Quality* **23**, 810-815.

Wollum II AG, Cassel DK (1978) Transport of microorganisms in sand columns. *Soil Science Society of America Journal* **42**, 72-76.

Yao KM, Habibian MT, O'Melia CR (1971) Water and waste water filtration: concepts and applications. *Environmental Science and Technology* **5**, 1105-112.

Yee N, Fein JB, Daughney CJ (2000) Experimental study of the pH, ionic strength, and reversibility behavior of bacteria-mineral adsorption. *Geochimica et Cosmochimica Acta* **64**, 609-617.

Zhang P, Johnson WP, Piana MJ, Fuller CC, Naftz DL (2001a) Potential artifacts in interpretation of differential breakthrough of colloids and dissolved tracers in the context of transport in a zero-valent iron permeable reactive barrier. *Ground Water* **39**, 831-840.

Zhang P, Johnson WP, Scheibe TD, Choi K-H, Dobbs FC, Mailloux BJ (2001b) Extended tailing of bacteria following breakthrough at the Narrow Channel focus area, Oyster, Virginia. *Water Resources Research* **37**, 2687-2698.

Appendix I

Two-site + AWI Model and Application to Bacterial Transport in Sand Columns

---

As discussed in chapter 5, one-site kinetic adsorption does not fully account for the real adsorption processes for bacterial deposition to sand grain surfaces. Thus, a two-site model which includes both equilibrium and first-order kinetic adsorption processes was developed to model unsaturated bacterial transport. The attachment of bacteria to air-water interfaces was still modeled as a first-order irreversible adsorption.

$$\frac{\partial c}{\partial t}+\frac{\rho_b}{\theta}\left(\frac{\partial s_1}{\partial t}+\frac{\partial s_2}{\partial t}\right)=D\frac{\partial^2 c}{\partial z^2}-v\frac{\partial c}{\partial z}-k_0 c \tag{39}$$

Where c is bacterial concentration in water (cfu/mL), s is attached bacteria on porous media surfaces (cfu/g), D is the dispersion coefficient (cm^2/min), v is the pore water velocity (cm/min), k_1 is the adsorption rate constant for adsorption at particle surfaces (min^{-1}), k_0 is the adsorption coefficient at air-water interfaces, t is time (min) and z is distance from inlet (cm).

$$\frac{\partial s_1}{\partial t}=f\cdot K_d\frac{\partial c}{\partial t} \tag{40}$$

The first-type of adsorption sites were modeled as an equilibrium process. f is the fraction of exchange sites assumed to be at equilibrium adsorption.

$$\frac{\partial s_2}{\partial t}=(1-f)\frac{\theta}{\rho_b}k_1 c-k_2 s_2 \tag{41}$$

The second-type of adsorption sites were modeled as a first-order kinetic process. This model could be modeled by STANMOD 2.2 by assuming k_0 to be the first-order decay coefficient. The attachment coefficients are calculated as follows.

$$\begin{aligned} k_1&=\alpha(R-1)\\ k_2&=\alpha \end{aligned} \tag{42}$$

Where α is the first-order kinetic coefficient in CXTFIT, and R is the retardation factor. Now the two-sites + AWI model has been developed as above, and STANMOD 2.1 (U.S. Salinity Laboratory) was used to model our sand column experimental breakthrough curves.

One-site and one-site + AWI models were also used in the modeling for comparison. Also, Equilibrium and equilibrium + AWI models were used if the software package STANMOD version 2.2 suggested the potential applicability. Estimated model parameters are listed in Table 16 to Table 18. Breakthrough and fitting curves are shown in Figure 35 to Figure 49. Methods and materials for the sand column transport were the same as described in chapter 5. Experimental parameters and recovery of bacteria and bromide in leachate were reported in Table 14 and Table 15. The equilibrium + AWI model was shown to be efficient to fit BTCs in coarse sand columns. The two-site model fitted BTC tailing better than the one-site or equilibrium models. The two-site + AWI model was the best among the models used.

Table 14. Experimental parameters for two-sites + AWI modeling.

Run[†]	*Sand*[*]	*Length (cm)*	*Suction (kPa)*	*Degree of saturation*[▲]	*Bacterial C_0 (cfu/mL)*	*Flow rate (mL/min)*[♦]
C1[♦]	COS	44	0	1	1.55×10^8	48.14
CA[♦]	COS	44	0	1	4.15×10^8	776.9
CB[♦]	COS	44	0.1	0.9999	4.14×10^8	805.6
CC[◊]	COS	44	1.0	0.6842	4.01×10^8	172.7
CD[♦]	COS	22	0	1	5.69×10^8	744.0
CE[◊]	COS	22	1.0	0.6842	4.59×10^8	217.9
CF[◊]	COS	22	1.4	0.3656	6.21×10^8	400.1
CG[♦]	COS	22	0	1	9.25×10^8	255.8
CH[◊]	COS	22	1.2	0.5022	1.06×10^9	209.2
FA[◊]	FOS	44	1.0	0.9999	4.15×10^8	63.0
FB[◊]	FOS	44	1.3	0.9996	3.74×10^8	63.0
FC[◊]	FOS	44	4.9	0.7254	5.49×10^8	8.0
FD[♦]	FOS	44	0.1	1	5.55×10^8	50.9
FH[◊]	FOS	22	1.5	0.9991	4.21×10^8	118.9
FI[♦]	FOS	22	0	1	4.80×10^8	146.7

[†] Some of the experiments were also reported in chapter five as CA to CD, corresponding to CA, CC, CG, and CH here; as FA to FD, corresponding to FD, FB, FI, and FH. Saturated and unsaturated columns are indicated by [♦] and [◊], respectively.

[*] COS: Coarse Oamaru Sand; FOS: Fine Oamaru Sand.

[▲] Degree of saturation was calculated as the average value.

[♦] Flow rate was calculated based on sample weights and sampling intervals.

Table 15. Recovery of bacteria and bromide after about 25 L of leachate collected.

Run[†]	*Volume of leachate (L)*	*Bacterial recovery (%)*	*Bromide recovery (%)*
C1♦	26.25	48.14	84.37
CA♦	25.64	89.00	74.34
CB♦	24.17	96.96	71.62
CC◊	25.90	54.36	71.45
CD♦	26.04	66.27	73.53
CE◊	26.15	46.81	74.44
CF◊	28.01	16.01	61.51
CG♦	28.14	80.71	73.03
CH◊	27.82	44.25	69.01
FA◊	29.63	0.01	70.83
FB◊	27.73	0.03	67.98
FC◊	18.24	0	64.95
FD♦	26.96	0.0022	66.64
FH◊	25.33	1.42	73.09
FI♦	25.23	17.45	73.31

[†] Saturated and unsaturated columns are indicated by ♦ and ◊, respectively.

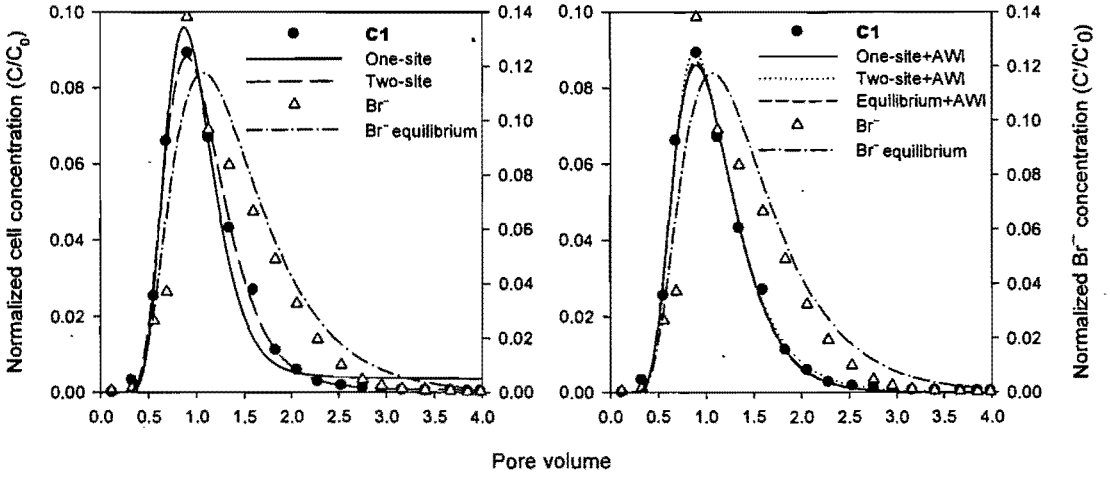

Figure 35. Breakthrough curves for C1 (saturated) simulated by equilibrium, one-site kinetic, two-site models and their AWI models.

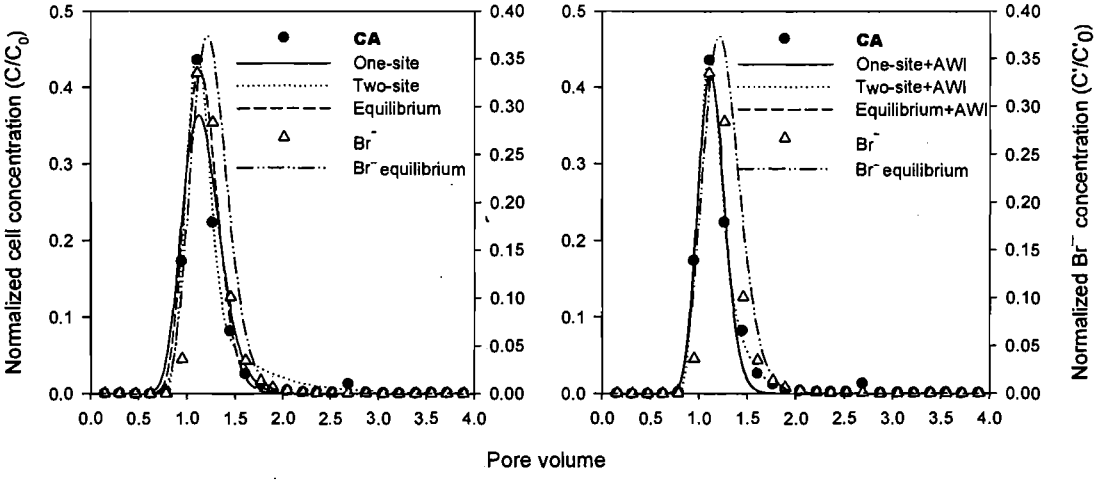

Figure 36. Breakthrough curves for CA (saturated) simulated by equilibrium, one-site kinetic, two-site models and their AWI models.

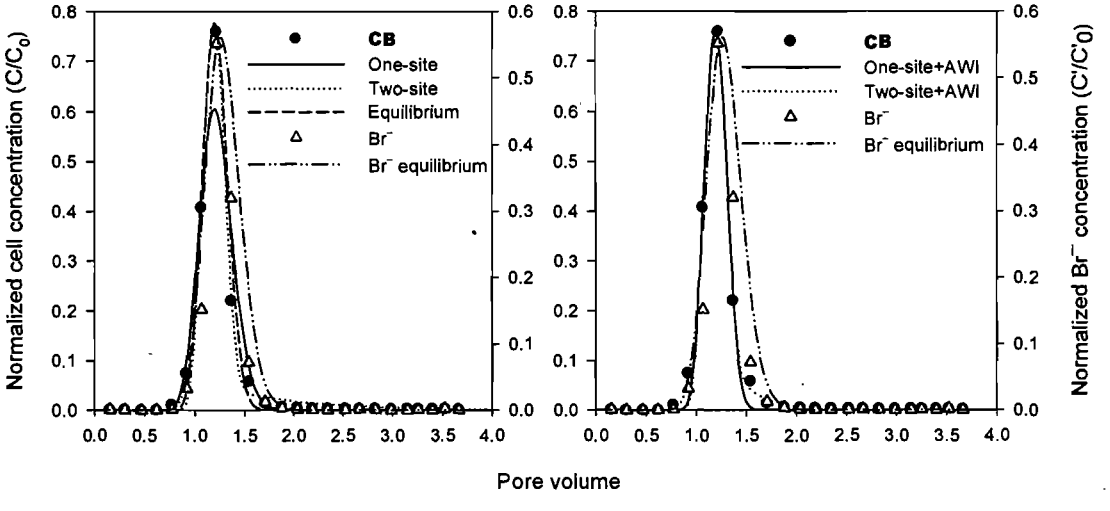

Figure 37. Breakthrough curves for CB (saturated) simulated by equilibrium, one-site kinetic, two-site models and their AWI models.

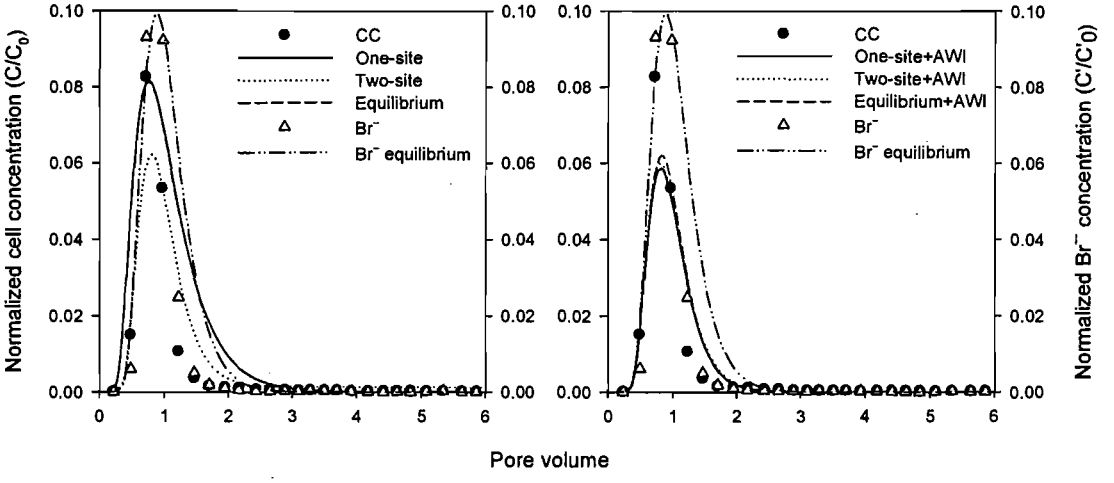

Figure 38. Breakthrough curves for CC (unsaturated) simulated by equilibrium, one-site kinetic, two-site models and their AWI models.

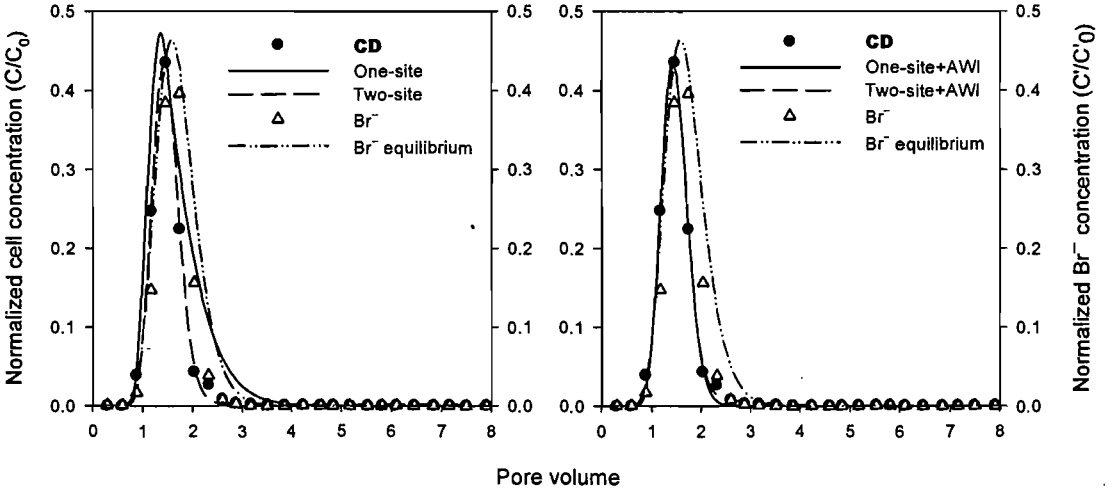

Figure 39. Breakthrough curves for CD (saturated) simulated by equilibrium, one-site kinetic, two-site models and their AWI models.

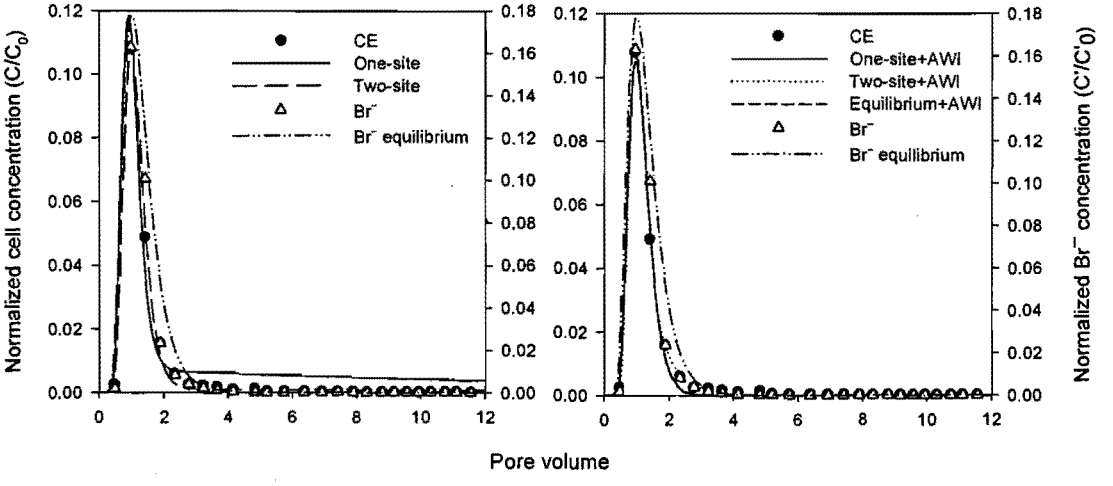

Figure 40. Breakthrough curves for CE (unsaturated) simulated by equilibrium, one-site kinetic, two-site models and their AWI models.

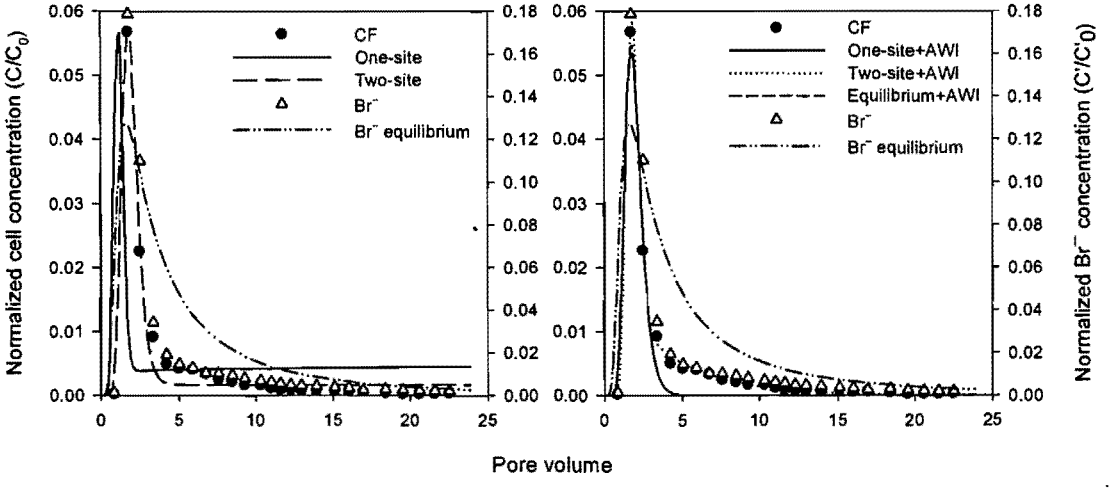

Figure 41. Breakthrough curves for CF (unsaturated) simulated by equilibrium, one-site kinetic, two-site models and their AWI models.

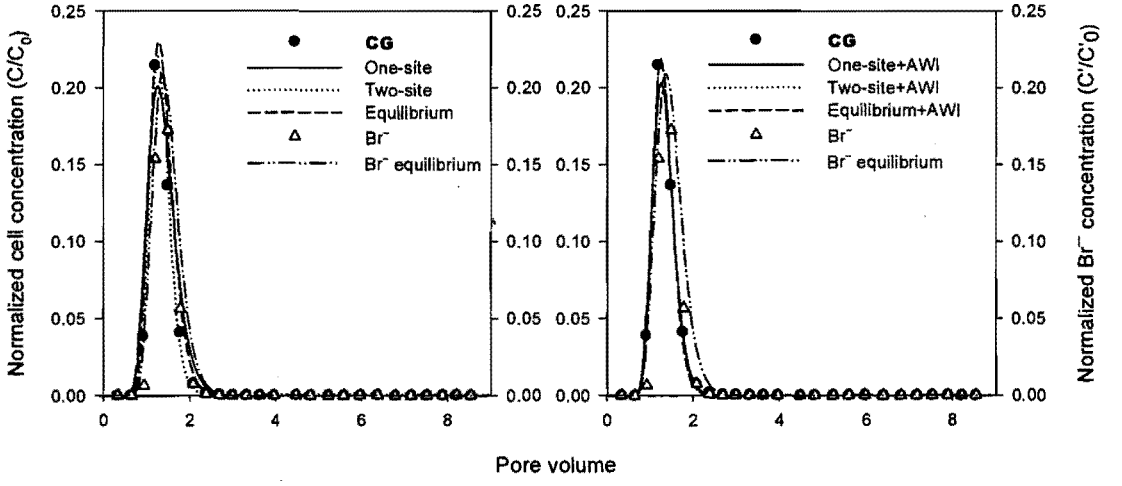

Figure 42. Breakthrough curves for CG (saturated) simulated by equilibrium, one-site kinetic, two-site models and their AWI models.

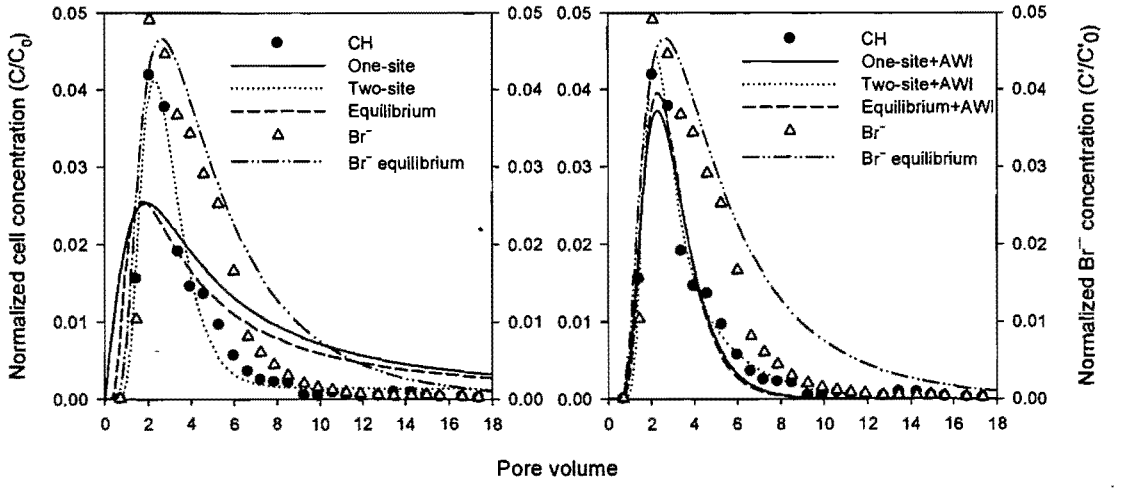

Figure 43. Breakthrough curves for CH (unsaturated) simulated by equilibrium, one-site kinetic, two-site models and their AWI models.

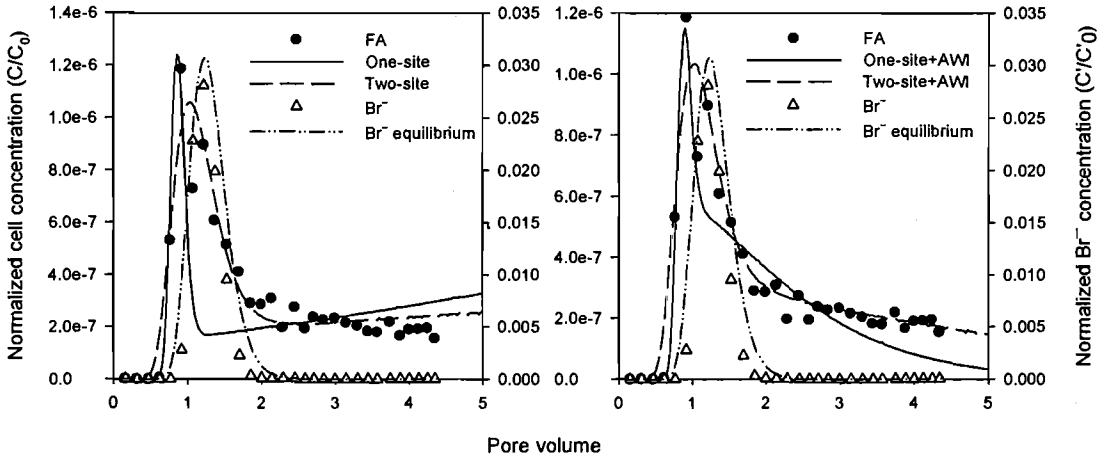

Figure 44. Breakthrough curves for FA (unsaturated) simulated by one-site kinetic, two-site models and their AWI models.

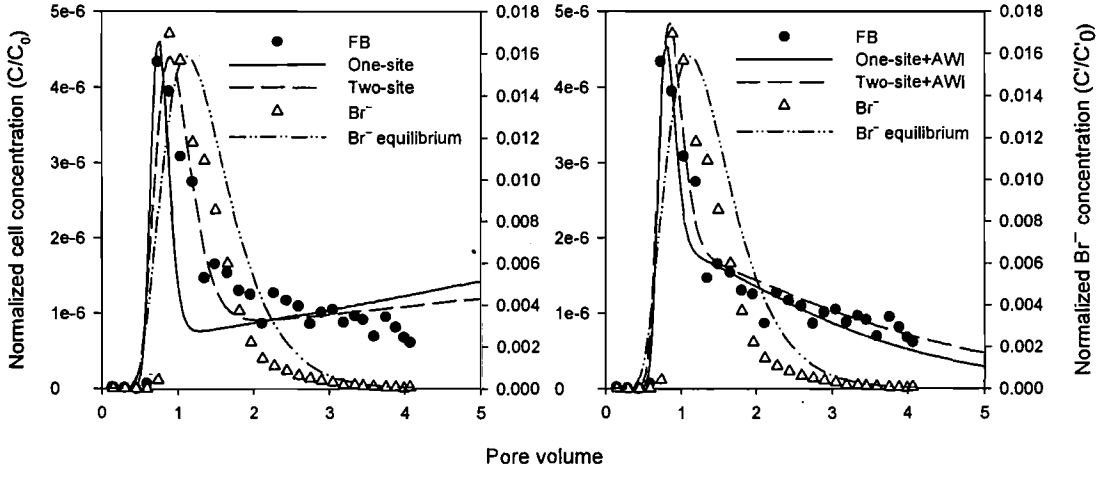

Figure 45. Breakthrough curves for FB (unsaturated) simulated by one-site kinetic, two-site models and their AWI models.

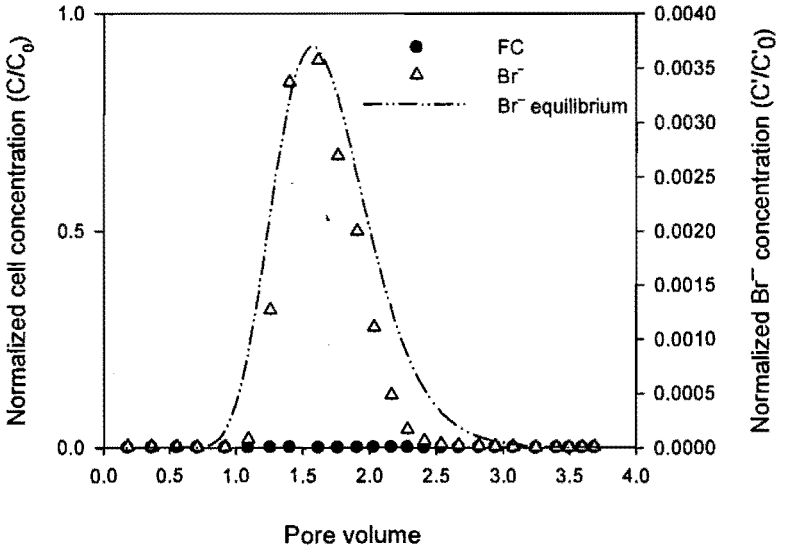

Figure 46. Breakthrough curves for FC (unsaturated). Bromide curve was simulated by equilibrium model.

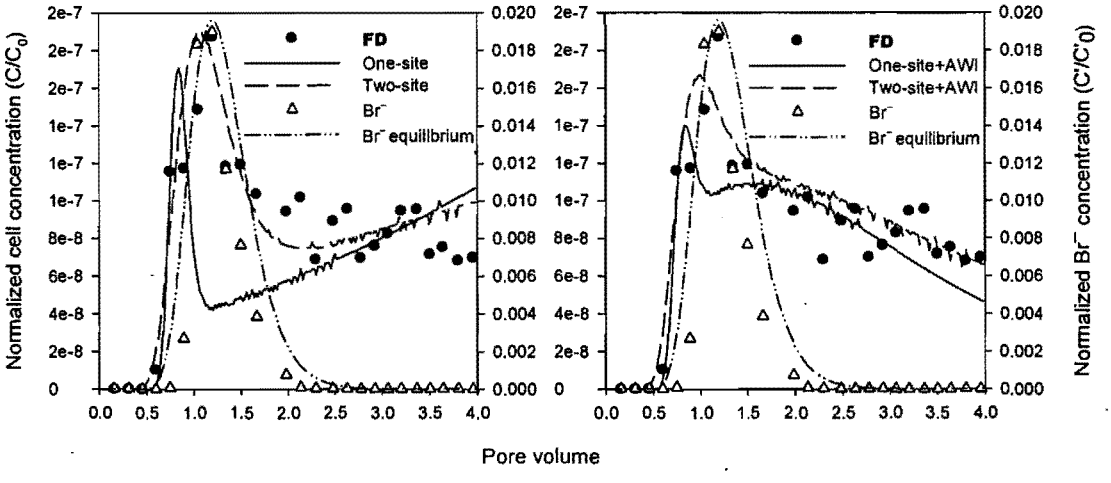

Figure 47. Breakthrough curves for FD (saturated) simulated by one-site kinetic, two-site models and their AWI models.

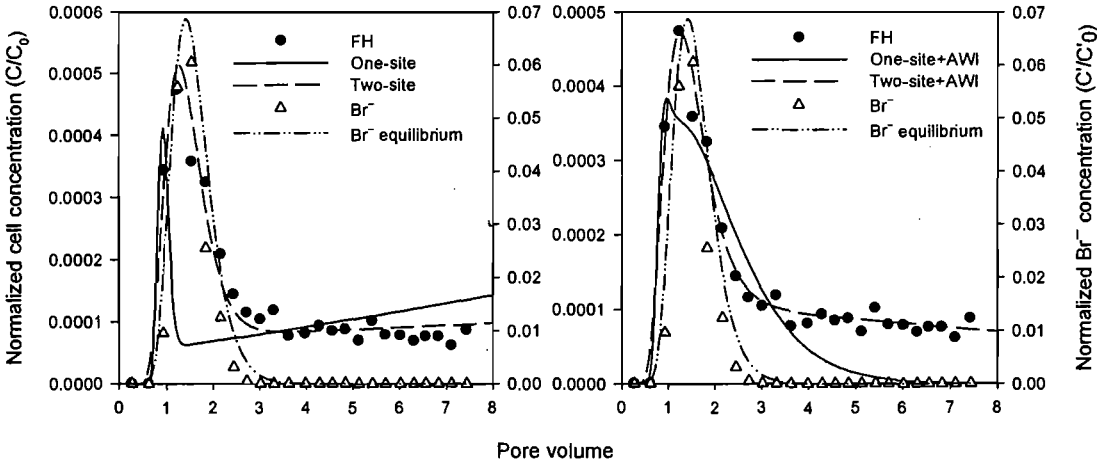

Figure 48. Breakthrough curves for FH (unsaturated) simulated by one-site kinetic, two-site models and their AWI models.

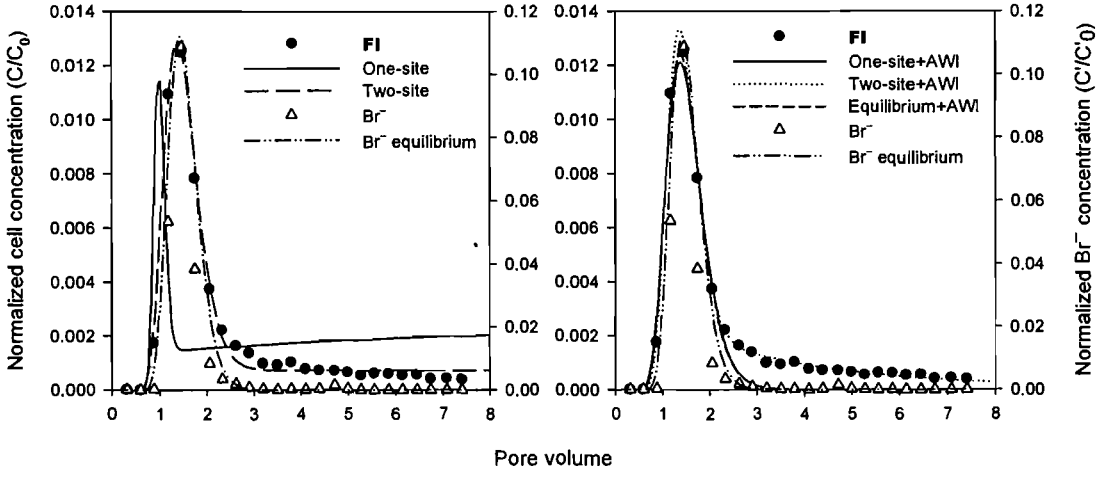

Figure 49. Breakthrough curves for FI (saturated) simulated by equilibrium + AWI, and one-site kinetic, two-site models and their AWI models.

Table 16. Estimated model coefficients by one-site and one-site + AWI models †

Run♠	k_0	k_1	k_2	k_1/k_2	D	R	Pe	r^2
C1♦		0.09	0.01	11.39	12.24	12.39	15.7	0.9712
	0.77	9.95	73.20	0.136	18.42	1.14	10.5	0.9959
CA♦		11.79	155.07	0.076	3.68	1.08	62	0.9324
	0.21	11.79	240.51	0.049	1.72	1.05	132.5	0.9827
CB♦		12.22	122.21	0.1	2.06	1.10	115.0	0.9325
	0.13	3.61	46.24	0.078	0.64	1.08	369.0	0.9900
CC◊		3.91	217.00	0.018	8.95	1.02	8.5	0.5817
	0.62	3.91	390.59	0.01	5.27	1.01	14.3	0.8677
CD♦		0.38	0.88	0.434	0.83	1.43	132.3	0.8108
	0.37	3.99	15.46	0.258	1.63	1.26	67.2	0.9968
CE◊		0.09	0.01	9	2.57	10.00	18.2	0.9435
	0.87	9.64	63.83	0.151	3.02	1.15	15.5	0.9944
CF◊		0.98	0.01	80.75	5.80	81.75	26.8	-0.2096
	2.51	32.18	28.37	1.134	10.86	2.13	14.3	0.9576
CG♦		7.76	26.67	0.291	1.18	1.29	31.8	0.9317
	0.23	7.76	30.09	0.258	0.73	1.26	51.8	0.9916
CH◊		13.06	0.65	20.15	125.6	21.2	0.5	0.5323
	1.04	13.06	5.02	2.6	7.84	3.6	8.1	0.9496

Run[♦]	k_0	k_1	k_2	k_1/k_2	D	R	Pe	r^2
FA[◊]		0.03	0.00	80.75	5.80	81.75	3.1	-0.2096
	10.11	0.02	0.02	1.243	0.11	2.24	158.9	0.8824
FB[◊]		0.10	0.00	173.5	0.3	174.5	59.7	0.5282
	8.85	0.02	0.01	1.841	0.23	2.8	78.5	0.9260
FD[♦]		0.11	0.00	164.3	0.11	165.3	131.4	-0.0195
	11.51	0.03	0.01	2.22	0.13	3.2	112.4	0.7574
FH[◊]		0.24	0.00	79.43	0.15	80.4	112.7	-0.0841
	4.77	0.10	0.08	1.244	0.22	2.2	77.8	0.7386
FI[♦]		0.15	0.01	24	0.15	25	138.9	-0.0074
	2.16	4.30	5.87	0.733	0.86	1.73	24.4	0.9556

[†] For each experiment, the first row of data was estimates from one-site model; the second row was estimates from one-site + AWI model.

[♦] Saturated and unsaturated columns are indicated by [♦] and [◊], respectively.

Table 17. Estimated model coefficients by two-sites and two-sites + AWI models †

Run♦	k_0	k_1	k_2	k_1/k_2	K_d	f	D	R	Pe	r^2
C1♦		0.08	0.00	49.02	11.49	0.0025	17.65	50.02	10.9	0.9965
	0.75	0.05	0.41	0.124	0.029	0	13.36	1.12	14.4	0.9979
CA♦		0.05	0.25	0.187	0.044	0.1291	1.28	1.19	178.5	0.9901
	0.14	0.08	0.88	0.089	0.021	0	1.72	1.05	242.0	0.9987
CB♦		0.02	0.11	0.202	0.0473	0.3651	0.61	1.20	387.4	0.9917
	0.08	0.02	0.19	0.113	0.0265	0.6208	0.52	1.11	455.5	0.9929
CC◊		0.02	0.00	8.872	1.3944	0	5.42	9.87	13.9	0.8706
	0.58	3.91	390.59	0.01	0.0016	0.5657	5.68	1.01	13.3	0.8722
CD♦		0.11	0.00	30.25	7.0898	0.0086	1.88	31.25	58.0	0.9970
	0.40	0.02	0.06	0.39	0.0914	0.6447	1.78	1.39	61.3	0.9974
CE◊		0.09	0.00	63.13	10.1506	0.0022	2.83	64.13	16.5	0.9959
	0.82	0.03	0.13	0.242	0.0389	0.2517	2.03	1.24	22.9	0.9996
CF◊		0.82	0.00	213.9	18.9149	0.0050	10.02	214.90	15.5	0.9775
	2.03	0.21	0.08	2.689	0.2378	0.3016	5.38	3.69	28.9	0.9986
CG♦		0.02	0.00	6.687	1.5672	0.0375	0.62	7.69	60.4	0.9971
	0.234	7.76	30.80	0.252	0.0591	0.9995	0.64	1.25	59.1	0.9969
CH◊		0.14	0.00	67.29	7.6672	0.0343	6.29	68.29	10.1	0.9775
	4.77	0.10	0.04	2.757	0.3141	0.5811	3.24	3.76	19.5	0.9986

Run[♦]	k_0	k_1	k_2	k_1/k_2	K_d	f	D	R	Pe	r^2
FA[◊]		0.26	0.00	663.3	158.2990	0.0060	3.00	664.30	5.97	0.8924
	21.94	0.04	0.00	13.52	3.2266	0.2615	2.75	14.52	6.51	0.9103
FB[◊]		0.16	0.00	319.6	76.2546	0.0053	1.10	320.60	16.3	0.8562
	9.58	0.02	0.01	2.893	0.6903	0.0938	0.47	3.89	38.1	0.9300
FD[♦]		0.33	0.00	573.9	136.9794	0.0110	3.35	574.90	4.3	0.8394
	21.99	0.05	0.01	9.67	2.3081	0.2631	1.57	10.67	9.2	0.8716
FH[◊]		0.26	0.00	176.2	42.0184	0.0101	1.65	177.20	10.2	0.9470
	5.95	0.11	0.01	20.45	4.8767	0.1400	2.89	21.45	5.9	0.9748
FI[♦]		0.10	0.00	65.68	15.6766	0.0105	0.80	66.68	26.0	0.9917
	1.78	0.02	0.01	1.913	0.4566	0.3119	0.63	2.91	33.1	0.9990

[†] For each experiment, the first row of data was estimates from two-site model; the second row was estimates from two-site + AWI models.

[♦] Saturated and unsaturated columns are indicated by [♦] and [◊], respectively.

Table 18. Estimated model coefficients by adsorption equilibrium and equilibrium + AWI models.

Run[♠]	*Model*	*D*	*R*	K_d	k_0	r^2
C1[♦]	EQ+AWI	18.01	1.13	0.0841	0.77	0.9961
CA[♦]	EQ	2.61	1.06	0.0148	–	0.9516
	EQ+AWI	1.67	1.05	0.0112	0.22	0.9829
CB[♦]	EQ	1.02	1.08	0.0185	–	0.9782
CC[◊]	EQ	8.95	1.02	0.0031	–	0.5817
	EQ+AWI	4.86	1.00	0.5889	0.0002	0.8737
CE[◊]	EQ+AWI	2.90	1.14	0.0232	0.87	0.9947
CF[◊]	EQ+AWI	11.58	2.17	0.1032	2.53	0.9601
CG[♦]	EQ	0.89	1.27	0.0635	–	0.9518
	EQ+AWI	0.63	1.25	0.0591	0.24	0.9969
CH[◊]	EQ	1190.00	180.50	20.4528	–	0.6608
	EQ+AWI	7.36	3.52	0.2873	1.04	0.9572
FI[♦]	EQ+AWI	0.87	1.74	0.1757	2.17	0.9582

[♠] Saturated and unsaturated columns are indicated by [♦] and [◊], respectively.

Appendix II

Water Infiltration Rate and Suctions in Sand Columns

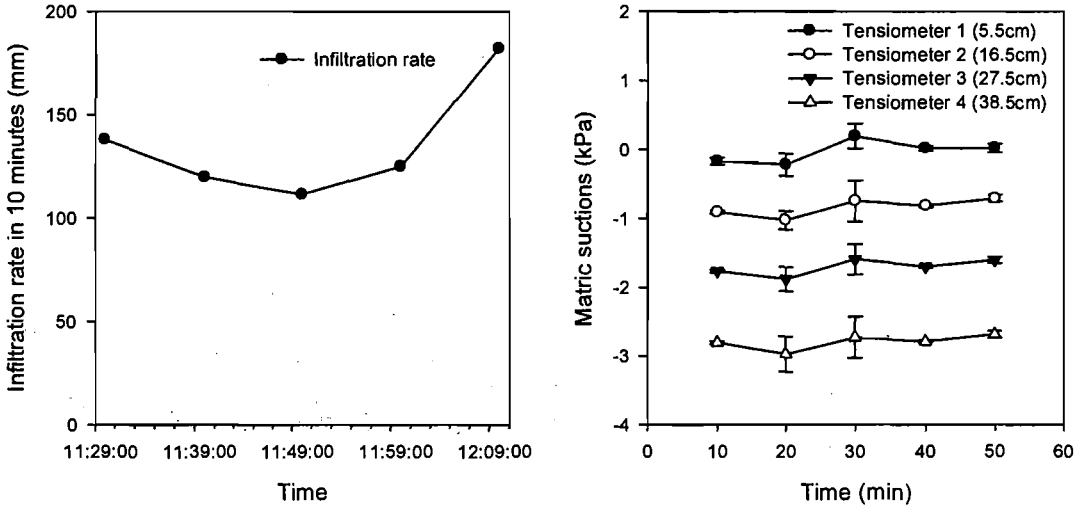

Figure 50. Ten-minute average infiltration rate and suctions for C1.

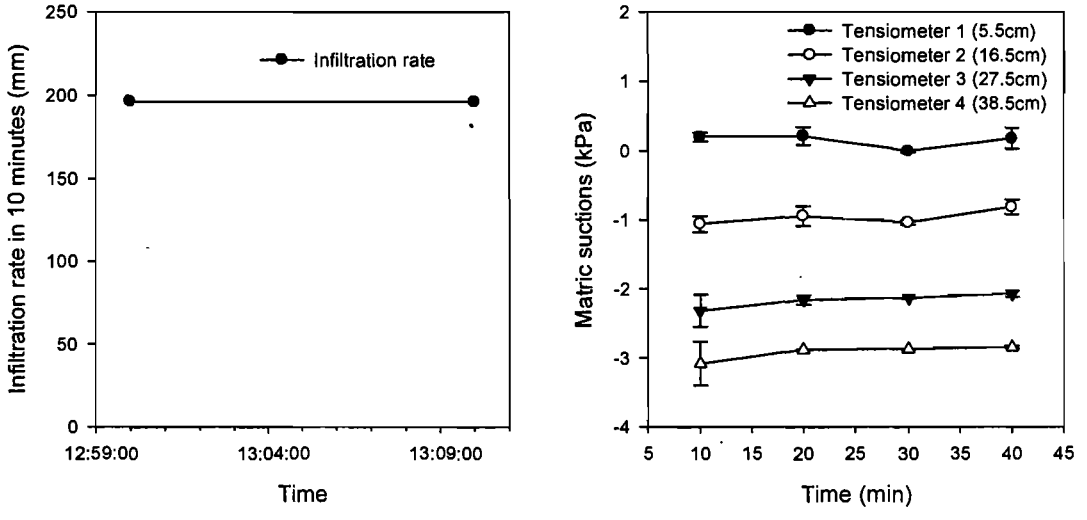

Figure 51. Ten-minute average infiltration rate and suctions for CA.

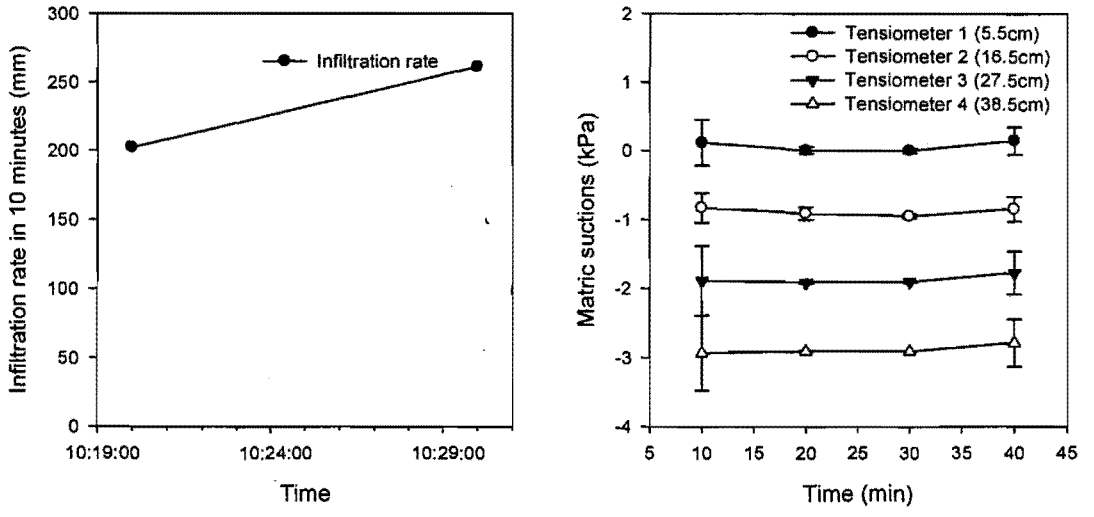

Figure 52. Ten-minute average infiltration rate and suctions for CB.

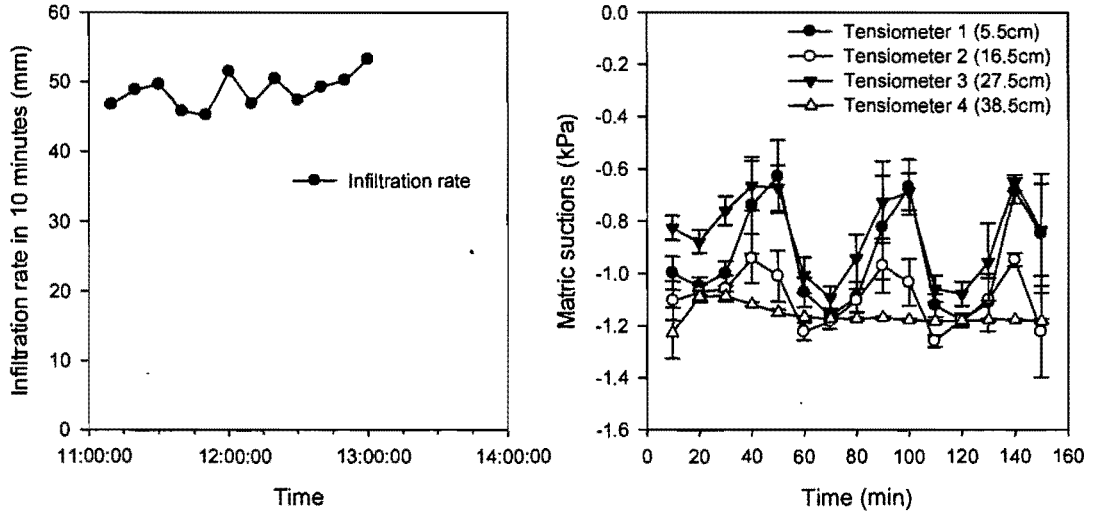

Figure 53. Ten-minute average infiltration rate and suctions for CC.

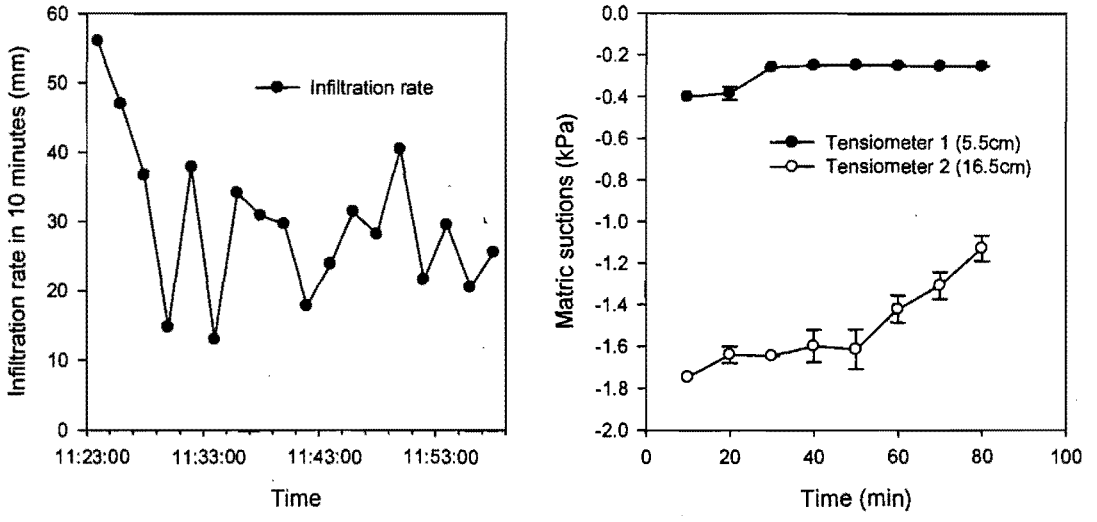

Figure 54. Ten-minute average infiltration rate and suctions for CD.

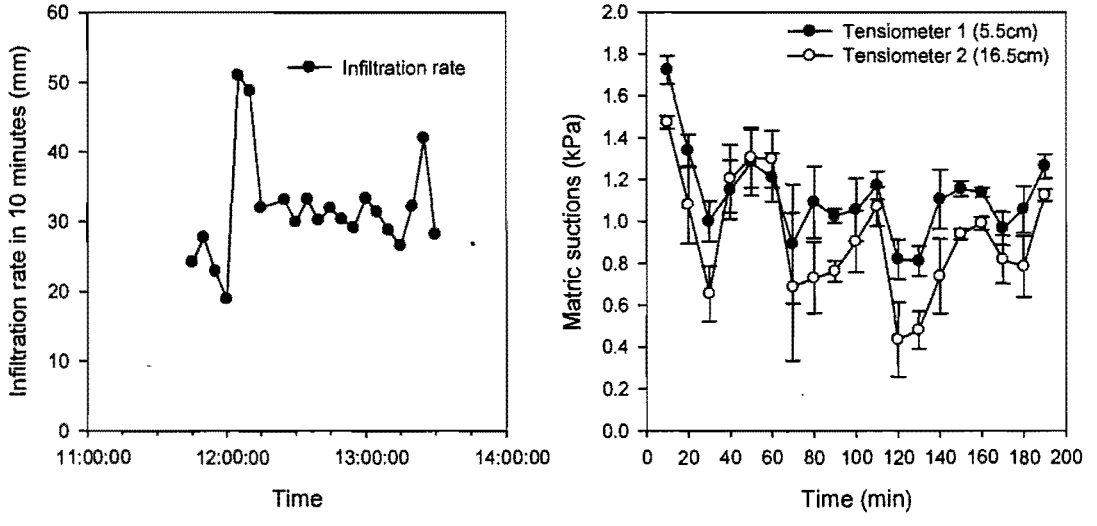

Figure 55. Ten-minute average infiltration rate and suctions for CE.

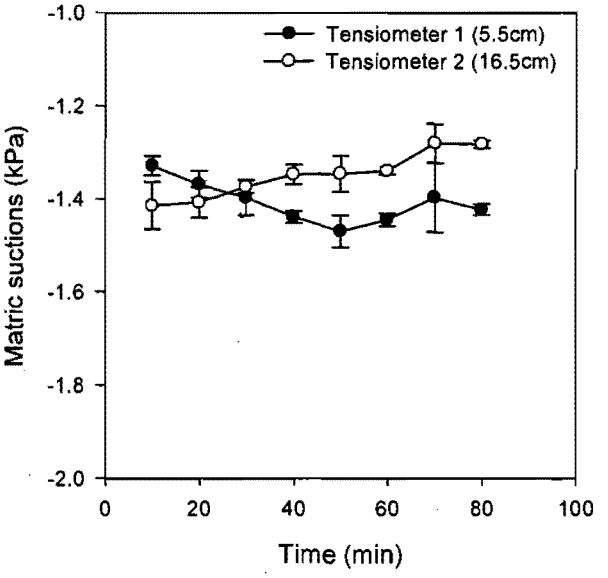

Figure 56. Ten-minute average suctions for CF.

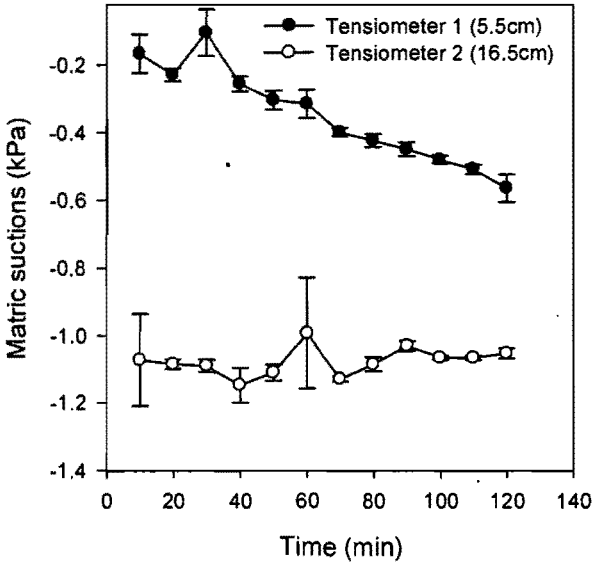

Figure 57. Ten-minute average suctions for CG.

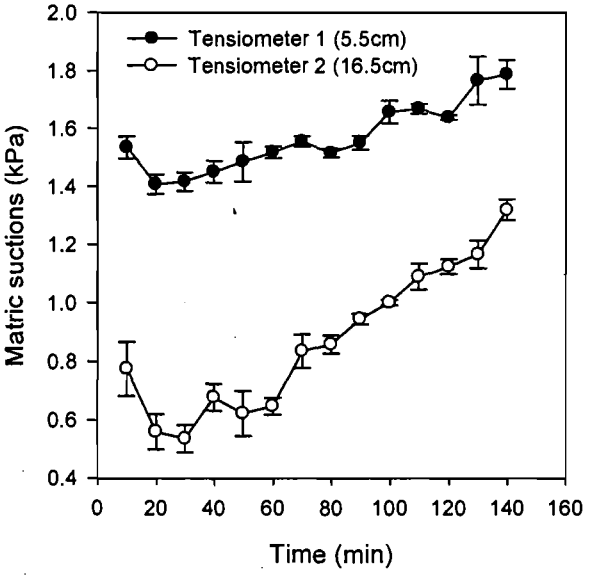

Figure 58. Ten-minute average suctions for CH.

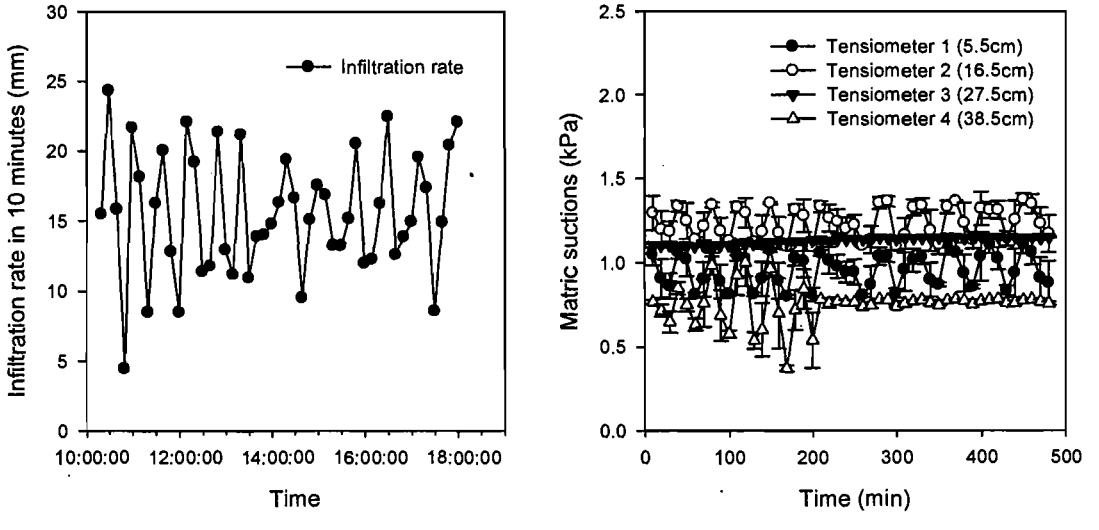

Figure 59. Ten-minute average infiltration rate and suctions for FA.

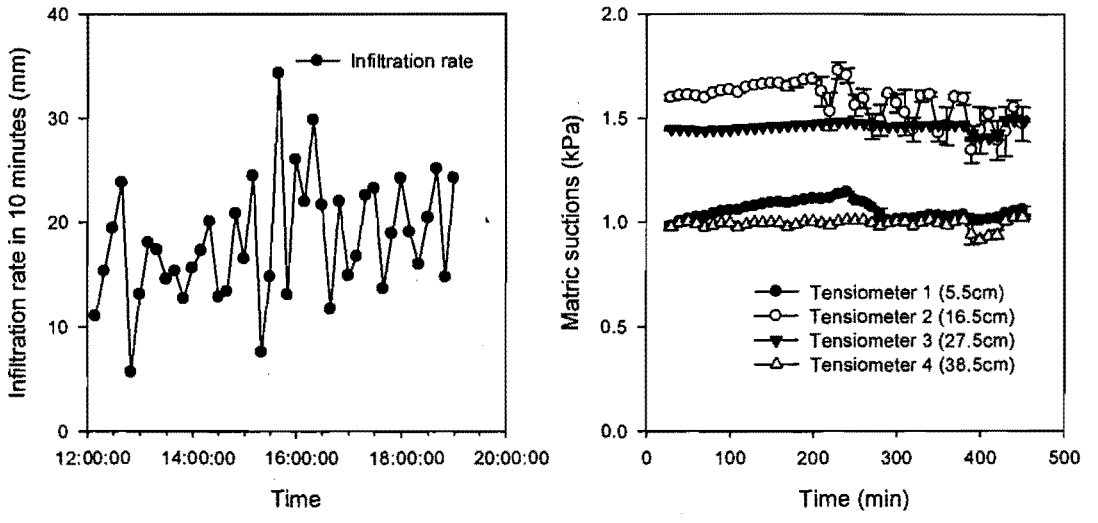

Figure 60. Ten-minute average infiltration rate and suctions for FB.

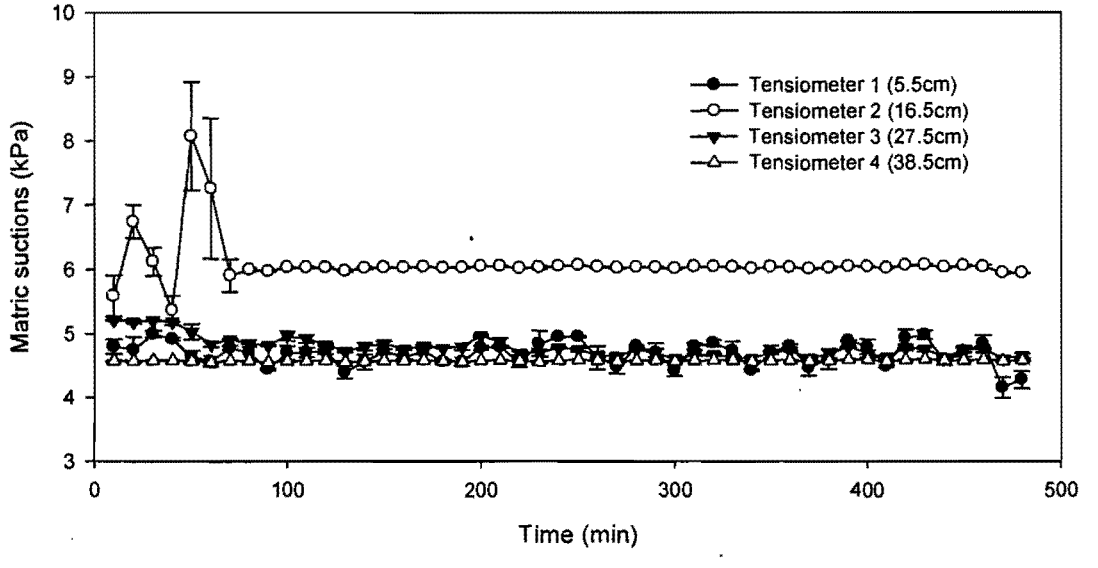

Figure 61. Ten-minute average suctions for FC.

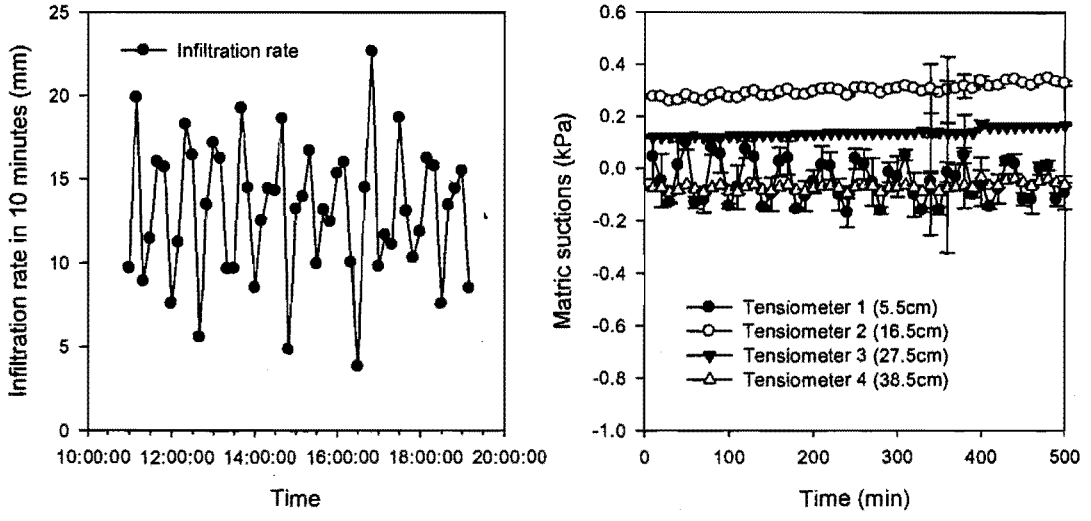

Figure 62. Ten-minute average infiltration rate and suctions for FD.

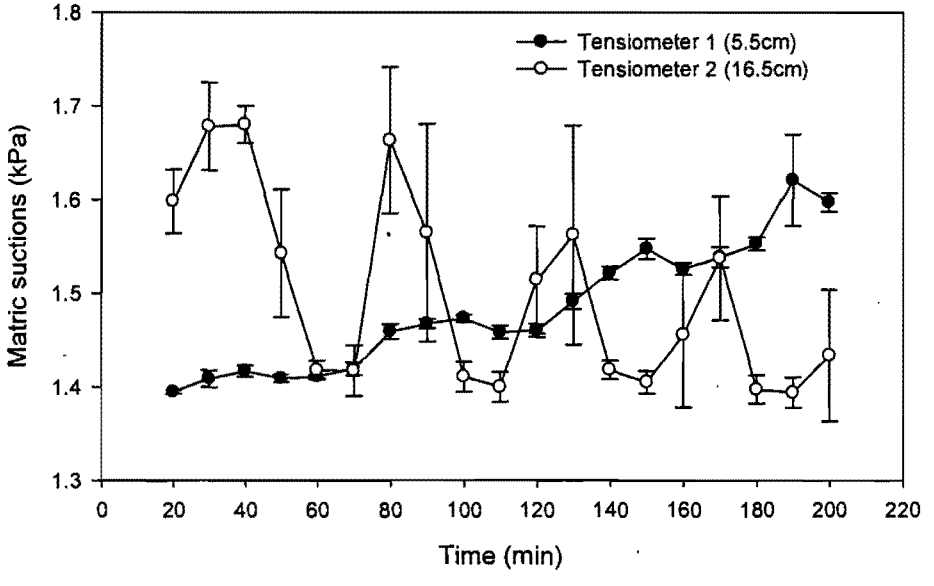

Figure 63. Ten-minute average suctions for FH.

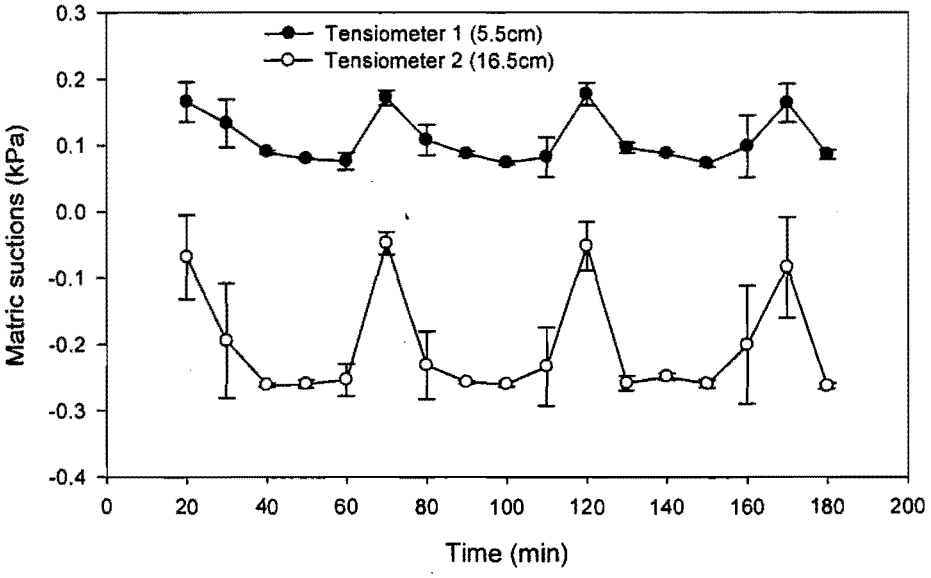

Figure 64. Ten-minute average suctions for FI.

Appendix III

Methods and Results for Sensor Calibration

1. Calibration of pressure transducers for matric suction

The pressure transducers, including three Micro Switch 170PC for soil lysimeter experiment and eight Honeywell 26PC sensors for sand column experiment, were calibrated before they are attached to tensiometers, which measured the change of matric suction in soil and sand. The programs used to calibrate these sensors are in Appendix I and II. Experimental setup was shown in Figure 65. Sensor and a syringe were connected via a 'T' connector with a tube, which held water and equilibrated by immersing the end of tube into a constant water level. A series of readings were acquired by changing the water height in the soft tube, which equals to the suction applied to the sensor.

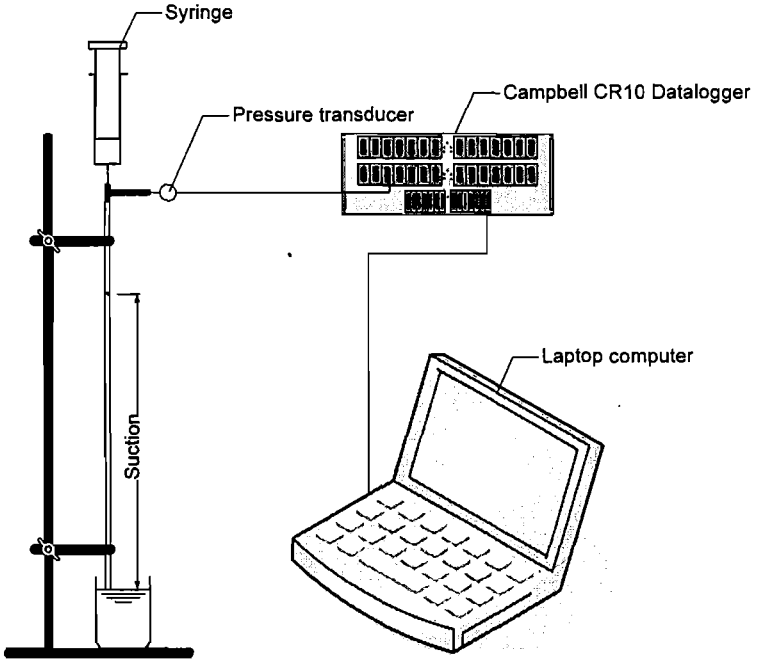

Figure 65. Calibration setup for pressure transducers.

The sensor readings coupled with measured water pressure or suction (see **Figure 65**) was used to get coefficients in datalogger programs. The linear regression was done in

Sigmaplot 9.0 (SYSTAT) and results are shown below in **Figure 66** and **Figure 67**.

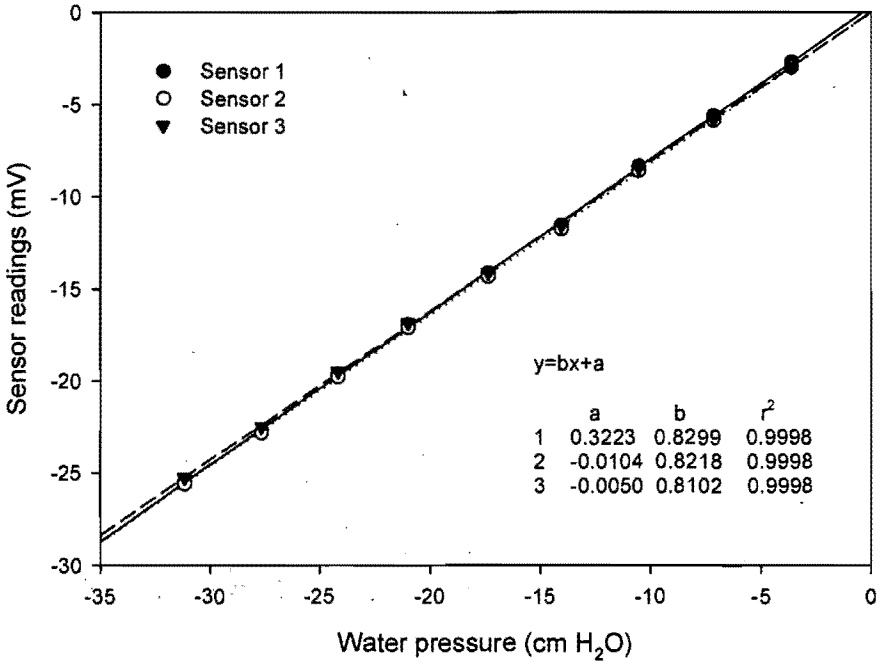

Figure 66. Linear regression for the calibration of 170PC sensors.

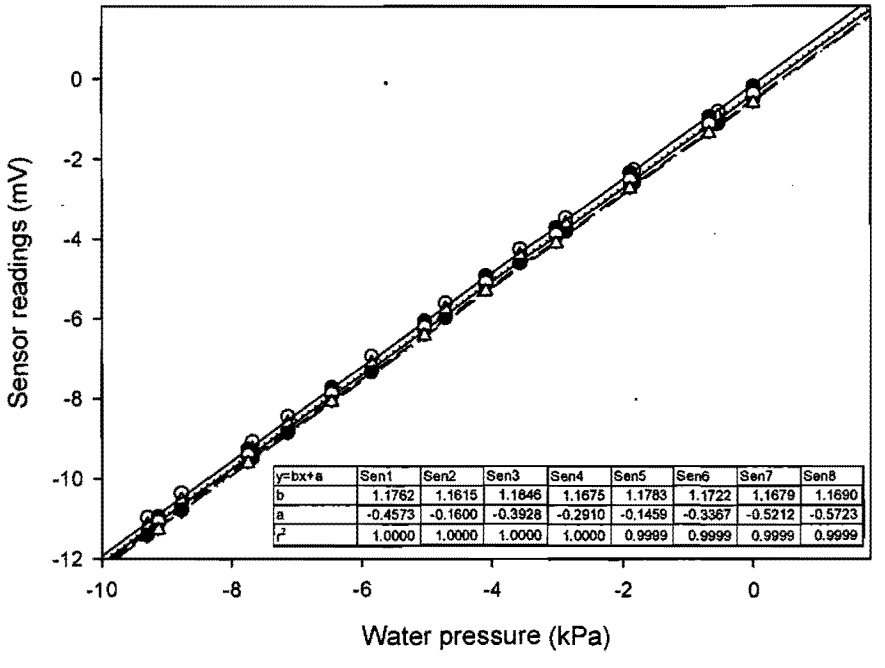

y=bx+a	Sen1	Sen2	Sen3	Sen4	Sen5	Sen6	Sen7	Sen8
b	1.1762	1.1615	1.1846	1.1675	1.1783	1.1722	1.1679	1.1690
a	-0.4573	-0.1600	-0.3928	-0.2910	-0.1459	-0.3367	-0.5212	-0.5723
r^2	1.0000	1.0000	1.0000	1.0000	0.9999	0.9999	0.9999	0.9999

Figure 67. Linear regression for the calibration of 26PC pressure sensors.

2. Calibration of pressure transducers for infiltration rate

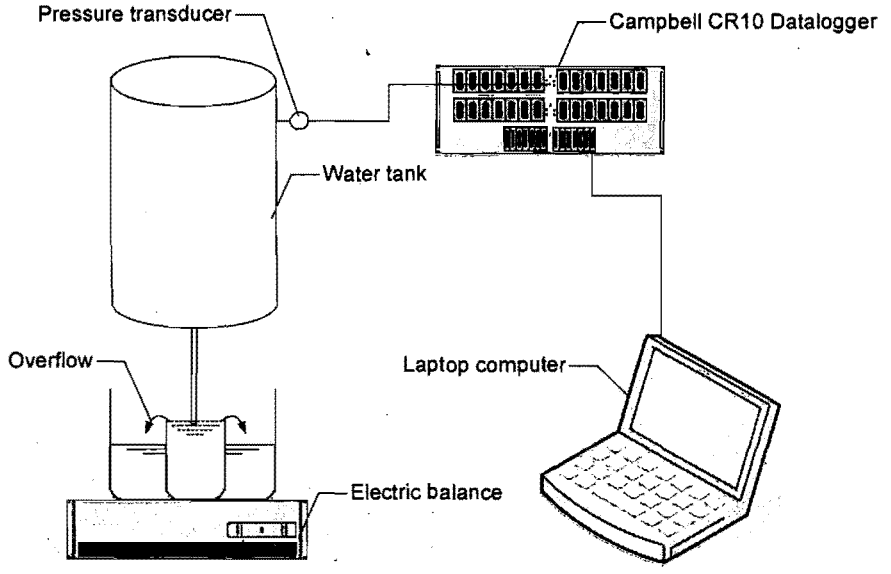

Figure 68. Calibration setup for sensors monitoring infiltration rate.

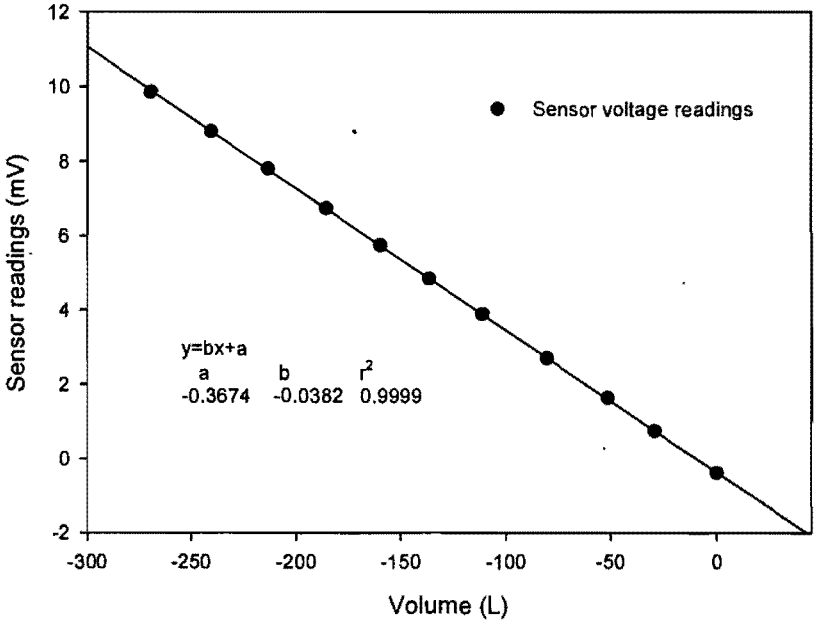

Figure 69. Linear regression for the calibration of infiltration rate sensor SCX01DNC.

An electric balance with two different sized water containers was employed to measure

the volume of water outflow from the water tank. The pressure sensor (SCX01DNC in soil lysimeter experiments and 26PC in sand column experiments) measured the pressure in the airtight water tank. The volume of water in water tank was calculated as the total volume of tank minus the weight of water on balance. After getting a series of pressure readings and volume of water in the tank, a linear regression was carried out to find the sensor coefficients. **Figure 68** shows the setup of calibration experiment. Linear regression results and sensor coefficients were shown in **Figure 69** and **Figure 70.**

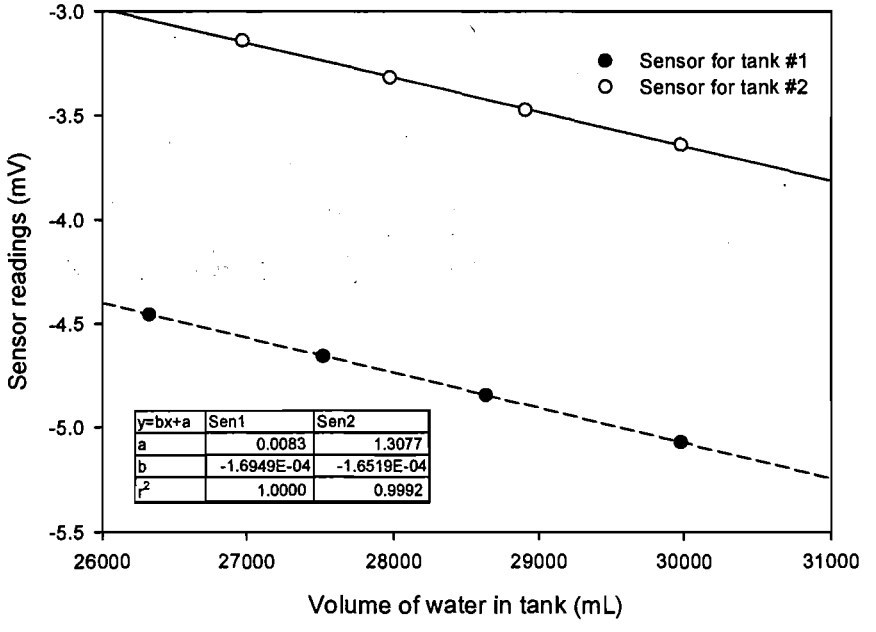

Figure 70. Linear regression for the calibration of infiltration rate sensors 26PC.

3. Calibration of temperature sensor

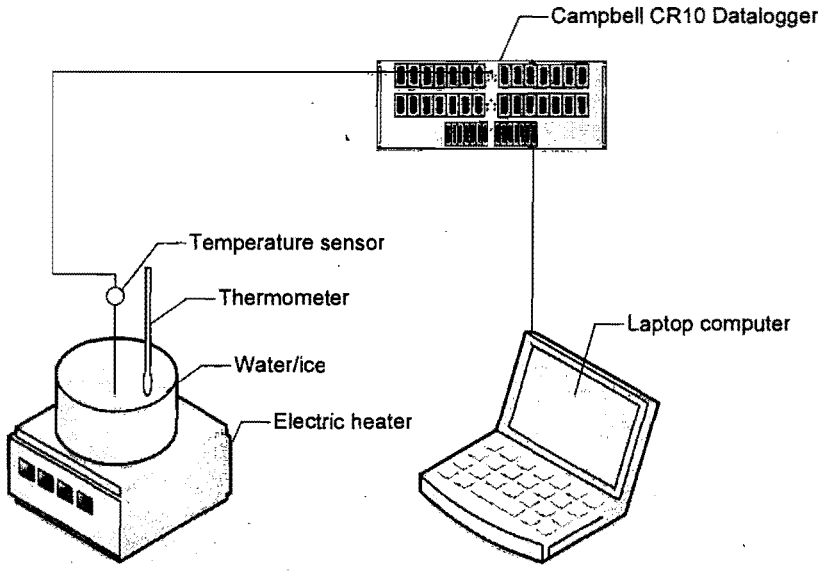

Figure 71. Calibration setup for temperature sensor.

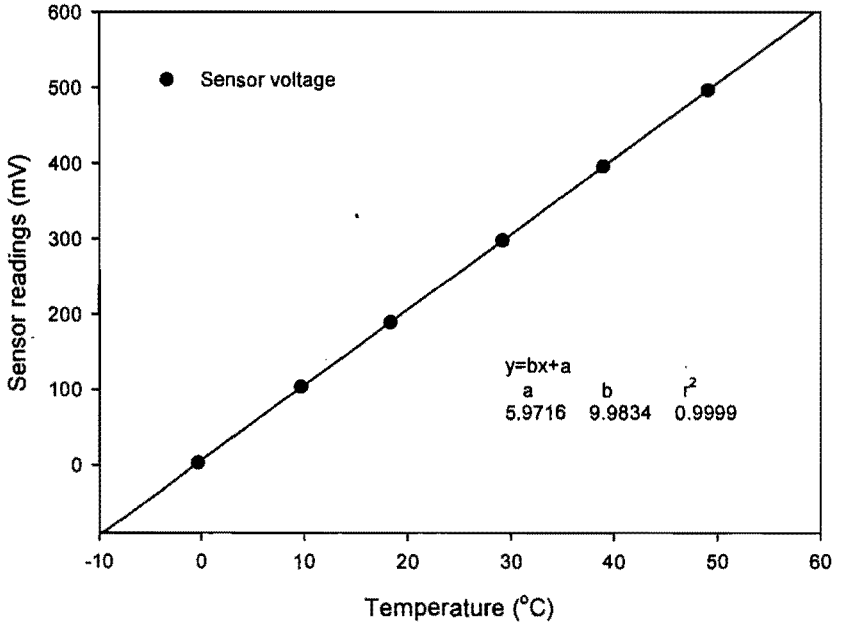

Figure 72. Linear regression for the calibration of temperature sensor LM35CZ.

Temperature sensor (LM35CZ) was inserted into a water container with ice water, which was sitting on an electric heater. Water temperature was read from a thermometer. When

nearly stable temperature reached (0.1 °C variations in 30 seconds), the flag was set to indicate the datalogger to read voltage from sensor. The calibration was done from 0 °C to 50 °C, which covers the temperature range in the bacterial transport experiments. Diagram of setup and results of calibration was shown in **Figure 71** and **Figure 72**, respectively.

Appendix IV

Datalogger Programs for Field Soil Lysimeter Experiment

---

1. Calibration program for pressure transducers (176PC)

```
;{CR10}
;
*Table 1 Program
  01: 10        Execution Interval (seconds)

1:  Volt (Diff) (P2)
 1: 3         Reps
 2: 34        250 mV 50 Hz Rejection Range
 3: 1         DIFF Channel
 4: 2         Loc [ Tens_1    ]
 5: 1.0       Mult
 6: 0.0       Offset

2:  If Flag/Port (P91)
 1: 11        Do if Flag 1 is High
 2: 30        Then Do

    3:  Z=Z+1 (P32)
     1: 5         Z Loc [ Counter    ]

    4:  If (X<=>F) (P89)
     1: 5         X Loc [ Counter    ]
     2: 1         =
     3: 10        F
     4: 10        Set Output Flag High

    5:  Average (P71)
     1: 4         Reps
     2: 1         Loc [ Std        ]

    6:  Standard Deviation (P82)
     1: 3         Reps
     2: 2         Sample Loc [ Tens_1     ]

    7:  If Flag/Port (P91)
     1: 10        Do if Output Flag is High (Flag 0)
     2: 30        Then Do

        8:  Z=F (P30)
         1: 0.0       F
         2: 00        Exponent of 10
         3: 5         Z Loc [ Counter    ]

        9:  Do (P86)
```

```
        1: 21          Set Flag 1 Low

    10:  End (P95)

11:  End (P95)

*Table 2 Program
  02: 0.0000      Execution Interval (seconds)

*Table 3 Subroutines

End Program

-Input Locations-
1 Std          1 1 0
2 Tens_1       5 2 1
3 Tens_2       9 2 1
4 Tens_3       9 2 1
5 Counter      17 1 3
6 _____        0 0 0
7 _____        0 0 0
8 _____        0 0 0
9 _____        0 0 0
10 _____       0 0 0
11 _____       0 0 0
12 _____       0 0 0
13 _____       0 0 0
14 _____       0 0 0
15 _____       0 0 0
16 _____       0 0 0
17 _____       0 0 0
18 _____       0 0 0
19 _____       0 0 0
20 _____       0 0 0
21 _____       0 0 0
22 _____       0 0 0
23 _____       0 0 0
24 _____       0 0 0
25 _____       0 0 0
26 _____       0 0 0
27 _____       0 0 0
28 _____       0 0 0
29 _____       0 0 0
-Program Security-
0000
0000
0000
-Mode 4-
-Final Storage Area 2-
0
```

2. Calibration program for temperature sensor (LM35CZ)

```
;{CR10}
;
*Table 1 Program
  01: 10          Execution Interval (seconds)
```

```
1:  Excite-Delay (SE) (P4)
 1: 1          Reps
 2: 35         2500 mV 50 Hz Rejection Range (Delay must be zero)
 3: 01         SE Channel
 4: 01         Excite all reps w/Exchan 1
 5: 0000       Delay (units 0.01 sec)
 6: -1000      mV Excitation
 7: 2          Loc [ Temp        ]
 8: 1.0        Mult
 9: 0.0        Offset

2:  If Flag/Port (P91)
 1: 11         Do if Flag 1 is High
 2: 30         Then Do

    3:  Z=Z+1 (P32)
     1: 3          Z Loc [ Counter    ]

    4:  If (X<=>F) (P89)
     1: 3          X Loc [ Counter    ]
     2: 1          =
     3: 10         F
     4: 10         Set Output Flag High

    5:  Average (P71)
     1: 2          Reps
     2: 1          Loc [ Std         ]

    6:  Standard Deviation (P82)
     1: 1          Reps
     2: 2          Sample Loc [ Temp        ]

    7:  If Flag/Port (P91)
     1: 10         Do if Output Flag is High (Flag 0)
     2: 30         Then Do

        8:  Z=F (P30)
         1: 0.0        F
         2: 00         Exponent of 10
         3: 3          Z Loc [ Counter    ]

        9:  Do (P86)
         1: 21         Set Flag 1 Low

   10:  End (P95)

11:  End (P95)


*Table 2 Program
  02: 0.0000     Execution Interval (seconds)

*Table 3 Subroutines

End Program

-Input Locations-
1 Std        1 1 0
2 Temp       1 2 1
3 Counter    1 1 2
```

4 _____ 0 0 0
5 _____ 0 0 0
6 _____ 0 0 0
7 _____ 0 0 0
8 _____ 0 0 0
9 _____ 0 0 0
10 _____ 0 0 0
11 _____ 0 0 0
12 _____ 0 0 0
13 _____ 0 0 0
14 _____ 0 0 0
15 _____ 0 0 0
16 _____ 0 0 0
17 _____ 0 0 0
18 _____ 0 0 0
19 _____ 0 0 0
20 _____ 0 0 0
21 _____ 0 0 0
22 _____ 0 0 0
23 _____ 0 0 0
24 _____ 0 0 0
25 _____ 0 0 0
26 _____ 0 0 0
27 _____ 0 0 0
28 _____ 0 0 0
29 _____ 0 0 0
-Program Security-
0000
0000
0000
-Mode 4-
-Final Storage Area 2-
0

3. Soil lysimeter monitoring program

```
;{CR10}
;{CR10}  Created 11/02/2004  {New Voltage Range For Tensiometers}
;Flag Usage: 1 - Reset References
;Control Port Usage: 1-Power Temperature Probe
;Diff Inut Channel Usage: 1..3 - Tens2..3; 4 - Volume
;SE Channel Usage: 11 - Temp


*Table 1 Program
  01: 60.0000    Execution Interval (seconds)

1:  If Flag/Port (P91)
 1: 11          Do if Flag 1 is High
 2: 30          Then Do

    2:  Z=F (P30)
     1: 0.0000    F
     2: 0         Exponent of 10
     3: 7         Z Loc [ RefVol     ]

    3:  Z=F (P30)
     1: 0.0000    F
```

```
    2: 0        Exponent of 10
    3: 8        Z Loc [ RefVol2   ]

  4:  Do (P86)
    1: 21       Set Flag 1 Low

5:  End (P95)

6:  Batt Voltage (P10)
  1: 1        Loc [ Batt       ]

7:  Volt (Diff) (P2)
  1: 1        Reps
  2: 4        250 mV Slow Range
  3: 1        DIFF Channel
  4: 2        Loc [ Ten_1      ]
  5: .11836   Mult
  6: .50202   Offset

8:  Volt (Diff) (P2)
  1: 1        Reps
  2: 4        250 mV Slow Range
  3: 2        DIFF Channel
  4: 3        Loc [ Ten_2      ]
  5: .11963   Mult
  6: .54248   Offset

9:  Volt (Diff) (P2)
  1: 1        Reps
  2: 4        250 mV Slow Range
  3: 3        DIFF Channel
  4: 4        Loc [ Ten_3      ]
  5: .12111   Mult
  6: .53933   Offset

10:  Volt (Diff) (P2)
  1: 1        Reps
  2: 3        25 mV Slow Range
  3: 4        DIFF Channel
  4: 5        Loc [ Volume     ]
  5: -22.757  Mult
  6: 0.0000   Offset

11:  Do (P86)
  1: 41       Set Port 1 High

12:  Excite-Delay (SE) (P4)
  1: 1        Reps
  2: 5        2500 mV Slow Range
  3: 11       SE Channel
  4: 1        Excite all reps w/Exchan 1
  5: 1        Delay (units 0.01 sec)
  6: 1      – mV Excitation
  7: 6        Loc [ Temperat   ]
  8: .10016   Mult
  9: -.59815  Offset

13:  Do (P86)
  1: 51       Set Port 1 Low
```

```
14:  If time is (P92)
 1: 0          Minutes (Seconds --) into a
 2: 60         Interval (same units as above)
 3: 30         Then Do

    15:  If (X<=>F) (P89)
     1: 7          X Loc [ RefVol     ]
     2: 1          =
     3: 0.0000     F
     4: 30         Then Do

        16:  Z=X (P31)
         1: 5          X Loc [ Volume     ]
         2: 7          Z Loc [ RefVol     ]

        17:  Z=X (P31)
         1: 5          X Loc [ Volume     ]
         2: 8          Z Loc [ RefVol2    ]

    18:  End (P95)

    19:  Z=X-Y (P35)
     1: 5          X Loc [ Volume     ]
     2: 7          Y Loc [ RefVol     ]
     3: 9          Z Loc [ CumVol     ]

    20:  Z=X-Y (P35)
     1: 5          X Loc [ Volume     ]
     2: 8          Y Loc [ RefVol2    ]
     3: 10         Z Loc [ VolInc     ]

    21:  Z=X (P31)
     1: 5          X Loc [ Volume     ]
     2: 8          Z Loc [ RefVol2    ]

    22:  Z=X*F (P37)
     1: 9          X Loc [ CumVol     ]
     2: 5.3030     F
     3: 11         Z Loc [ CumInfil   ]

    23:  Z=X*F (P37)
     1: 10         X Loc [ VolInc     ]
     2: 5.3030     F
     3: 12         Z Loc [ InfilRate ]

24:  End (P95)

25:  If time is (P92)
 1: 0          Minutes (Seconds --) into a
 2: 60         Interval (same units as above)
 3: 10         Set Output Flag High

26:  Real Time (P77)
 1: 110        Day,Hour/Minute (midnight = 0000)

27:  Average (P71)
 1: 1          Reps
 2: 6          Loc [ Temperat   ]
```

```
28:  Average (P71)
 1: 3        Reps
 2: 2        Loc [ Ten_1      ]

29:  Sample (P70)
 1: 4        Reps
 2: 9        Loc [ CumVol     ]

*Table 2 Program
  01: 0.0000     Execution Interval (seconds)

*Table 3 Subroutines

End Program

-Input Locations-
1 Batt        1 0 1
2 Ten_1       1 1 1
3 Ten_2       1 1 1
4 Ten_3       1 1 1
5 Volume      1 5 1
6 Temperat    1 1 1
7 RefVol      1 2 2
8 RefVol2     1 1 3
9 CumVol      1 2 1
10 VolInc     1 2 1
11 CumInfil   1 1 1
12 InfilRate 1 1 1
13 _________ 0 0 0
14 _________ 0 0 0
15 _________ 0 0 0
16 _________ 0 0 0
17 _________ 0 0 0
18 _________ 0 0 0
19 _________ 0 0 0
20 _________ 0 0 0
21 _________ 0 0 0
22 _________ 0 0 0
23 _________ 0 0 0
24 _________ 0 0 0
25 _________ 0 0 0
26 _________ 0 0 0
27 _________ 0 0 0
28 _________ 0 0 0
-Program Security-
0000
0000
0000
-Mode 4-
-Final Storage Area 2-
0
```

Appendix V

Datalogger program for sand column experiment

---

1. Calibration program for pressure sensor (26PCAFB6G)

```
;{CR10}

;Program to calibrate 1 PSI Pressure Sensors  (HoneyWell 26PCAFB6G)

*Table 1 Program
  01: 10.00      Execution Interval (seconds)

1:  Batt Voltage (P10)
 1: 1           Loc [ Batt      ]

2:  Volt (Diff) (P2)
 1: 4           Reps
 2: 33          25 mV 50 Hz Rejection Range
 3: 1           DIFF Channel
 4: 3           Loc [ Sens_1    ]
 5: 1.0         Mult
 6: 0.0         Offset

3:  If Flag/Port (P91)
 1: 11          Do if Flag 1 is High
 2: 30          Then Do

    4:  Z=Z+1 (P32)
     1: 7           Z Loc [ Counter    ]

    5:  If (X<=>F) (P89)
     1: 7           X Loc [ Counter    ]
     2: 1           =
     3: 10          F
     4: 10          Set Output Flag High (Flag 0)

    6:  Resolution (P78)
     1: 1           High Resolution

    7:  Average (P71)^22559
     1: 5           Reps
     2: 2           Loc [ CalVal    ]

    8:  Standard Deviation (P82)^12650
     1: 4           Reps
     2: 3           Sample Loc [ Sens_1    ]

    9:  If Flag/Port (P91)
     1: 10          Do if Output Flag (Flag 0) is High
     2: 30          Then Do
```

```
        10:  Z=F x 10^n (P30)
          1: 0          F
          2: 00         n, Exponent of 10
          3: 7          Z Loc [ Counter    ]

        11:  Do (P86)
          1: 21         Set Flag 1 Low

    12:  End (P95)

13:  End (P95)
*Table 2 Program
  02: 0.0000      Execution Interval (seconds)

*Table 3 Subroutines

End Program

-Input Locations-
1 Batt        1 0 1
2 CalVal      1 1 0
3 Sens_1      5 2 1
4 Sens_2      9 2 1
5 Sens_3      9 2 1
6 Sens_4      17 2 1
7 Counter     1 1 2
8 _________ 0 0 0
9 _________ 0 0 0
10 _________ 0 0 0
11 _________ 0 0 0
12 _________ 0 0 0
13 _________ 0 0 0
14 _________ 0 0 0
15 _________ 0 0 0
16 _________ 0 0 0
17 _________ 0 0 0
18 _________ 0 0 0
19 _________ 0 0 0
20 _________ 0 0 0
21 _________ 0 0 0
22 _________ 0 0 0
23 _________ 0 0 0
24 _________ 0 0 0
25 _________ 0 0 0
26 _________ 0 0 0
27 _________ 0 0 0
28 _________ 0 0 0
-Program Security-
0000
0000
0000
-Mode 4-
-Final Storage Area 2-
0
-DLD File Labels-
0
-Final Storage Labels-
0,CalVal_AVG~2,22559
0,Sens_1_AVG~3
```

```
0,Sens_2_AVG~4
0,Sens_3_AVG~5
0,Sens_4_AVG~6
1,Sens_1_STD~3,12650
1,Sens_2_STD~4
1,Sens_3_STD~5
1,Sens_4_STD~6
```

2. Sand column data acquisition program

```
;{CR10}
;
;04/Nov/2004
;Program 1 for Guangming
;Measurement of soil water potential and infiltration of water via water infiltrometers.

;Flag Usage: 1- Set initial infiltration references.
;5V Port Usage:  Power pressure all sensors, including tensiometers.
;Diff Input Port Usage: 1-4 Tensio1..4; 5 Infiltration Sensor.

*Table 1 Program
  01: 60          Execution Interval (seconds)

1:  Volt (Diff) (P2) ;Measure Tensiometers.
 1: 4          Reps
 2: 33         25 mV 50 Hz Rejection Range
 3: 1          DIFF Channel
 4: 1          Loc [ Tensio_1   ]
 5: 1.0        Mult
 6: 0          Offset

2:  Scaling Array (A*Loc+B) (P53) ;Apply tensiometer calibrations.
 1: 1          Start Loc [ Tensio_1   ]
 2: .85017     A1
 3: .74574     B1
 4: .86096     A2
 5: .49474     B2
 6: .84417     A3
 7: .68856     B3
 8: .85653     A4
 9: .60623     B4

;Routine to send Tensiometer Data to final storage.

3:  Do (P86)
 1: 10         Set Output Flag High

4:  Real Time (P77)^26026
 1: 110        Day,Hour/Minute (midnight = 0000)

5:  Sample (P70)^32495
 1: 4          Reps
 2: 1          Loc [ Tensio_1   ]

6:  If time is (P92)
 1: 5          Minutes (Seconds --) into a
 2: 10         Interval (same units as above)
 3: 10         Set Output Flag High
```

```
7:  Real Time (P77)^6680
 1: 110        Day,Hour/Minute (midnight = 0000)

8:  Average (P71)^16285
 1: 4          Reps
 2: 1          Loc [ Tensio_1   ]

9:  Standard Deviation (P82)^12675
 1: 4          Reps
 2: 1          Sample Loc [ Tensio_1   ]

*Table 2 Program
  02: 0.5        Execution Interval (seconds)

1:  Volt (Diff) (P2)
 1: 1          Reps
 2: 33         25 mV 50 Hz Rejection Range
 3: 5          DIFF Channel
 4: 5          Loc [ Volsen     ]
 5: -5900.0    Mult
 6: 48.807     Offset

2:  If time is (P92)
 1: 0          Minutes (Seconds --) into a
 2: 1          Interval (same units as above)
 3: 10         Set Output Flag High

3:  Set Active Storage Area (P80)
 1: 3          Input Storage Area
 2: 6          Loc [ VolsAv     ]

4:  Resolution (P78)
 1: 1          High Resolution

5:  Average (P71)^24967
 1: 1          Reps
 2: 5          Loc [ Volsen     ]

6:  If time is (P92)
 1: 0          Minutes (Seconds --) into a
 2: 10         Interval (same units as above)
 3: 30         Then Do

;Routine to set initial references for infiltration calculations.

    7:  If Flag/Port (P91)
     1: 11         Do if Flag 1 is High
     2: 30         Then Do

        8:  Z=X (P31)
         1: 6          X Loc [ VolsAv     ]
         2: 7          Z Loc [ VolRefAbs ]

        9:  Z=X (P31)
         1: 6          X Loc [ VolsAv     ]
         2: 8          Z Loc [ VolRef10   ]

        10:  Z=F x 10^n (P30)
         1: 0          F
```

```
    2: 0        n, Exponent of 10
    3: 15       Z Loc [ TimeCount ]

   11:  Do (P86)
    1: 21       Set Flag 1 Low

12:  End (P95)

;Infiltration calculations routine.


13:  Z=X+F (P34)
 1: 15      X Loc [ TimeCount ]
 2: 10      F
 3: 15      Z Loc [ TimeCount ]

14:  Z=X-Y (P35)
 1: 7       X Loc [ VolRefAbs ]
 2: 6       Y Loc [ VolsAv    ]
 3: 9       Z Loc [ CumVol    ]

CumInfil=CumVol/39.761

CumInfilR=Cuminfil/(TimeCount/60)

15:  Z=X-Y (P35)
 1: 8       X Loc [ VolRef10  ]
 2: 6       Y Loc [ VolsAv    ]
 3: 10      Z Loc [ Vinc10    ]

Infil10=Vinc10/39.761

16:  Z=X*F (P37)
 1: 12      X Loc [ Infil10   ]
 2: 6       F
 3: 14      Z Loc [ Infil10R  ]

17:  Z=X (P31)
 1: 6       X Loc [ VolsAv    ]
 2: 8       Z Loc [ VolRef10  ]

;Output Infiltration results to final storage.

18:  Do (P86)
 1: 10      Set Output Flag High

19:  Set Active Storage Area (P80)^12088
 1: 1       Final Storage Area 1
 2: 1       Array ID

20:  Real Time (P77)^17521
 1: 110     Day,Hour/Minute (midnight = 0000)

21:  Sample (P70)^28497
 1: 6       Reps
 2: 9       Loc [ CumVol    ]

22:  End (P95)

*Table 3 Subroutines
```

End Program

-Input Locations-
1 Tensio_1 5 4 2
2 Tensio_2 9 4 2
3 Tensio_3 9 4 2
4 Tensio_4 17 4 2
5 Volsen 3 1 1
6 VolsAv 1 5 1
7 VolRefAbs 3 1 1
8 VolRef10 3 1 2
9 CumVol 3 1 1
10 Vinc10 3 1 1
11 CumInfil 3 1 0
12 Infil10 3 2 0
13 CumInfilR 3 1 0
14 Infil10R 3 1 1
15 TimeCount 3 1 2
16 CSI_R 0 0 0
17 CSI_1 0 0 0
18 CSI_2 0 0 0
19 _____ 0 0 0
20 _____ 0 0 0
21 _____ 0 0 0
22 _____ 0 0 0
23 _____ 0 0 0
24 _____ 0 0 0
25 _____ 0 0 0
26 _____ 0 0 0
27 _____ 0 0 0
28 _____ 0 0 0
-Program Security-
0000
0000
0000
-Mode 4-
-Final Storage Area 2-
0
-DLD File Labels-
0
-Final Storage Labels-
0,Day_RTM,26026
0,Hour_Minute_RTM
1,Day_RTM,6680
1,Hour_Minute_RTM
2,Tensio_1_AVG~1,16285
2,Tensio_2_AVG~2
2,Tensio_3_AVG~3
2,Tensio_4_AVG~4
3,Day_RTM,17521
3,Hour_Minute_RTM
4,CumVol~9,28497
4,Vinc10~10
4,CumInfil~11
4,Infil10~12
4,CumInfilR~13
4,Infil10R~14
5,Tensio_1~1,32495
5,Tensio_2~2

5,Tensio_3~3
5,Tensio_4~4
6,Tensio_1_STD~1,12675
6,Tensio_2_STD~2
6,Tensio_3_STD~3
6,Tensio_4_STD~4
7,Volsen_AVG~5,24967
8,1,12088